Integrated Characterization of Cellular Physiology Underlying Hepatic Metabolism

by

Matthew Sing Wong

Bachelor of Chemical Engineering, 1999
Rice University, Houston, Texas

Submitted to the Department of Chemical Engineering
in Partial Fulfillment of the Requirements for the Degree of

DOCTOR OF PHILOSOPHY
in Chemical Engineering

at the

MASSACHUSETTS INSTITUTE OF TECHNOLOGY
June 2006

Author _____
Department of Chemical Engineering
February 16, 2006

Certified by _____
Gregory Stephanopoulos
Professor of Chemical Engineering
Thesis Supervisor

Accepted by _____
William Deen
Professor of Chemical Engineering
Chairman, Committee for Graduate Students

Integrated Characterization of Cellular Physiology Underlying Hepatic Metabolism

by

Matthew Sing Wong

Submitted to the Department of Chemical Engineering
on February 16, 2006 in Partial Fulfillment of the Requirements
for the Degree of Doctor of Philosophy in Chemical Engineering

Abstract

The macroscopic metabolic phenotype of a cellular system, such as insulin resistance, is the result of the integration of many hundreds or thousands of preceding cellular events, which culminates in the cell's final response to a perturbation in the environment. The data provided by DNA microarrays and multiple types of metabolic measurements can be integrated to reconstruct the actions taken by a cellular system to arrive at a particular metabolic response to a stimulus, elucidating the underlying physiology. We employed this integrated approach for the characterization of hepatic metabolism.

First, we implemented a novel method for functional genomics. The metabolic response of hepatoma cells to the depletion and repletion of glutamine was characterized in time course measurements of metabolic fluxes and metabolite pool sizes. DNA microarrays characterized the expression profiles. The metabolic data were correlated with the microarray data to identify coregulated clusters of genes. This study contributed to our understanding of glutamine metabolism in hepatomas, and advanced the field of functional genomics.

Next, we identified the hexosamine biosynthetic pathway (HBP) as a mechanism for hyperglycemia-induced hepatic insulin resistance. Glycogen deposition and glucose production data in mouse hepatocytes confirmed that HBP activity was negatively correlated with insulin sensitivity. Metabolite profiling data confirmed that prolonged incubation in hyperglycemic conditions raised the levels of hexosamine intermediates by saturating upper glycolysis. Our data, along with previous work in muscle and adipose tissue, underline the increasingly important role of the HBP in regulating insulin action and energy homeostasis. A dysfunctional HBP may contribute to the pathophysiology of Type 2 diabetes.

Finally, we analyzed the control structure of the glucose production bioreaction network. We systematically perturbed the network and analyzed the effects on the fluxes. We found that gluconeogenesis was the dominant flux, and therefore regulation of gluconeogenesis determined the glucose production phenotype. G6Pase was identified

as the enzyme in gluconeogenesis controlling the glucose production phenotype, whereas PEPCK played a secondary role. Our conclusions here give insight into the physiology underlying the regulation and dysregulation of hepatic glucose production with possible application to the treatment of Type 2 diabetes.

Thesis Supervisor: Gregory Stephanopoulos
Title: Professor of Chemical Engineering

To my parents,

Joe,

And Lisa

Acknowledgements

During my graduate school application process, I wrote in my application essays that I already knew that a Ph.D. required intelligence and persistence in equal parts. During my stay here, I have realized that another component is also necessary. The kind assistance and guidance of people who traveled this road ahead of me and people who walked this road with me were also needed to bring me to the end of this journey. To these people, I owe my sincere thanks and gratitude.

First thanks go to my thesis advisor, Greg, whose patient guidance and gentle prodding shaped not only my research but also my outlook on science. Thanks for providing the financial support for this work, giving me wise direction when it was warranted, and letting me think independently to formulate my own goals and methods. My thesis committee members, Professors Joanne Kelleher, K. Dane Wittrup, and David Rhoads, also provided crucial input on my project. I thank Joanne for sharing her valuable laboratory and medical experience, and for helping me think through those pesky experimental details. I thank Dave especially for his assistance in straightening out the hepatocyte isolation protocols, his enthusiasm for research, and his constant support throughout the process.

My current and former colleagues inside and outside the Stephanopoulos lab also deserve much gratitude. Arvind Ramanathan, for our very fruitful collaboration in metabolite profiling and Xbox. Javier Femenia, for telling me to leave as soon as possible. Saliya Silva, for always being a willing conversation partner and lunch buddy. Jeff Swers, for all those good times evaluating the Sox's pitching rotation while waiting for an incubation to finish. Other people also deserve a special mention for making the

lab a vibrant community: Jose Aleman, Keith Tyo, Brett Roth, Collin Martin, and Pooya Iranpour. Thanks to Maciek Antoniewicz and Mike Raab for their direct assistance in this project. This work could not have been completed without your hard work and expertise. Double thanks to Jose Aleman for proofing this thesis; it takes a lot of effort to slog through a thesis! Thanks to all the rest of the Stephanopoulos group members, past and present, who have made my time at MIT more interesting. It was experience I will remember fondly for years to come.

And finally, nothing would be possible without the love and support of my dear family. Mom and Dad sacrificed so much to give me opportunities in life. Thank you for cheering for me every step of the way, and I hope to follow the example you have set for me in life. My brother, Joe, with whom I shared an apartment for 3 years here in Cambridge. Thank you for providing stress relief and a good game of stickball. And of course, Lisa, my wife. Thank you for your unconditional support and love, your companionship, and your patience.

Thank you all, for without you, I would have never made it to MIT, made it out of MIT, and had such great memories here that I will cherish for the rest of my life.

Matthew S. Wong

February 2006

Table of Contents

Table of Figures

Table of Tables

List of Abbreviations

CAP	Cbl associated protein
Cbl	Casitas B-lineage lymphoma
CSPR3	Controlled processed serum replacement 3
DPP-IV	Dipeptidyl peptidase IV
FBPase	Fructose-1,6-bisphosphatase
FBS	Fetal bovine serum
FDA	Food and Drug Administration
FFA	Free fatty acids
G6Pase	Glucose-6-phosphatase
GFAT	Glutamine:fructose-6-phosphate amidotransferase
Ggn	Glucagon
GlcNAc	*N*-acetyl glucosamine
GLP1	Glucagon-like peptide 1
GLUT	Facilitated glucose transporter
GK	Glucokinase
GP	Glycogen phosphorylase
GS	Glycogen synthase
GSK-3	Glycogen synthase kinase-3
HBP	Hexosamine biosynthetic pathway
HNF	Hepatocyte nuclear factor
Ins	Insulin
IRE	Insulin responsive element

IRS	Insulin receptor substrate
ISA	Isotopomer spectral analysis
KIR6·2	Potassium-inward rectifier 6·2
MODY	Maturity-onset diabetes of the young
PC	Pyruvate carboxylase
PDH	Pyruvate dehydrogenase
PDK1	Phosphoinositide-dependent kinase 1
PEP	Phosphoenolpyruvate
PEPCK	Phosphoenolpyruvate carboxykinase
PGC-1	PPARγ co-activator-1
PI3-K	Phospho-inositide-3-kinase
PIP2	Phosphatidyl-inositol-3,4-bisphosphate
PIP3	Phosphatidyl-inositol-3,4,5-trisphosphate
PK	Pyruvate kinase
PKB	Protein kinase B
PKC	Protein kinase C
PP1	Protein phosphatase 1
PPARγ	Peroxisome proliferators-activated receptor γ
PS	Penicillin streptomycin
PTEN	Phosphatase and tensin homologue
PTP1B	Protein-tyrosine-phosphatase 1B
SHIP2	SH2-containing 5'-inositol phosphatase
SREBP-1	Sterol regulatory element binding protein 1

SUR1	Sulfonylurea receptor 1
TNFα	Tumor necrosis factor α
TZD	Thiazolidinedione
UDP	Uridine diphosphate
VNTR	Variable number tandem repeat

1 INTRODUCTION

The macroscopic metabolic phenotype of a cellular system, such as insulin resistance, is the result of the integration of many hundreds or thousands of preceding cellular events, which culminates in the cell's final response to a perturbation in the environment. In the context of mammalian systems, a cell exchanges information with the environment through endocrine, paracrine, and autocrine signals, through which information is transferred between organs and between organ systems. The binding of a ligand, or hormone, to a receptor is the event that initiates a signaling cascade within the cell. The net effect of this cascade will depend on the particular cascade. Some cascades will activate transcription factors that control gene expression, and other cascades will directly control enzyme activity, perhaps through phosphorylation. If the cascade affects gene expression, the synthesis rate of mRNA will be upregulated or downregulated. In turn, the translation of mRNA into proteins will also be affected. The proteins then carry out the final cellular response to the original perturbation, functioning as enzymes for metabolic reactions and regulators of metabolic enzymes. Changes in the intracellular metabolite levels may feed back into the regulation of proteins. The data provided by DNA microarrays and multiple types of metabolic measurements can be integrated to reconstruct the actions taken by a cellular system to arrive at a particular metabolic response to a stimulus, and gain a deeper understanding of the underlying physiology.

The elucidation of sufficient metabolic information may require several tools, due to the limitations of individual techniques. Release or incorporation of radioisotopes (^{3}H and ^{14}C) from labeled substrates has been a long-used technique for measuring metabolic flux. The advantages of this technique are that it is cheap, relatively quick, and the analysis of the data is simple. The major disadvantage of this technique is that the majority of reactions do not release or incorporate radioisotopes. True fluxes cannot be calculated from the data due to the unknown specific activity of intracellular metabolite pools. Incorporation of stable isotopes (^{2}H and ^{13}C) from labeled substrates has also been used for many decades. Detailed mathematical models of biochemistry can extract a cornucopia of flux data from the isotopomer labeling patterns of metabolic intermediates. The inert nature of stable isotopes allows them to be used in human studies. And finally, as mentioned above, the actual metabolite levels themselves may contain information about the metabolism. Biochemical methods of measuring metabolites or GC/MS methods of metabolite profiling are useful in this regard.

We employed this integrated approach for the characterization of hepatic metabolism. In the functional genomics portion, metabolic data were combined with DNA microarray data to examine gene function. In the bioreaction network analysis portion, biochemical metabolite measurements were combined with stable isotope flux data to create true intracellular flux maps.

1.1 Motivation

The thesis work consisted of three parts: a study in functional genomics, a study in insulin resistance pathophysiology, and a study in bioreaction network control. In the

first section, we demonstrated a novel method of functional genomics in which we characterized the metabolic and transcriptional changes in mouse hepatoma central carbon metabolism that occurred during glutamine depletion and repletion. In the hepatoma studies, the motivation was two-fold. First, glutamine metabolism in mouse hepatoma cells was not well studied, particularly with regard to the use of glutamine in lipogenesis. Our stable isotope studies established the important role of glutamine in hepatoma lipogenesis. Second, we felt that the use of time-course metabolic flux data in conjunction with microarray data would represent a significant advance in functional genomics. Such an approach would supply a powerful method to select genes from the genome-wide pool with functions that were relevant to the flux in question with more precision than previous methods.

The second part of the thesis dealt with the modulation of liver insulin action by the hexosamine biosynthetic pathway. The resistance of muscle, liver, and fat to insulin is the central pathophysiological event in the development of Type 2 diabetes. The precise pathogenesis of insulin resistance is unknown, but it is known that multiple genetic and environmental factors are involved. In an attempt to add to this knowledge, we investigated the hexosamine biosynthetic pathway as a mechanism of hyperglycemia-induced insulin resistance in the liver. A promising hypothesis states that excess flux through the hexosamine biosynthetic pathway results in the increased glycosylation of proteins. Some of these proteins are insulin signaling proteins and glycosylation leads to a decrease in their activity, thus leading to insulin resistance. The effect of excess hexosamine biosynthetic pathway activity has been thoroughly studied in muscle and adipose tissue since the pathway's discovery in 1991 (111). The work detailed in this

thesis complements the previous knowledge of insulin resistance pathophysiology. The identification of the molecular pathophysiological mechanisms of insulin resistance and Type 2 diabetes is essential for the development of novel and more effective therapies to better treat patients with insulin resistance and Type 2 diabetes.

The third part of the thesis examined the control structure of the glucose production network. The response of the network was tested by a series of systematic perturbations in Preincubation glucose level, hormone administration, glycerol availability, and hexosamine biosynthetic pathway activity. These perturbations produced an array of data with many different glucose production phenotypes, and analysis of that data gave us insight into the fluxes and the enzymes that most influenced the glucose production phenotype. Since overactive hepatic glucose production is characteristic of Type 2 diabetes, the identification of the key network control points is essential for more effective therapies.

1.2 Thesis Objectives

The general objective of this thesis was to develop and apply metabolic assays for the characterization of hepatocellular systems. In accomplishing this overall goal, the following specific aims were pursued:

- Develop methods for the use of radioisotopes for the measurement of enzymatic fluxes
- Develop methods for the measurement of metabolite levels using GC/MS

- Characterize the metabolic and transcriptional response of Hepa1-6 mouse hepatoma cells to glutamine oscillations for the implementation of a novel functional genomics strategy
- Develop methods for the isolation and culture of mouse hepatocytes
- Quantify the relationship between the activity of the hexosamine biosynthetic pathway and liver insulin action
- Dissect the control structure of the glucose production flux network

1.3 Thesis Description

The thesis then describes the context for this work, methods used, the results obtained, and the conclusions drawn from the results. The thesis is organized into 7 chapters:

- *Chapter 1*: The motivation behind the present work is presented. The objectives of the thesis are provided.
- *Chapter 2*: Literature review of functional genomics and insulin resistance is given to the reader.
- *Chapter 3*: The materials and methods used in the hepatoma work and the hepatocyte work are listed. More detailed protocols are provided in the appendix.
- *Chapter 4*: The work involving the study of the response of mouse hepatoma cells to glutamine oscillations is presented. This work explored methods to

correlate metabolic flux data with gene expression data in order to advance the field of functional genomics.

- *Chapter 5*: The work studying the role of the hexosamine biosynthetic pathway in liver insulin action is presented. These results advanced the understanding of the pathophysiology of hepatic insulin resistance and Type 2 diabetes.
- *Chapter 6*: The work studying the control structure of the glucose production network is presented. The results advanced the understanding of the control of hepatic glucose production with possible application to the treatment of hyperglycemia in Type 2 diabetes.
- *Chapter 7*: The conclusions and the recommendations for future work are provided.

2 Literature Review

This chapter will provide the background in which our studies of functional genomics and Type 2 diabetes took place. In the area of functional genomics, we attempted to develop a new method that coupled flux measurements with DNA microarray data. The context for this study will be reviewed first. We will then review the existing knowledge base in insulin resistance and Type 2 diabetes, which set the landscape for our hepatocyte studies.

2.1 Functional Genomics

The explosion of genomic knowledge in the past 15 years has left us with an abundance of genes with unknown or poorly characterized function. To understand physiological systems, we must identify gene function and the regulatory interactions between genes. In a study from 1998, RT-PCR measurement sets for 112 genes at various times during rat central nervous system development (198) revealed features of the regulatory cascade. The advent of microarrays, of course, enabled a sampling of genome-wide expression data, and DNA microarrays have become the key experimental tool in functional genomics. The power of expression profiling is most evident in systematic experiments that explore a varied set of conditions. Sampling a smoothly

varying process over time provides data redundancy, and coregulation of genes across a set of biological conditions or across time reveals hypothetical functional gene groups.

Early studies focused on applying these principles. DeRisi et al. (44) followed essentially all the genes in the yeast *Saccharomyces cerevisiae* growing in culture through its diauxic shift. Genes with related known metabolic function showed similar expression evolution over time. The transcriptional changes observed in other genes helped flesh out knowledge of the metabolic pathways involved. Their study helped demonstrate the feasibility and utility of this approach to genome-wide exploration of gene expression patterns. *Caenorhabditis elegans* was profiled over a set of developmental phases, growth conditions, and genetic mutations. The diversity of these conditions yielded strong groupings of co-regulated genes. They visualized the data as a gene expression map, which they used as a gene discovery tool (88). Progression of expression during development was followed during early metamorphosis in *Drosophila* (199), and genes were grouped according to their pattern of expression over the different phases of development. Spellman et al. (174) followed the yeast *S. cerevisiae* through two cell cycles, first synchronizing the cells in the culture with multiple cycle arrest and release methods. Using periodicity and correlation algorithms, they identified 800 genes that met an objective minimum criterion for cell cycle regulation, and functional relationships between different phases of the cycle were suggested. Despite the visually clear and alluring expression patterns that resulted, the detailed conclusions of this and subsequent synchronization studies with microarrays have been called into question over statistical issues and whether most cells are in fact synchronized (33). These early applications of DNA microarrays illustrated the possibilities for the technology and the

challenges in dealing with these large data sets that come with uncertain error behavior and biology.

Increasing diversity of the conditions set, up to a point, yields stronger and more informative groupings of genes by coregulation. The usefulness of more experiments is determined by considering biological complexity and using algorithms to find patterns. Despite the rigor of any mathematical algorithm, these clusters still are subject to the caveat that similarity of response results in a "guilt by association" inference (28) and not proof of functional relatedness. These results are merely a starting point for more confirmatory experiments to pin down the role of a particular gene. Marcotte et al. (110) were able to group proteins by correlated evolution, correlated messenger RNA expression patterns and patterns of domain fusion to determine functional relationships among the 6,217 proteins of the yeast *S. cerevisiae*. Comparing these predictions to accepted functional annotations indicated fairly limited accuracy of the coregulation based inferences, although this depends on the set of conditions over which the expression profiles are obtained.

One study in particular stands out for its novelty. Hughes et al. (74) profiled a large set of different single-gene disruption mutants in yeast, comparing their transcriptional state to the wild-type strain. The resulting patterns (Fig. 2.1) provided a visualization of major pathway groupings and provided functional inferences for previously unannotated genes. Figure 2.1, in which rows and columns of the expression ratio data were reordered according to agglomerative hierarchical similarity clustering, illustrates the important distinction between two modes of functional inference. Proximity of two genes in the horizontal dimension indicates the degree of coregulation.

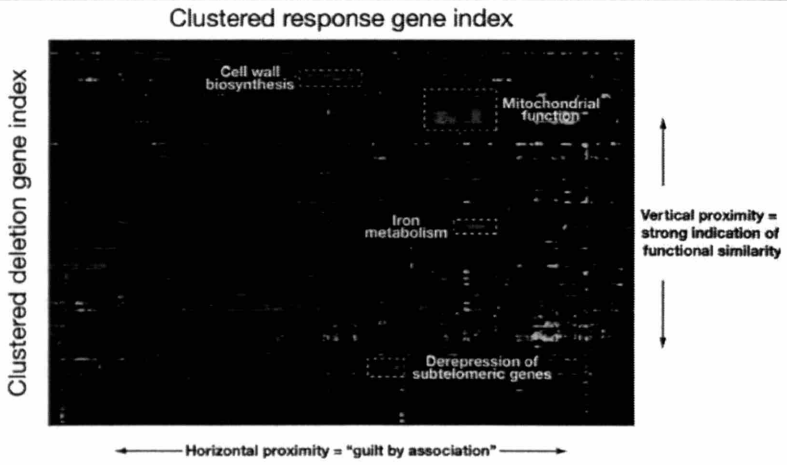

Figure 2.1. Expression responses to single-gene deletions in yeast. Each row represents the up- (*red*) or downregulation (*green*) of expression in response to a single-gene disruption in yeast. Only 300 genes (*columns*) are shown. These were the most responsive among the ~6000 yeast genes measured in each two-color hybridization experiment. Columns, and independently the rows, have been rearranged via agglomerative hierarchical clustering to place rows with similar response patterns near each other, and columns with similar response patterns near each other. Each red or green island then represents a coordinated transcriptional response that is similar for each of a set of gene disruptions.

These genes respond similarly to the disruptions of other genes. However, this kind of similarity often is the result of a fairly uninteresting downstream convergence of pathways, such as a global stress signature. Proximity on the vertical axis means two disrupted genes produced similar cell responses at the gene expression level, which was a stronger indication of functional similarity. The utility of this approach was validated by examining profiles caused by deletions of uncharacterized genes. They identified and experimentally confirmed that eight uncharacterized open reading frames encoded proteins required for sterol metabolism, cell wall function, mitochondrial respiration, or protein synthesis. (74). This approach was extended even further to characterize pharmacological perturbations by the identifying the target of a drug compound. The expression pattern of a knockout mutant that matched the pattern of the drug revealed the drug's probable target.

This leads to a second class of functional genomics experiments that uses microarray expression data as the signature of a perturbation. Genes that are differentially expressed when the system is exposed to a perturbation such as a toxin become indicators of an inflamed state. In this case, we are not so interested in the functions of these differentially expressed genes as we are in how their expression pattern can uniquely describe the toxin. As examples, toxicity patterns in rat liver were produced by profiling the response to compounds of known toxicity (118, 194). The expression profiles produced by compounds under study then can be interpreted for the mechanism and likelihood of toxicity. Biological interpretation of the responding genes also gives clues to the mechanisms of toxicity. Similarly, efficacy landmarks can be provided by profiling drugs with known mechanisms of action. Expression responses to psychoactive

compounds in primary human neurons in vitro were used to develop classifiers for antidepressant, antipsychotic, and opioid drug action (63). The products of such projects can be thought of either as biomarkers for particular classification decisions or as a general resource for interpreting the bioactivity of new compounds.

Finally, one of the most common experiment types in the drug discovery and diagnostics arena is the search for biomarkers of a particular human phenotypic end point. Cancer outcome prognosis is a very popular category because genetic variation is critical to cancer phenotype. Alizadeh et al. (4) found expression patterns indicative of survival in B-cell lymphoma patients and characteristics of two subtypes of large diffuse lymphoma B cells. In this study, the microarray probes were chosen to target genes expressed in lymphoid cells and to be relevant to immune response. A subset of the predictive markers was confirmed in follow-up validation studies with PCR. Van t' Veer et al. (188) used DNA microarray analysis on primary breast tumors of 117 young patients. After applying supervised classification, they were able to find an arithmetic function of the expression levels of 70 transcripts that predicted metastasis of breast tumors out of ~25,000 profiled. This predictor was validated in a larger follow-up study of almost 300 patients (189). However, the use of a supervised classification, as opposed to an unsupervised method such as principal component analysis, was a weakness of that study. A recent meta-analysis of 84 microarray-based cancer outcome studies found that very few of them accomplished thorough validation and that, not surprisingly, larger cohorts and larger probe sets increased the chances of finding good biomarkers (131). There is a close relationship in these studies between developing predictors and recognizing subphenotypes of disease. In general, the detailed molecular phenotype

provided by expression profiling allows discrimination between multiple states that may at one moment have the same gross phenotype (lymph node status or histological grade) but for which the subsequent progression of events differs.

2.2 Insulin Resistance and Type 2 Diabetes

In the past few decades, diabetes mellitus has pushed its way to the forefront of public health consciousness. In conjunction with the spread of obesity, Type 2 diabetes mellitus has reached epidemic proportions in many developed countries, most notably in the United States. As of 2004, there were an estimated 16 million people with Type 2 diabetes in the US (33% were undiagnosed) and approximately 1.3 million more are newly diagnosed each year. As of 2002, Type 2 diabetes was the 6th leading cause of death in the United States. This disease is caused by multiple genetic factors, but diet and lifestyle are also factors. The etiology of this complex disease has not been unraveled, but its symptoms and the various organs and molecules involved in glucose homeostasis have been described since ancient times (89, 148).

2.2.1 Historical Review of Diabetes

In 1500 B.C., the Papyrus Ebers of Ancient Egyptians had a number of remedies for combating the passing of too much urine (polyuria). Hindus in the Ayur Veda recorded that insects and flies were attracted to the urine of some people, that the urine tasted sweet, and that this was associated with certain diseases. Between that time and the 19th century, many physicians and scientists such as Arataeus of Cappadocia (1st century A.D.), Celsus (1st century A.D.), Chen Chuan of China (7th century A.D.)

Thomas Willis of Oxford (17th century A.D.), and Avicenna the Arab (11th century A.D.), noted the symptoms of excessive urination and sweetness of urine.

Attempts at treatment began when no more was known of diabetes than the polyuria. John Rollo, Surgeon-General to the Royal Artillery, treated Captain Meredith in 1796 by dietary restriction with considerable success. The patient survived for at least a year. Rollo also noticed the smell of acetone on the breath of diabetics, presumably those in the advanced stage of Type 1 diabetes. Around the same time, Thomas Cawley made the observation that the pancreas of a patient who had died of diabetes showed stones and tissue damage. The significance of this was not apparent until Minkowski's work 101 years later.

In 1889, Mehring and Minkowski produced diabetes mellitus in dogs by removing the pancreas. The results were glycosuria, polyuria, intense thirst, ravenous hunger, and loss of weight despite normal food intake. Glycogen disappeared from the liver and skeletal muscle. These results were unexpected because the prevailing view at the time was that the pancreas only produced digestive enzymes. The removal of the pancreas had been for an experiment exploring the role of the pancreas in digestion. But once Minkowski saw the results of the pancreatectomy, he realized immediately what they meant and tested the urine for glucose. With these results, he knew that the pancreas produced some antidiabetic substance, but he could not purify it. In 1921, Banting and Best successfully extracted insulin from the pancreas. The news of this discovery spread quickly throughout the world and brought hope to sufferers of Type 1 diabetes mellitus.

It soon became apparent that there were two types of diabetes mellitus – insulin dependent, and non-insulin dependent. Physicians had long appreciated the clinical

distinction, but they did not know that the two types of diabetes were caused by different pathogenic mechanisms. In 1936, Harold Himsworth demonstrated insulin sensitivity in Type 1 and insulin resistance in Type 2 diabetes.

Forms of oral treatment for Type 2 diabetes have been used since the 1930's, but none were really effective. In 1942, M.J. Janbon, a professor at Montpellier, France, discovered that a substance in the class of sulphonylureas could induce the fall of blood glucose. They were able to infer that sulphonylureas stimulated the secretion of insulin, although this did not fully explain their mode of action. G. Unger first described the use of biguanides for Type 2 diabetes therapy in 1957 (186). Metformin (dimethylgibuanide) reduced hepatic glucose output as its mode of action, but did not receive FDA approval for Type 2 diabetes until 1994.

2.2.2 Pathogenesis of Type 2 Diabetes

Diabetes mellitus is the most common endocrine disorder, currently affecting over 170 million people worldwide (202). More than 90% of the patients are of the Type 2 diabetes variety. The major pathophysiological event contributing to the development of Type 2 diabetes mellitus is resistance of target tissues to insulin (Fig. 2.2). Insulin stimulates glucose uptake in mainly skeletal muscle and fat, and inhibits the glucose production from the liver. In a pre-diabetic insulin resistant state, these organs do not respond properly to insulin, leading to hyperglycemia. The pancreas can partially compensate for this by increasing its output of insulin, but fasting glucose will remain mildly high. This increased secretory load on the pancreas, combined with glucose toxicity, will result in progressive beta cell dysfunction. Eventually, complete beta cell

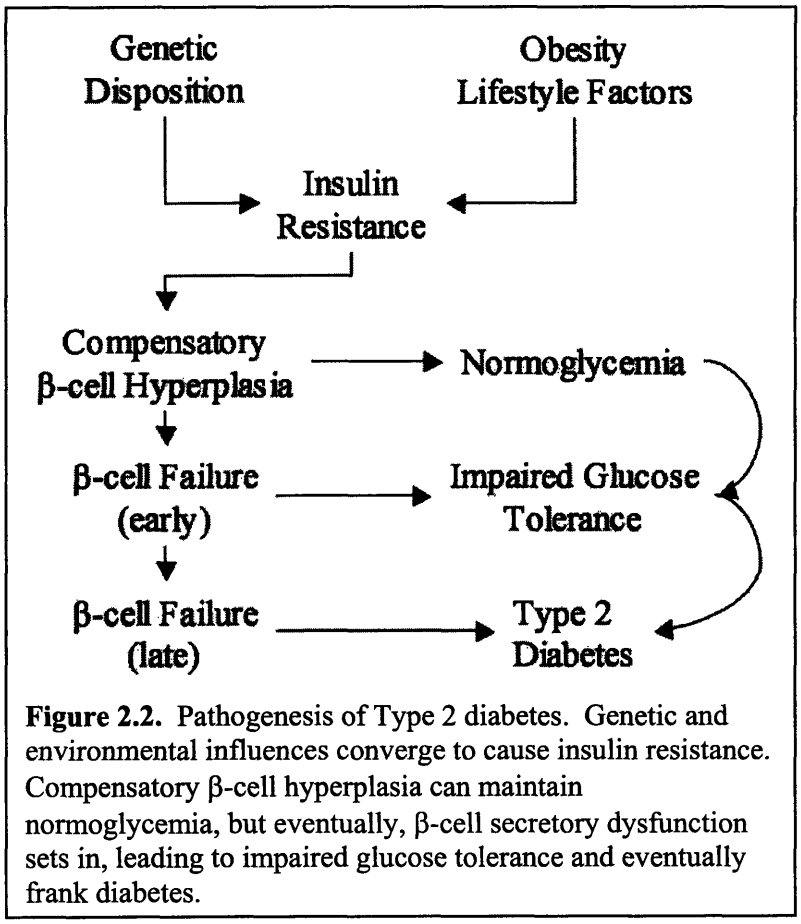

Figure 2.2. Pathogenesis of Type 2 diabetes. Genetic and environmental influences converge to cause insulin resistance. Compensatory β-cell hyperplasia can maintain normoglycemia, but eventually, β-cell secretory dysfunction sets in, leading to impaired glucose tolerance and eventually frank diabetes.

failure occurs and Type 2 diabetes will manifest itself in uncontrolled plasma glucose levels.

The development arc of Type 2 diabetes is a process that takes many years, and the precise sequence of pathophysiological events is unknown. However, recent advances have contributed to our understanding of the underlying molecular mechanisms of insulin resistance. Investigators have attacked the problem with

- Biochemical *in vitro* studies
- Gene targeting in mice
- Analysis of natural mutations in insulin resistant mice
- Analysis of natural mutations in insulin resistant human patients.

The development of novel effective therapies for Type 2 diabetes depends on the advancement of our understanding of the disease. The following sections in this chapter will concentrate on the existing knowledge of hepatic insulin resistance. The contributions of other tissues such as the pancreas, skeletal muscle, and adipose tissues to insulin resistance are outside the scope of this project, as we are working with isolated cultured hepatocytes.

2.2.3 The Insulin Signaling Pathway

The insulin signaling pathway (Fig. 2.3) is mostly conserved across the insulin sensitive tissues. The insulin receptor consists of extracellular ligand binding and intracellular tyrosine kinase domains. When insulin binds the extracellular portion of the receptor, the kinase is activated and the receptor autophosphorylates specific intracellular

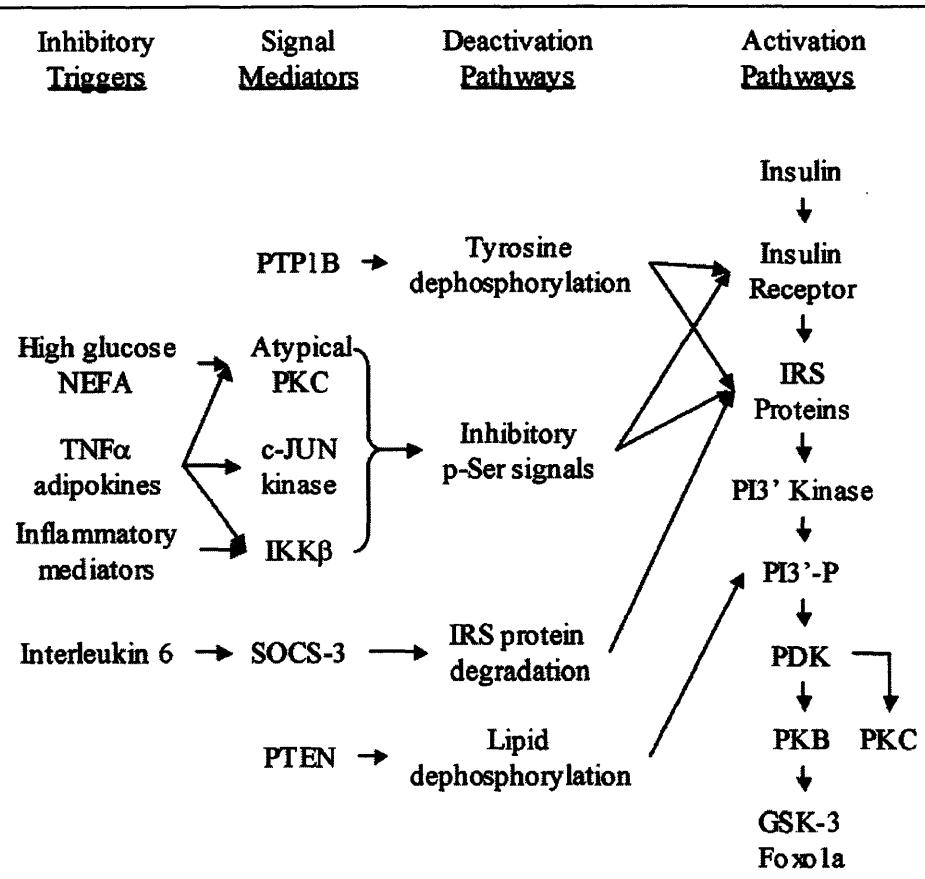

Figure 2.3. Insulin signaling and deactivation pathways across adipose, muscle, and liver tissue. Insulin signaling involves binding of insulin to its receptor followed by a cascade of intracellular events, depicted as activation pathways. Negative modulation of insulin action can be mediated via various pathways leading to insulin resistance. PKC = protein kinase C. PTEN = phosphatase and tensin homologue. PI = phospho-inositol. PKB = protein kinase B. GSK-3 = glycogen synthase kinase-3. PDK = phosphoinositide-dependent kinase.

tyrosine residues. This recruits a number of scaffolding proteins: insulin receptor substrate (IRS) proteins, casitas B-lineage lymphoma (Cbl), or Cbl associated protein (CAP). These proteins themselves then become phosphorylated (14, 27, 101, 130, 139). IRS proteins are not catalytic themselves, but harbor several interaction domains to recruit other signaling molecules like phospho-inositide-3-kinase (PI3-kinase) to form large protein complexes at the plasma membrane. There are multiple IRS proteins, but the most important ones in the regulation of carbohydrate metabolism appear to be IRS-1 and IRS-2 (200). Knockouts of IRS-2 in mice show insulin resistance in muscle, fat, and liver, and develop overt diabetes as a result of β-cell failure (146). In mice, disruption of the IRS-1 gene results only in insulin resistance of muscle and fat (205). Rare mutations of the IRS-1 protein found in humans are associated with insulin resistance (201). There are also data showing that IRS dysfunction in muscle may be a result of adipocyte action. For example, circulating free fatty acids (FFA) and the adipokine tumor necrosis factor α (TNFα) may increase serine phosphorylation of IRS proteins, disrupting insulin signaling (200). Finally, prolonged excess stimulation with insulin (hyperinsulinemia) may result in regulated degradation of IRS protein (160).

Downstream of the IRS proteins, the PI 3-kinase is a central mediator of insulin signaling. PI 3-kinase isoforms can be divided into three classes, but only Class Ia PI 3-kinases participate in insulin signaling. Binding of PI 3-kinase to phosphorylated site on IRS proteins leads to activation of PI 3-kinase. PI 3-kinase generates of phosphatidyl-inositol-3,4-bisphosphate (PIP2) and phosphatidyl-inositol-3,4,5-trisphosphate (PIP3), which bind to the phosphoinositide-dependent kinase 1 (PDK1). Therefore, these two phospholipids may attract PDK1 and the putative PDK2 to the plasma membrane.

Known substrates of the PDKs are the protein kinase B (PKB) and also atypical forms of protein kinase C (PKC) (93).

PKB (also called Akt) is a serine/threonine kinase with high homology to PKA and PKC. So far, three different isoforms of PKB have been identified in mammals (α, β, γ). PKB is conserved from invertebrates to mammals and shows high homology among different species emphasizing its pivotal role in development, cell proliferation, and metabolism (190). PKB mediates effects of insulin on glucose transport, glycogen synthesis, protein synthesis, lipogenesis, and suppression of hepatic gluconeogenesis. PKB regulates both glucose uptake via facilitated glucose transporters (GLUT family) and intracellular glucose metabolism in insulin sensitive tissues, such as skeletal muscle (3). Under non-stimulated conditions, PKB is located in the cytoplasm and stimulation with insulin results in translocation of PKB to the plasma membrane, where it may bind to PIP2 and PIP3 (90, 190). At the plasma membrane, PKB co-localizes with PDK and becomes activated by phosphorylation of its two principal regulatory sites, Thr308 and Ser473. Phosphorylation of both sites is essential for the activation of PKB. PDK1 is the kinase phosphorylating Thr308, while the mechanism of phosphorylation of the Ser473 residue remains controversial and the corresponding kinase PDK2 still needs to be identified (69). Following activation, PKB detaches from the plasma membrane to affect metabolic processes such as glycogen synthesis and glucose transport. Parts of the activated PKB also translocate through the cytoplasm into the nucleus by an unknown mechanism to affect gene expression (5, 119, 190). Substrates for a direct phosphorylation by PKB include glycogen synthase kinase-3 (GSK-3) and members of

the Foxo-family of transcription factors, which are critically involved in the insulin-dependent regulation of glucose homeostasis.

Termination of the insulin signal is critical for the maintenance of metabolic control. Signaling of the insulin receptor cascade is terminated by specific phosphatases. One of the key phosphatases in this context is the protein-tyrosine-phosphatase 1B (PTP1B). Mice lacking the PTP1B gene exhibit increased insulin sensitivity and fail to develop insulin resistance under a high-fat diet (48). In addition, the inhibition of PTP1B activity by systemic application of antisense oligonucleotides specific for PTP1B improved insulin sensitivity and glycemic control in diabetic mice (216). Other phosphatases relevant for the termination of insulin signaling include phosphatase and tensin homologue (PTEN), which inactivates the lipid products of the PI 3-kinase and also SH2-containing 5'-inositol-phosphatase (SHIP2). Knockout mice with a homozygous deletion of the SHIP2 gene display increased insulin sensitivity and hypoglycemia because of an inhibition of hepatic glucose production (29). Also, antisense oligonucleotides specific for PTEN drastically improved glycemic control in diabetic ob/ob and db/db mice (26). Therefore, PTP1B, SHIP2, and PTEN can be regarded as potential therapeutic targets for the treatment of Type 2 diabetes.

2.2.4 Hepatic Glucose Production

The fasting hyperglycemia in patients with Type 2 diabetes is the clinical correlate of the increased glucose production by the liver caused by insulin resistance. Hepatic glucose production is the sum of gluconeogenesis and glycogenolysis, and insulin and glucagon have opposite regulatory effects on key enzymes in both pathways

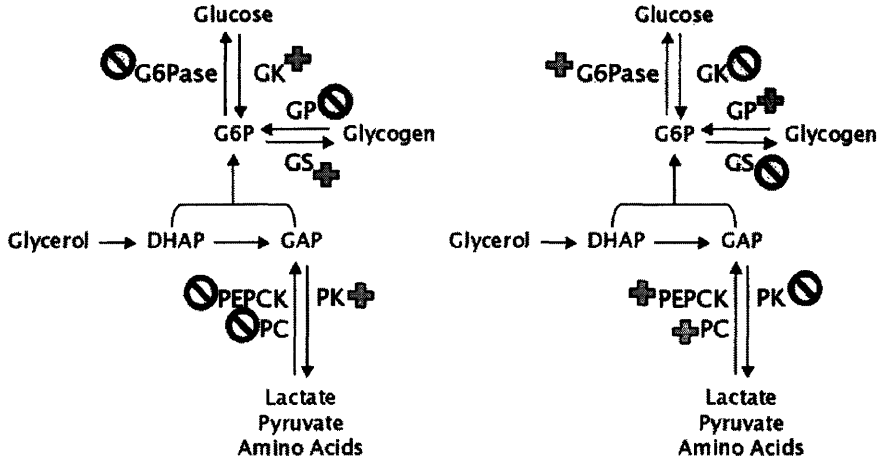

Figure 2.4. Regulatory actions of insulin and glucagon on central carbon metabolism. The symbols indicate an upregulation or downregulation of the particular enzyme at the activity or transcriptional level. G6Pase = glucose-6-phosphatase; GK = glucokinase; GP = glycogen phosphorylase; GS = glycogen synthase; PEPCK = phosphoenolpyruvate carboxykinase; PC = pyruvate carboxylase; PK = pyruvate kinase.

(Fig. 2.4). Insulin activates glucokinase at the transcriptional level, and glucagon, when present, exerts a dominant repressive effect on glucokinase transcription (79). Insulin suppresses the expression of key gluconeogenic enzymes phosphoenolpyruvate carboxykinase (PEPCK) and the glucose-6-phosphatase catalytic subunit (G6Pase) (12), opposing the effect of glucagon. Insulin also inhibits pyruvate carboxylase (PC) expression, whereas glucagon activates the PC protein (80) and increases flux through PC (2). Glucagon converts pyruvate kinase (PK) to a lower activity form, and insulin is able to convert PK back to a high activity form (17). Insulin also increases expression of PK and lengthens the half-life of the mRNA, while glucagon has the opposite effect for both of these mechanisms in isolated hepatocytes (39) and intact rats (191). Glucagon activates glycogen phosphorylase through cAMP production, and insulin antagonizes this through phosphodiesterase-catalyzed destruction of cAMP (78). By the same cAMP mechanism, glucagon also phosphorylates and inhibits glycogen synthase activity (51). It is mentioned in the next section that insulin activates glycogen synthase through PP1, which opposes glycogenolysis.

There is a consensus that hepatic glucose overproduction is the result of dysregulation of the two key gluconeogenic enzymes, PEPCK and G6Pase (13, 156, 184, 187). Insulin inhibits the expression of both of these enzymes at the transcriptional level (12) and it is widely accepted that this process is mediated by activation of PKB (100, 163). The promoters of both the PEPCK and G6Pase genes contain so called insulin-responsive elements (IREs) that are essential for the effect of insulin on the regulation of those genes. Data from *in vitro* studies have shown that three Foxo-family transcription factors (Foxo1a, Foxo3a, and Foxo4) are capable of binding to these structures (65, 163,

207) and that phosphorylation of Foxo-proteins by PKB results in transcriptional inactivation, nuclear export, and consequently inhibition of target gene expression (65, 204). There is increasing evidence that Foxo-proteins are critically involved in the insulin-dependent regulation of gluconeogenic gene expression and insulin resistance *in vivo*. For example, the partial knockout of the Foxo1 gene in insulin resistant mice resulted in reduced G6Pase mRNA and insulin levels comparable with metabolically unaffected control animals (128). Furthermore, transgenic animals with liver and pancreatic β-cell specific expression of a constitutively active, non-insulin-regulatable Foxo1 point mutant (Ser253Ala) have a diabetic phenotype (127, 214). Therefore, these results demonstrate a causal relationship between Foxo1 regulation by insulin and glycemic control *in vivo*. In addition, the PPARγ co-activator-1 (PGC-1), a factor integrating the effects of glucocorticoids and cAMP on gluconeogenic gene expression in the liver (68, 192, 211) is also regulated by PKB and Foxo1 (147), therefore providing additional evidence that PKB and Foxo1 are critical parts of the network integrating hepatic glucose production.

In addition to the Foxo transcription factors, members of the hepatocyte nuclear factor (HNF) family of transcription factors may be involved in the regulation of glucose metabolism by insulin. For example, HNF1 enhances the effect of insulin on the promoter of the G6Pase gene via interaction with an IRE (177). In addition, consensus sequences for HNF3 and HNF4 have been identified in the G6Pase promoter, although the functional implications with respect to the regulation of the promoter by insulin are unclear (206). As an aside, the HNF3 family of proteins has been renamed as the Foxa family. HNF3α, HNF3β, and HNF3γ have been renamed Foxa1, Foxa2, and Foxa3,

respectively (82). Knockout mice homozygous for a null mutation of HNF3 display a phenotype with a complex impairment of glucose metabolism including persistent hypoglycemia (83). Recently, there is increasing evidence for an involvement of HNF4 in the insulin-dependent regulation of hepatic gene expression. For example, HNF4 is involved in the PI 3-kinase/PKB-dependent stimulation of glucokinase gene expression by insulin, an important mechanism to increase glycolysis (159). On the molecular level, HNF4 may directly interact with Foxo1, and Foxo1 may act as an inhibitor of HNF4. In this setting, insulin stimulates HNF4 transcriptional activity by sequestering Foxo1 from HNF4 (70). However, although genetic defects of some HNF transcription factors (e.g., HNF1α, HNF4α) are the basis for some forms of maturity-onset diabetes of the young (MODY), the role of HNF transcription factors in the pathogenesis of Type 2 diabetes remains unclear.

2.2.5 Hepatic Glycogen Synthesis

Glycogen synthase, the rate-limiting enzyme in glycogen synthesis, is regulated through a complex cascade of protein kinases and phosphatases. The activity of glycogen synthase is determined by the phosphorylation state of the enzyme and is under hormonal control (30). The enzyme can be phosphorylated at multiple sites by more than 10 protein kinases (153) that in general inhibit enzyme activity (54). Insulin activates glycogen synthase by stimulating its dephosphorylation (43, 97, 98). An insulin-stimulated protein kinase has been shown *in vitro* to phosphorylate and activate PP1G (43), the glycogen-bound form of type-1 protein phosphatase. Glucosamine downregulates basal PP1 activity with greater potency than glucose, and both

glucosamine and high glucose significantly reduce insulin's ability to stimulate PP1 (35). Glycogen synthase activity may also be regulated by the addition of a single GlcNAc monosaccharide on serine/threonine residues (136, 137). Insulin also antagonizes the activation of glycogen phosphorylase through destruction of cAMP (78). Glycogen phosphorylase is not activated in the absence of glucagon, but the presence of insulin may keep the basal activity to a minimum.

Currently, probably the best-characterized substrate of PKB is the GSK-3, a critical enzyme regulating glycogen synthesis. There is abundant evidence that PKB-mediated inhibition of GSK-3 is the key mechanism through which insulin promotes glycogen synthesis. The major part of glucose taken up from the blood after insulin stimulation is stored as glycogen in skeletal muscle. Dysregulated glycogen synthesis is a critical feature in diabetes mellitus as glycogen synthesis rates in diabetic patients are approximately 50% lower than in healthy subjects (167). Under basal conditions, GSK-3 is constitutively active and phosphorylation of glycogen synthase by GSK-3 inhibits glycogen synthesis. The phosphorylation of GSK-3 by PKB results in inhibition of this kinase. Furthermore, expression of a GSK-3 mutant that is insensitive to phosphorylation by PKB results in a reduction of insulin-mediated glycogen synthesis (179).

Impaired hepatic glycogen storage and glycogen synthase activity is a common finding in insulin resistance (19, 37) and polymorphisms in the glycogen synthase gene have been described in insulin resistant patients. The most frequent mutations are the so-called *Xba*I mutations and Met416Val within intron 14 and exon 10, respectively. Currently, there are conflicting data on the correlation of these polymorphisms with insulin resistance and Type 2 diabetes mellitus (7, 62, 81, 152, 176).

2.2.6 Mutations Associated with Insulin Resistance

Although there is little doubt about the existence of a genetic component in Type 2 diabetes, the heterogeneity of the disease is a confounding factor for the interpretation of genetic studies. In general, two methods have been used for the study of genetic factors: the candidate gene approach and the genome-wide scan approach. The candidate gene approach examines genes with a rational role in the disease. The statistical association of a given allele and a phenotype (insulin resistance) is tested in unrelated individuals. The genome-wide scan or linkage approach locates genes through their genomic position. Family members sharing a specific phenotype will also share genetic markers surrounding the gene(s) involved.

Mutations found in candidate genes are listed first in Table 2.1, and relatively few mutations have strong evidence supporting the association thus far. A naturally occurring Ala1134Thr mutation in the insulin receptor resulted in markedly deficient insulin-stimulated phosphorylation (124). An Arg1174Gln mutation was discovered in the intracellular receptor β-subunit (123). A Met614Val mutation in IRS-1 was associated with insulin resistance (201). The Gly972Arg polymorphism in IRS-1 may have a weak association with Type 2 diabetes (134), although possibly through β-cell dysfunction rather than insulin resistance (141, 178). A Met326Ile mutation in PI3-K has some data in support of its association with insulin resistance, but the data are not currently definitive (15, 66). PKB/Akt was found to have a dominant negative missense mutation within the kinase domain (55).

Several different mutations have been described for glycogen synthase (7, 62, 81, 152, 176), but the associations with insulin resistance remain controversial. The most

Table 2.1. *Mutations in molecules that are reported to be associated with insulin resistance in humans.*

Molecule	Nature of the Mutation	Mechanism	Reference
IR	Ala1134Thr	Insulin signaling disruption	124
	Arg1174Gln (β subunit)		123
IRS-1	Met614Val	Insulin signaling disruption	201
	Gly972Arg		134, 141, 178
PI3-K	Met326Ile	Insulin signaling disruption	15, 66
PKB/Akt	Arg274His	Insulin signaling disruption	55
GS	Met416Val, Gln71His, Xba-mutation;	Altered glycogen storage	7, 62, 81, 152, 176
PPARG	Pro12Ala	Insulin resistance	102, 134
INS	Class III VNTR	β-cell dysfunction	134
KCJN11	Glu23Lys	β- or α-cell dysfunction	59
ABCC8	T761 (exon 18)	β-cell dysfunction	59
PPARGC-1	Ser482	Unclear, possibly pleiotropic	47
CAPN10	Intronic SNP43, G	Unclear, possibly pleiotropic	73
	Intronic SNP44, C		42, 50, 171, 195

VNTR = variable number tandem repeat;

robust single candidate variant is the highly prevalent Pro12Ala polymorphism in peroxisome proliferator-activated receptor γ (PPARγ) (102, 134). In this case, the alanine genotype results in greater insulin sensitivity (40, 47, 126). The Gly483Ser polymorphism in PGC1α, a transcriptional cofactor, might also be associated with Type 2 diabetes via as yet unknown mechanisms (47).

Among the many candidate genes for insulin secretory dysfunction, those encoding Sulfonylurea receptor 1 (SUR1) and Potassium-inward rectifier 6·2 (KIR6·2) have been most extensively studied. The two genes – ABBC8 and KCNJ11, respectively – are adjacent to one another on chromosome 11. There is insufficient evidence for association of two widely studied SUR1 polymorphisms (exon 16-3t/c, exon 18 T759T) with Type 2 diabetes (59). Meta-analyses on the Glu23Lys variant in the KIR6·2 gene are more robust, suggesting that the risk of Type 2 diabetes increased by about 15% for the Lys allele, probably through decreased insulin secretion (59).

Several findings from genome-wide scans have been replicated in multiple studies, but generally, positional cloning of the causative gene has not successful. The first diabetes gene cloned was CAPN10 on chromosome 2 (34, 73). It encodes for calpain-10, a cysteine protease, which is ubiquitously expressed (104, 180). Polymorphisms UCSNP-43 (73) and UCSNP-44 (42, 50, 171, 195) were found to be associated with Type 2 diabetes. Genetic variants might affect insulin sensitivity (8), reduced insulin secretion (175), or both (185).

A peculiar possibility is the relation of diabetes to imprinted genes, whose expression varies depending on the sex of the transmitting parent. The class III allele of the variable number tandem repeat near the insulin gene (chromosome 11p15) might

relate to Type 2 diabetes (133). The class III allele is associated with decreased amount of insulin mRNA. Only paternally transmitted class III alleles were found to be associated with diabetes in one study (76).

2.2.7 Current Therapies for Hepatic Insulin Resistance

The final piece of the diabetes puzzle is to take the knowledge of the biology and the pathophysiology and implement a therapeutic strategy. The major goal of Type 2 diabetes therapy is protecting patients from the long-term complications of the disease. Interventions are initially aimed at increasing tissue insulin sensitivity because insulin resistance plays such a fundamental role in the pathogenesis of Type 2 diabetes. Changes in diet and exercise habits can improve insulin sensitivity, and can be combined with drugs that further enhance insulin sensitivity. Figure 2.5 describes current therapies available and their sites of action. Only thiazolidinediones and metformin will be discussed below, as the scope will be limited to liver insulin resistance.

Drugs that enhance insulin sensitivity are primarily those of the thiazolidinediones (TZDs) class, which not only reduce glycemia, but also enhance vascular function and ameliorate the dyslipidemia and inflammatory milieu of Type 2 diabetes (210). TZDs affect liver insulin sensitivity in an indirect manner. They primarily activate PPARγ in adipose tissue and alter adipose metabolism and distribution. The redistribution of tissue triglyceride from visceral stores reduces levels of circulating FFA apparently by sequestration in a less lipolytic subcutaneous compartment (208). TZDs also reduce circulating concentrations of pro-inflammatory cytokines that promote insulin resistance (e.g., TNFα and interleukin 6) and at the same time increase

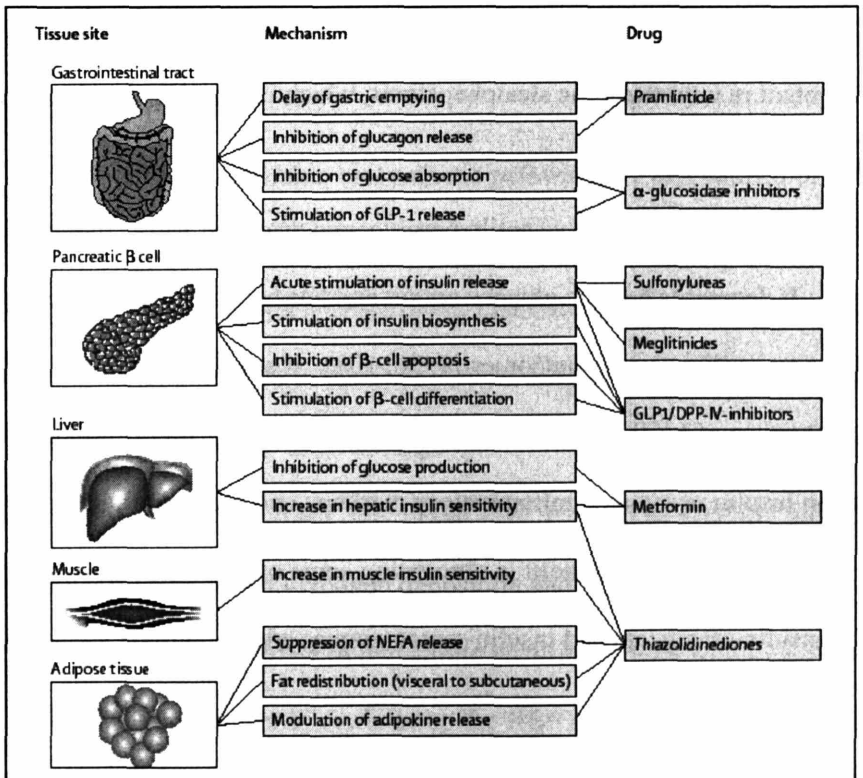

Figure 2.5. Pharmacological treatment of hyperglycemia according to site of action. GLP1 = glucagon-like peptide 1. DPP-IV = dipeptidyl peptidase IV.

concentrations of adiponectin, which has insulin-sensitizing and anti-inflammatory properties. The multiple effects of TZDs on adipose tissue metabolism and cross-talk of these signals with liver and skeletal muscle, as well as pancreatic β-cells and the vascular endothelium, might account for the enhancement of insulin action and improvement in insulin secretion with these agents, as well as several beneficial effects on vascular function (120). The action of the TZDs to redistribute visceral triglyceride can reduce hepatic lipid content in non-alcoholic steatohepatosis, which is closely related to obesity and insulin resistance (210).

Metformin is a highly effective antihyperglycemic drug that works independently of the pancreas. It decreases hepatic glucose output and has been shown to have a beneficial effect on cardiovascular outcomes (9, 36, 108). It acts through the recently discovered mechanism of LKB1 phosphorylation of AMPK (166). Metformin has less robust effects on insulin resistance, inflammatory markers, and vascular function compared with the TZDs, but its benefit in abrogating some of the weight gain commonly observed with insulin sensitizers and insulin secretagogues adds important value to this drug.

A potential new class of therapeutics inhibits fructose-1,6-bisphosphatase (FBPase) to control gluconeogenesis in Type 2 diabetes (49). Inhibition of this enzyme, which catalyzes the second-to-last step in gluconeogenesis, decreases gluconeogenesis while avoiding direct effects on glycogenolysis, glycolysis, and the tricarboxylic acid cycle. Furthermore, the near normal clinical profile of patients genetically deficient in FBPase who manage their diet and avoid prolonged fasting (56) suggests that FBPase inhibitors may exhibit an adequate safety margin.

2.3 Research Opportunities

In this background, we saw opportunities to contribute to the advancement of fields of functional genomics and Type 2 diabetes research. The correlation of metabolic flux to gene expression patterns was a novel method to discover more meaningful clusters of coregulated genes. The hepatoma system provided a platform that was amenable to rapid experiments.

The study of the hexosamine biosynthetic pathway as a mechanism of liver insulin resistance was complementary to the data in the literature for muscle and adipose tissue. The studies in muscle and adipose tissue concentrated on the insulin sensitivity of the glucose transporter system, and there was only a single publication examining glycogen deposition, which was done in adipocytes (114). This landscape offered an opportunity to break new ground not only in the liver, but also in studying the effect of modulating the HBP activity on glycogen deposition and glucose production. Our laboratory developed new expertise in metabolite profiling, which would allow us to examine the intracellular effects of modulating the HBP activity in a way that was novel to the field of hexosamine pathway study.

Finally, the intracellular flux maps allowed us to examine the control structure of the glucose production network in unprecedented detail and gain physiological insight into the determination of the glucose production phenotype, which is dysregulated in Type 2 diabetes. The stable isotope flux estimation expertise contained in the software Metran is unique to our laboratory, and allowed us to estimate the effect of systematic perturbations to the glucose production network.

Taken together, we felt that this work would be extremely novel and contribute greatly to the fields of functional genomics and Type 2 diabetes. With this context and these goals in mind, we moved forward to test our hypotheses.

3 Materials And Methods

3.1 Hepatoma Experiments

The following section pertains to materials and methods used in hepatoma experiments discussed in Chapter 4.

3.1.1 Cell Line and Culture Conditions

The mouse hepatoma line Hepa1-6 was obtained from the ATCC (Manassas, VA) and maintained in DMEM containing 25 mM glucose, 4 mM glutamine, and supplemented by 10% (vol/vol) fetal bovine serum (FBS) (Sigma, St. Louis, MO) and 1% (vol/vol) penicillin/streptomycin (PS) (Gibco). Confluent cells grown in this medium were used to investigate the effects of removing glutamine from the medium for 24 h followed by glutamine repletion to 4 mM and incubation for 24 h (Fig. 3.1). The transcriptional and metabolic activities of cells undergoing this 48-h glutamine depletion/repletion protocol were compared to control cells maintained in 4 mM glutamine for the entire 48 h. To reduce the unknown amount of hormones and endogenous lipids in the medium during the 48-h glutamine depletion/repletion, FBS was replaced with 10% Controlled Processed Serum Replacement 3 (CPSR3) (Sigma) in both the control and experimental samples. Metabolites and actinomycin D were obtained

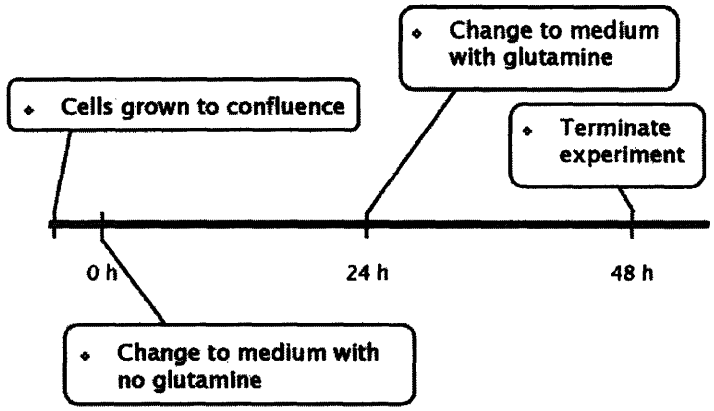

Figure 3.1. Incubation protocol for glutamine oscillations in hepatoma cells.

from Sigma. Stable isotopes were purchased from Isotec (Miamisburg, OH) and radioisotopes from American Radiolabeled Chemicals (St. Louis, MO).

3.1.2 Isotopic Metabolite Flux Assays

Isotopic metabolic flux assays were conducted at specified intervals across the 48-h glutamine depletion/repletion protocol. Fluxes were monitored as the release of labeled atoms from labeled glucose as it was metabolized, either $^{3}H_2O$ from ^{3}H-labeled glucose or $^{14}CO_2$ from ^{14}C-labeled glucose. The forward flux of hexose-phosphate isomerase was estimated from release of $^{3}H_2O$ from [2-^{3}H] glucose while the flux through the normally irreversible glycolytic step, phosphofructokinase, followed by triose-phosphate isomerase was estimated from release of $^{3}H_2O$ from [3-^{3}H] glucose. The flux through pyruvate dehydrogenase (PDH) was monitored by $^{14}CO_2$ production from [3,4-^{14}C] glucose. The oxidation of glucose in the TCA cycle was monitored by $^{14}CO_2$ production from [6-^{14}C] glucose. It should be noted that flux estimates using these labeled precursors supplied exogenously do not include flux of pre-existing intracellular metabolites through the same reactions. Modifications of the traditional versions of these assays (23) were developed to allow the assays to be performed in a higher throughput 96-well format and to limit the incubation time for the assays to 1 h. The absolute flux values of these assays varied between experiments, but were self-consistent within each experiment. The absolute flux values may not compared between experiments or between assays.

At specified intervals, the medium prescribed by the glutamine depletion/repletion protocol was removed from designated wells and replaced with isotope flux assay medium consisting of DMEM modified to contain 0.6 mM glucose and 1 mM glutamine.

In addition, each well contained 0.1 – 0.2 μCi of one ^{3}H- or ^{14}C-labeled glucose isotope at a specific activity of 0.8 to 1.6 Ci/mole. To quantify $^{3}H_2O$ production from ^{3}H-labeled glucose, the traditional assay using a borate resin to trap the labeled glycolytic compounds (46) was modified for use in a 96-well format. After a 1-h incubation with isotopes in the 96-well plate, the medium was removed and dispensed onto 0.4 ml of Dowex 1 × 400 borate resin (Sigma) in Spin-X centrifuge filter tubes (Costar). The tubes were agitated, incubated for 30 minutes, and centrifuged for 5 minutes at 5,000 rpm. The filtrate, which contained the $^{3}H_2O$, was quantified by liquid scintillation counting.

To allow for $^{14}CO_2$ collection, breakaway 96-well clusters (Costar) were used for the ^{14}C-glucose studies. To measure the $^{14}CO_2$ produced, individual wells were suspended in a 7 ml scintillation vial and gassed with 95/5 O_2/CO_2 immediately following addition of the ^{14}C-glucose the wells. The vial was then closed with a rubber septum cap and incubated for 1 h at 37°C. After the 1-h incubation, a syringe deposited ~20 μl of 30% perchloric acid through the septum into the well to terminate metabolic activity. A second syringe delivered 0.2 ml of hyamine hydroxide (ICN Pharmaceuticals, Costa Mesa, CA) to the bottom of the scintillation vial to absorb the CO_2. The trapped $^{14}CO_2$ was quantified by liquid scintillation counting.

3.1.3 ^{13}C Metabolite Pool Measurements

Metabolite pools were measured using a GC/MS method that included the addition of heavy ^{13}C-labeled internal standards at the time of cell lysis. The internal standards were heavy ^{13}C-labeled versions of each compound to be quantified. The area of each internal standard was compared to its naturally labeled counterpart. At the time

of the assay, metabolism was terminated with addition of 3 ml of 2% perchloric acid. The internal standards were added. Intracellular anions and cations were isolated by ion-exchange chromatography (203). These fractions were dried and derivatized with *N*-Methyl-*N*-[*tert*-butyldimethylsilyl]trifluoroacetamide + 1% *tert*-butyldimethylchlorosilane (MTBSTFA + 1% TBDMCS) (Pierce, Rockford, IL). Seventy microliters of MTBSTFA + 1% TBDMCS and 50 µl of dimethylformamide (DMF) (Pierce) were added to the dried sample. The sample was then capped, vortexed, and heated at 70°C for 30 min. The samples were analyzed with a Varian model Saturn 2000 GC/MS in electron ionization mode. One microliter of each sample was injected onto a 30 m CP-SIL 8 CB low bleed column (Varian, Walnut Creek, CA). The GC oven temperature was held at 140°C for 2 minutes after sample injection, before increasing it at a rate of 3°C/min to a final temperature of 250°C. This final temperature was held for 6.33 min for a total run time of 45 min.

3.1.4 ^3H_2O Lipogenesis Indicator Assay

Total lipid synthesis was estimated by the ^3H_2O incorporation method (103) using a protocol designed for cultured cells (22) and modified for a 1-h incubation. Cells in 6-well plates were incubated as prescribed by the glutamine depletion/repletion protocol. At 4-h intervals, the medium in individual wells was replaced with isotope flux assay medium containing 2-3 mCi ^3H_2O in 1.5 ml. The assay was terminated with 2% perchloric acid. Saponifiable lipids were extracted and quantified by liquid scintillation counting.

3.1.5 Isotopomer Spectral Analysis

Isotopomer Spectral Analysis (ISA) provides a method for quantifying the sources of carbon for *de novo* lipogenesis using stable isotope incorporation into products and analysis by nonlinear regression (87). As shown in Figure 3.2, a ^{13}C-labeled substrate (on all carbons) is introduced into the incubation. This substrate is metabolized to ^{13}C-labeled acetyl-CoA (on both carbons), which mixes with naturally labeled acetyl-CoA in the precursor pool. Eight units of acetyl-CoA are polymerized to form newly synthesized palmitate. The labeling pattern of the newly synthesized palmitate will reflect the percentage of acetyl-CoA that is ^{13}C-labeled, which we call D. Pre-existing palmitate in the cell mixes with this new palmitate. The labeling pattern of the pre-existing palmitate will reflect natural labeling of carbon, hydrogen, and oxygen. The mixed palmitate that we assay at a certain time point will yield a labeling pattern that reflects a weighted average of the newly synthesized and pre-existing labeling patterns. These weights reflect the percentage of palmitate that is newly synthesized, which we call g(t).

Unlike the 1-h radioisotope assays, ISA was performed over a 24-h period to estimate the overall effect of glutamine depletion on lipogenesis. Cells were preincubated for 24 h in media with 4 mM or 0 mM glutamine and then transferred to media containing one ^{13}C-labeled substrate for an additional 24 h. Control cells were evaluated in media containing 25 mM glucose and 4 mM glutamine with either [U-^{13}C] glucose (25 mM) or [U-^{13}C] glutamine (4 mM). This allowed estimation of the roles of both glucose and glutamine as lipogenic precursors. Glutamine-depleted cells were evaluated in media containing [U-^{13}C] glucose (25 mM). Following the 24-h incubation, the experiment was terminated with perchloric acid and cells were processed for ISA.

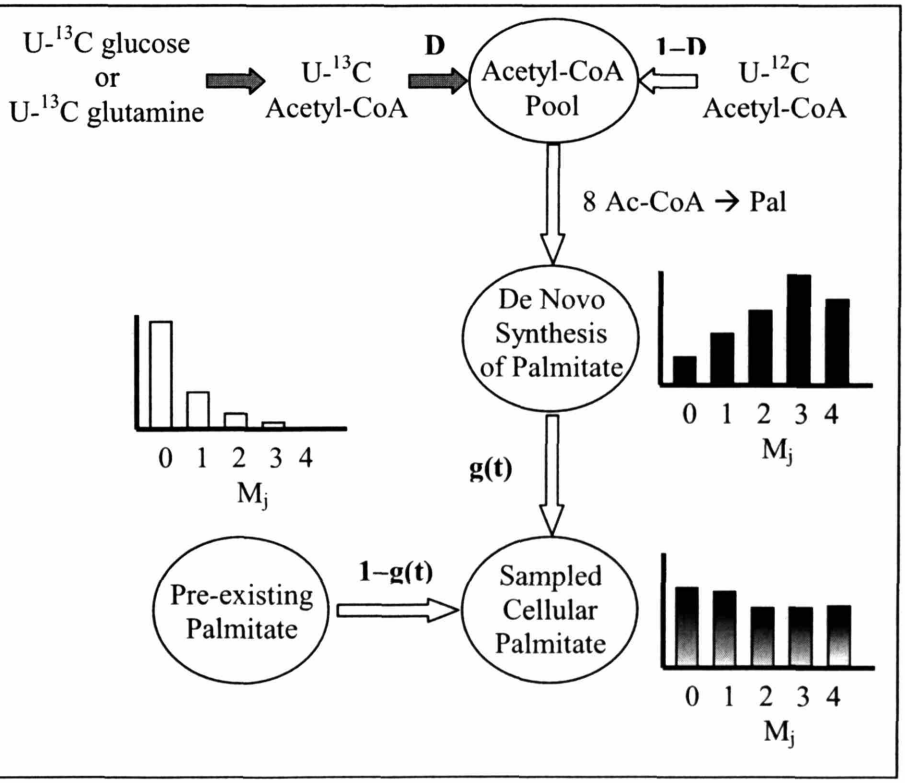

Figure 3.2. Isotopomer Spectral Analysis schematic. Labeled substrates are metabolized to acetyl-CoA and mix with natural acetyl-CoA. The acetyl-CoA is polymerized to newly synthesized palmitate, which mixes with pre-existing palmitate. Analysis with GC/MS measures the isotopomer distribution of the mixed palmitate pool.

Total lipids were extracted into 3:2 hexane:isopropanol (67), containing heptadecanoic acid (20 μg per well) as an internal standard for quantification of fatty acids. After solvent evaporation, the residue was treated with BF_3/MeOH (14%) to derivatize total fatty acids as methyl esters (72). Methyl esters were dissolved in DMF before analysis by GC/MS. Mass isotopomer analysis focused on palmitate to determine the ISA parameters D, the fractional contribution of the labeled substrate to the lipogenic acetyl-CoA, and g(24 h), the fraction of newly synthesized fatty acid present after 24 h.

3.1.6 DNA Microarray Experimental Protocol

Cells were seeded onto T25 flasks for the DNA microarrays and onto 96-well breakaway clusters for the hexose isomerase flux indicator assay. Data were taken at the following time points: 0.5, 12, 18, 24, 36, 39, and 48. At each time point, the cells were assayed for hexose isomerase flux and for mRNA expression. The protocols for the RNA extraction, labeling of probes, hybridization, and printing of arrays are listed at the Gene Expression Omnibus: http://www.ncbi.nlm.nih.gov/geo/query/acc.cgi, with the accession numbers GSE404, GPL285, and GSM5974 - GSM5993. The resulting data were downloaded and formatted in Excel (Microsoft, Redmond, WA), and then analyzed using Matlab (The MathWorks, Inc., Natick, MA). The DNA microarrays were performed with duplicate flasks of cells for each condition and each time point. Any unacceptable data points, flagged by scanning software were eliminated. The data in the duplicate arrays were then merged and averaged to create a union data set. Genes were retained in the union set only if data were available for each of the 7 time points. To capture genes with significant changes in gene expression, the data were filtered to eliminate genes that

did not have at least one time point with a log2 ratio greater than 0.6 or less than –0.6. These values were selected to insure 95% confidence for significant expression changes. Previous validation studies (not shown) demonstrated that the median coefficient of variation across duplicate arrays was 10.2%.

3.2 Hepatocyte Experiments

The following section pertains to materials and methods used in hepatocyte experiments discussed in Chapters 5 and 6.

3.2.1 Reagents and Materials

Bovine insulin, dexamethasone, glucagon, Dulbecco's modified Eagle's medium powder (DMEM), fetal bovine serum (FBS), and other cell culture reagents were purchased from Sigma (St. Louis, MO). [6-^{3}H] glucose was purchased from American Radiolabeled Chemicals (St. Louis, MO). Stable isotopes (D_2O, [U-^{13}C] glycerol) were purchased from Cambridge Isotope Laboratories (Andover, MA).

3.2.2 Animals

Male C57/BL6 mice were obtained from Taconic (Germantown, NY). Animals were housed in a facility approved by the American Association for Accreditation of Laboratory Animal Care. All animals received humane care in compliance with institutional guidelines. Mice had free access to water and chow *ad libitum* before the study. Mice were between 7 and 12 weeks old and 25-32 g body wt at their time of sacrifice.

3.2.3 Composition of Hepatocyte Medium Base

DMEM powder (Sigma) was supplemented with 3.7 g/L $NaHCO_3$, 30 mg/L proline, 100 mg/L ornithine, 610 mg/L niacinimide, 0.544 mg/L $ZnCl_2$, 0.75 mg/L $ZnSO_4 \cdot 7H_2O$, 0.2 mg/L $CuSO_4 \cdot 5H_2O$, 0.025 mg/L $MnSO_4$, 146 mg/L glutamine, 2 g/L bovine serum albumin, 100,000 units/L penicillin, and 100,000 μg/L streptomycin. The medium was sterilized by filtration through a 0.22 μm filter and stored at –20°C. Hormones, glucose, and fetal bovine serum were added to this base medium as specified by the incubation protocol.

3.2.4 Mouse Hepatocyte Isolation

Mouse hepatocytes were prepared for primary culture by nonrecirculating collagenase perfusion, as adapted from Seglen (165). In brief, the mouse was anesthetized with Avertin at a dose of approximately 0.025 ml Avertin/g body weight. The liver was initially infused with Ca^{2+}-free perfusion buffer and then dissociated with collagenase type IV (100 units/ml; Sigma). Isolated hepatocytes were scraped from the liver sac in preservation buffer. Hepatocytes were filtered through a 100 μm nylon mesh filter and then a 70 μm. The cell suspension was centrifuged at 50 × g, resuspended with 33% Percoll (GE Healthcare, Piscataway, NJ) and centrifuged at 50 × g. The pellet was resuspended in preservation buffer and centrifuged again at 50 × g. The resulting cell pellet was resuspended in Attachment medium, counted, and tested for viability using trypan blue exclusion. Cells were usually 85% to 90% viable.

3.2.5 Mouse Hepatocyte Culture

Primary mouse hepatocytes were seeded onto Type I collagen-coated tissue culture plates (BD Biosciences, Bedford, MA) in Attachment medium (Hepatocyte Medium Base supplemented with 1 nM insulin, 100 nM dexamethasone, 7% FBS, and 10 mM glucose). Glycogen synthesis experiments used 6-well plates with a density of 1.5×10^6 cells/well in 1.5 ml of Attachment medium. Glucose production and intracellular flux experiments used 12-well plates with a density of 6.1×10^5 cells/well in 600 µl of Attachment medium. Metabolite profiling experiments used T12.5 flasks with a density of 2.0×10^6 cells/flask in 2.0 ml of Attachment medium. The cells were allowed to attach for 1 h at 37°C in a humidified atmosphere containing 5% CO_2. Cells were then washed with PBS and given Maintenance medium (Hepatocyte Medium Base supplemented with 5 nM insulin, 100 nM dexamethasone, 7% FBS, and 20 mM glucose). 6-well plates received 1.0 ml/well, 12-well plates received 400 µl/well, and T12.5 flasks received 1.3 ml/well. After 24 h, cells were washed with PBS and given Preincubation medium (Hepatocyte Medium Base supplemented with 1 nM insulin, 100 nM dexamethasone, and 5 mM or 20 mM glucose). The medium volumes were identical to those given for Maintenance medium. Any modulators (glucosamine, azaserine, and alloxan) to be used were also added at this time. Cells were treated in the Preincubation medium for 16 to 18 h. For metabolite profiling experiments, a reference treatment of Preincubation medium with 1 mM glucose and no modulators was included.

3.2.6 Analysis of Glycogen Synthesis

After treatment in Preincubation medium, cells were incubated for 1 h in 1.0 ml of Glycogen Assay medium (Hepatocyte Medium Base supplemented with 25 nM or 0 nM insulin) (Fig. 3.3A). 5 mM glucose was then added to the Assay medium, spiked with 2 μCi [6-^{3}H] glucose (60 Ci/mmol), for a period of 2 h. The analysis of glycogen synthesis was adapted from Kaibori et al. (84). After 2 h, the experiment was terminated by aspirating the medium and washing the cells twice with ice-cold PBS. Cells were solubilized with 0.5 ml 30% KOH for 1.5 h. 0.4 ml of each sample was transferred to tubes and heated at 70°C for 20 min. 50 μl of glycogen carrier (25 mg/ml), 50 μl of saturated $NaSO_4$, and 1.4 ml of ethanol were added to the tubes. Samples were kept overnight at –20°C. Precipitated glycogen was centrifuged at 3,000*g* for 10 min. Pellets were resuspended in 0.4 ml water, heated at 70°C for 20 min, and reprecipitated with 1.5 ml ethanol. After 0.5 h at –20°C, precipitated glycogen was centrifuged at 3,000*g* for 10 min. Pellets were resuspended in 0.5 ml water and counted by scintillation counting.

The glycogen deposition data represent the flux of radiolabeled extracellular glucose to glycogen. The term "insulin sensitivity" was used during comparisons between treatments with insulin in the Assay medium. A change in sensitivity was considered significant if the difference between the glycogen deposited in the two insulin treatments was significant ($P < 0.05$).

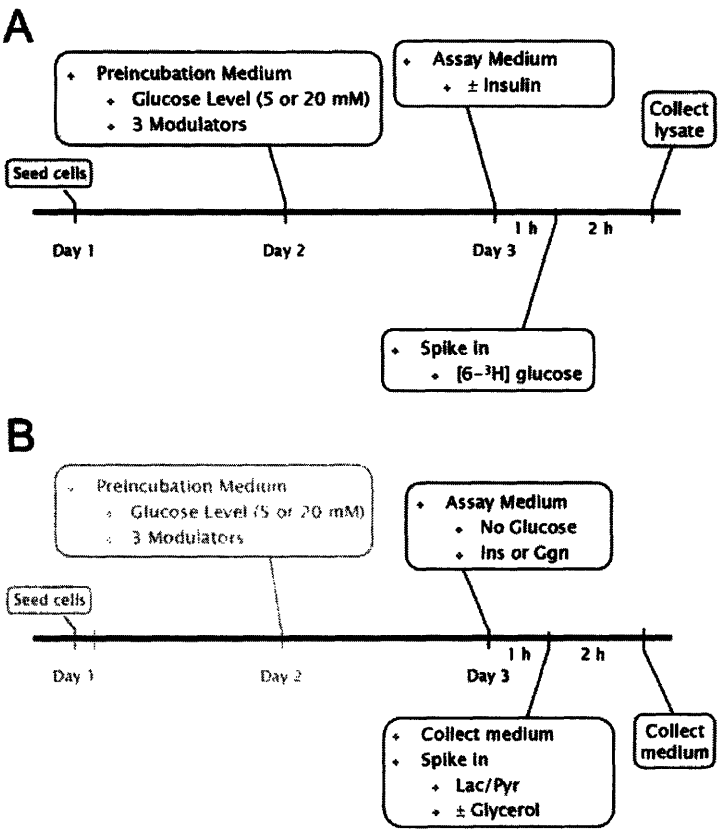

Figure 3.3. Protocols for analysis of glycogen synthesis (A) and analysis of glucose production (B). Both protocols are identical up to the completion of Day 2. On Day 3, different protocols are followed for the assay of glycogen synthesis and glucose production.

3.2.7 Analysis of Glucose Production

After treatment in Preincubation medium, cells were incubated for 1 h in 400 µl of Glucose Assay medium (Hepatocyte Medium Base supplemented with 10 nM glucagon, or 25 nM insulin) (Fig. 3.3B). At the end of the 1 h incubation (t = 0 h), 0.4 ml of medium were taken for analysis from a subset of samples treated with 25 nM insulin. The remaining samples then had 9 mM lactate/0.9 mM pyruvate, or 1.5 mM glycerol and 9 mM lactate/0.9 mM pyruvate added to their Assay medium, depending on the specific experiment. After a 2 h incubation (t = 2 h), 0.4 ml of medium were taken from each sample for analysis. Glucose and lactate concentrations were measured by a YSI 2700 Select glucose/lactate analyzer (YSI Inc., Yellow Springs, OH). The glucose measured at t = 0 h was subtracted from every sample measured at t = 2 h in order to eliminate any residual glucose from the Preincubation medium.

The term "insulin sensitivity" was used during comparisons between treatments with insulin in the Assay medium. A change in sensitivity was considered significant if the difference between the glucose produced in the two insulin treatments was significant ($P < 0.05$).

3.2.8 Metabolite Profiling

Immediately after treatment in Preincubation medium, the metabolites were isolated and analyzed with a method used by Fiehn et al. (53) (Fig. 3.4A). Briefly, the medium was removed and the cells were lysed with 0.7 ml methanol. An internal standard of ribitol was added at this time (4 µg/sample) to correct for sample loss and differences in derivatization efficiency between samples. Water (0.7 ml) was added to

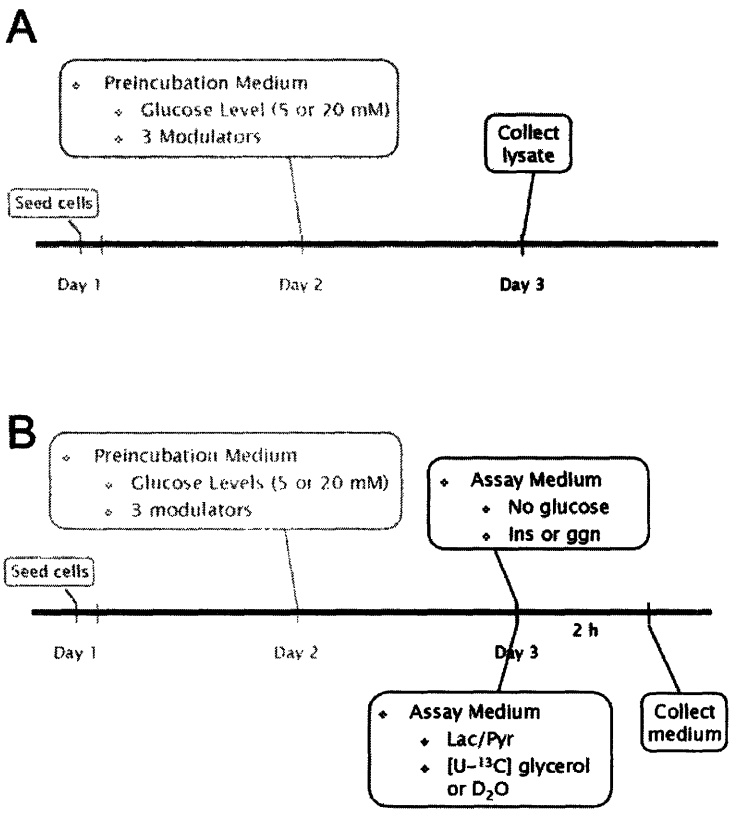

Figure 3.4. Protocols for metabolite profiling (A) and measurement of intracellular fluxes (B). Both protocols are identical up to the completion of Day 2. On Day 3, different protocols are followed for the assay of metabolite levels and intracellular fluxes.

the lysate and 0.38 ml chloroform was used to extract nonpolar metabolites. The remaining metabolites were dried in a vacufuge. To derivatize the metabolites, we added 50 µl of methoxyamine hydrochloride (20 mg/ml pyridine) to each sample and incubated for 90 min at 30°C. Then we added 80 µl of MSTFA + 1% TMCS (Pierce, Rockford, IL) to each sample and incubated at 37°C for 30 min. The samples were analyzed with a Varian model Saturn 2000 GC/MS in electron ionization mode. One microliter of sample was injected onto a 30-m CP-SIL 8 CB low-bleed column (Varian, Walnut Creek, CA). The GC oven temperature was held at a 70°C for 5 min after sample injection, before increasing at a rate of 5°C/min to a final temperature of 265°C. This final temperature was held for 1 min for a total run time of 45 min. During analysis of each sample, the area under the curve for each metabolite was normalized by the area of the ribitol peak for that sample to account for sample loss during processing. Each metabolite's normalized area was then divided by that metabolite's normalized area in the reference state (1 mM glucose, no modulators), which was run with every profiling experiment.

3.2.9 Stable Isotope Labeling of Glucose

After treatment in Preincubation medium, cells were treated for 2 h in 400 µl of Stable Isotope Assay medium (Hepatocyte Medium Base supplemented with 9 mM lactate, 0.9 mM pyruvate, and 10 nM glucagon or 25 nM insulin). In two different experiments, the Stable Isotope Assay medium was supplemented with 10% D_2O (no glycerol) and 1.5 mM [U-^{13}C] glycerol (Fig. 3.4B). At the end of the 2 h incubation, the medium from each sample was aspirated and stored at –20°C until analysis. This

protocol differs from the glucose production experiments in that there was no 1-h incubation period with the hormones.

3.2.10 Derivatization of Glucose

In both experiments, the samples were analyzed by quantifying the relative abundances of the isotopomers from several glucose fragments. To obtain as many glucose fragments as possible, we employed three different derivatization schemes to analyze the labeled glucose: aldonitrile pentapropionate, methyloxime pentapropionate, and di-O-isopropylidene propionate.

Briefly, the aldonitrile pentapropionate method was performed as follows. One hundred microliters of sample were mixed with 300 μl of cold acetone. The mixture was vortexed and then centrifuged at 14,000 rpm for 5 min. The supernatant was collected and then dried under airflow at 60°C. Fifty microliters of hydroxylamine hydrochloride in pyridine solution (20 mg/ml) were added to the sample, which was incubated at 90°C for 60 min. One hundred microliters of propionic anhydride were added to the sample, and the sample was incubated at 60°C for 30 min. The sample was dried under airflow at 60°C, and dissolved in 100 μl of ethyl acetate. The methyloxime pentapropionate method employed the same steps as listed for aldonitrile pentapropionate derivatization, except that a methylhydroxylamine hydrochloride in pyridine solution (20 mg/ml) was used instead of hydroxylamine hydrochloride solution.

Briefly, the di-O-isopropylidene propionate was performed as follows (64). One hundred microliters of sample were mixed with 300 μl of cold acetone. The mixture was

vortexed and then centrifuged at 14,000 rpm for 5 min. The supernatant was collected in screw-top glass tubes and then dried under airflow at 60°C. Five hundred microliters of 0.38 M sulfuric acid in acetone were added to the dried samples. The samples were vortexed and left at room temperature for 60 min. The reaction was stopped by adding 400 µl of 0.44 M sodium carbonate. Then 1 ml of saturated sodium chloride solution and 1 ml of ethyl acetate were added. The samples were vortexed for 15 seconds, and then left alone for phase separation. The top organic layer was collected in Eppendorf tubes, and dried under airflow at room temperature. One hundred and fifty microliters of propionic anhydride/pyridine solution (2:1 propionic anhydride/pyridine, v/v) were added to each sample, and the samples were incubated for 30 min at 60°C. The sample was dried under airflow at 60°C, and dissolved in 100 µl of ethyl acetate.

The D_2O samples were derivatized by the aldonitrile pentapropionate method and the methyloxime pentapropionate method. The [U-^{13}C] glycerol samples were derivatized by the aldonitrile pentapropionate and di-O-isopropylidene propionate methods.

3.2.11 GC/MS Analysis of Glucose

All samples were then analyzed on a Hewlett Packard 5890 Series II GC connected to a Hewlett Packard 5971 Series MS in electron ionization mode. One microliter of sample was injected onto a 60-m DB-XLB column (J & W Scientific, Folsum, CA). The GC oven temperature was held at 80°C for 1 min after sample

injection, before increasing at a rate of 20°C/min to a final temperature of 280°C. This final temperature was held for 4 min for a total run time of 15 min.

3.2.12 Analysis of GC/MS Data

The analysis of the D_2O data was as follows. The isotopic abundances were quantified for the fragment of glucose with the m/z ratio of 145 for the methyloxime method. The isotopomers quantified were 145-148 m/z. For the aldonitrile method, the isotopic abundances were quantified for the fragments of glucose with the m/z ratios of 173, 259, 284, and 370. The isotopomers quantified were 173-176, 259-263, 284-288, and 370-374 m/z.

The analysis of the [U-^{13}C] glycerol data was as follows. The aldonitrile pentapropionate method was analyzed differently from the D_2O data, and the isotopic abundances of glucose fragments 173 and 370 m/z were quantified. The isotopomers quantified for the 173 fragment were 173-178 and 370 to 377 m/z. For the di-O-isopropylidene propionate method, the isotopic abundances were quantified for the fragment of glucose with the m/z ratio of 301. The isotopomers quantified for the 301 fragment were 301-309 m/z.

3.2.13 Metabolic Network Model

The reactions in our gluconeogenesis model are shown in Figure 3.5. The network model contains two gluconeogenic precursors, i.e. oxaloacetate and glycerol. Oxaloacetate is the common intrahepatic precursor to glucose, which is first converted to phosphoenolpyruvate by the irreversible phosphoenolpyruvate carboxykinase (PEPCK).

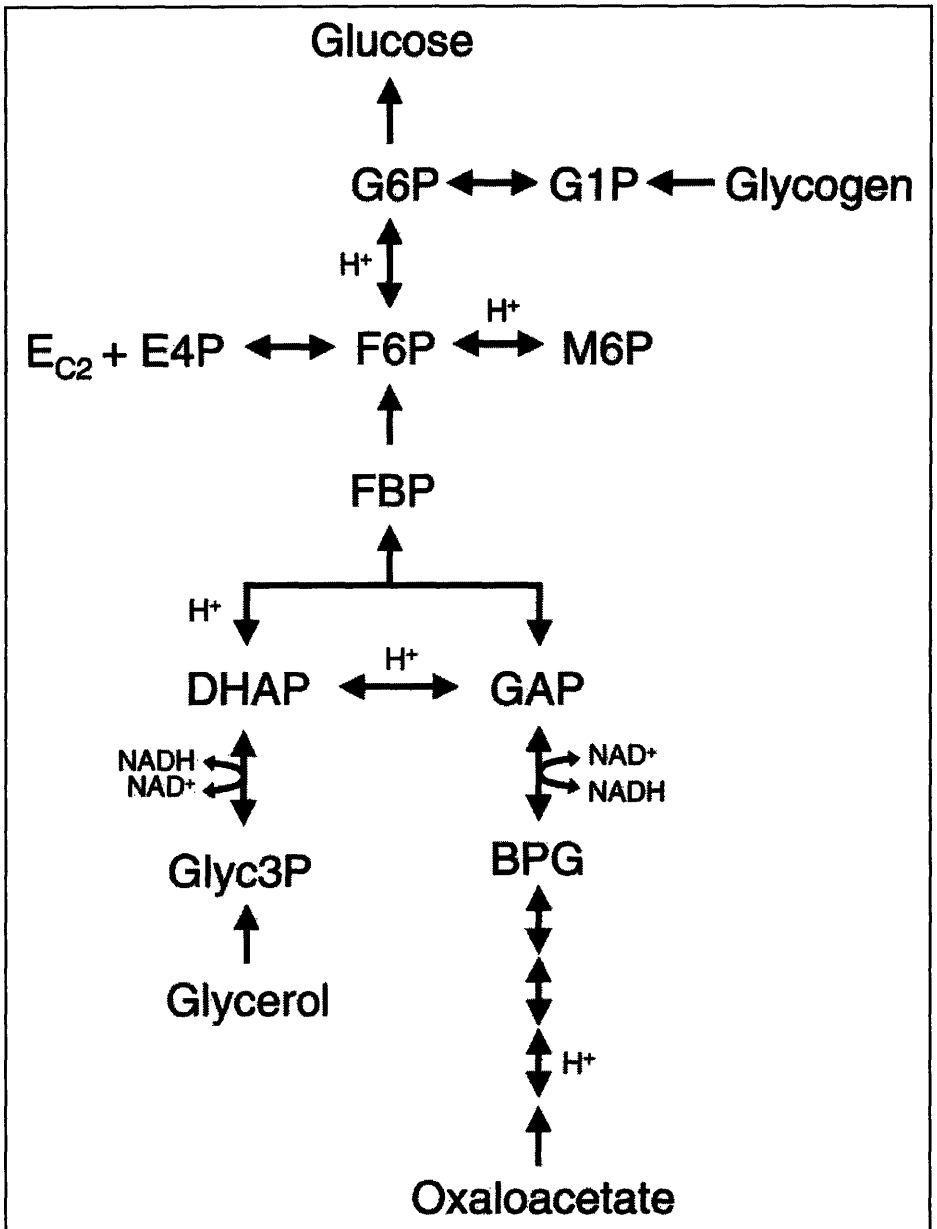

Figure 3.5. Metabolic network model for gluconeogenesis. This shows the full set of reactions used in the Metran calculations.

The PEPCK flux represents here the combined gluconeogenic contribution from lactate, pyruvate, glutamine, TCA cycle intermediates and related metabolites. We included glycerol's contribution to glucose explicitly in the model, allowing us to model isotope incorporation from glycerol to glucose. Glycerol is believed to contribute 10-30% to glucose production *in vivo* (96). Breakdown of endogenous glycogen, i.e. glycogenolysis, is an alternative pathway for glucose production in hepatocytes, and is modeled here by two reactions, i.e. phosphorylase and phosphoglucomutase. In our model, the reversibility of any reaction was assigned based on current knowledge. Many of the linear pathways in our model were lumped into single reactions, resulting in the flux map in Figure 6.1.

Furthermore, we assigned absolute stereochemistry to all reactions based on current knowledge. It has been long known that biochemical reactions are highly stereospecific (155), i.e. enzymes differentiate between prochiral hydrogen atoms and other prochiral groups. It is therefore important that we keep track of all prochiral hydrogen atoms in the model and assign stereospecific atom transitions for them. The absolute stereochemistry for many reactions has been worked out in detail. For example, it is known that phosphoglocose isomerase (PGI) abstracts specifically the pro-R hydrogen at C-1 of fructose 6-phosphate (F6P) (106, 107, 164) and transfers it to the C-2 position of glucose 6-phosphate (G6P), however, hydrogen exchange with the solvent is also observed in this conversion. Malaisse et al. reported for a single passage in the direction F6P $\rightarrow$ G6P, 65% intramolecular hydrogen transfer and 35% hydrogen exchange, and for a single passage in the direction G6P $\rightarrow$ F6P, 72% intramolecular hydrogen transfer and 28% hydrogen exchange. Triose phosphate isomerase (TPI) has the same stereochemistry as PGI. Phosphomannose isomerase (PMI), on the other hand, is

Table 3.1. Stoichiometry and atom transformations for gluconeogenesis model in Fig. 3.5.

No.	Enzyme	Stoichiometry	Atom transformations*
Upper gluconeogenesis			
1	glucose 6-phosphatase	G6P → Gluc	abcdef → abcdef
2	phosphoglucose isomerase	F6P + 0.3 H ↔ G6P + 0.3 H	abcdef ↔ abcdef
			(70%) C1-H^{proR} ↔ C2-H
			(30%) C1-H^{proR} + H ↔ H + C2-H
3	fructose 1,6-bisphosphatase	FBP → F6P	abcdef → abcdef
4	aldolase	DHAP + GAP ↔ FBP + H	abc + def ↔ cbadef
			(DHAP)C1-H^{proS} ↔ H
5	triose phosphate isomerase	DHAP + 0.3 H ↔ GAP + 0.3 H	abc ↔ abc
			(70%) C1-H^{proR} ↔ C2-H
			(30%) C1-H^{proR} + H ↔ H + C2-H
6	phosphomannose isomerase	F6P + H ↔ M6P + H	abcdef ↔ abcdef
			C1-H^{proS} + H ↔ H + C2-H
7	transketolase	F6P ↔ E-C2 + E4P	abcdef ↔ ab + cdef
Glycogenolysis			
8	phosphorylase	Glycogen → G1P	abcdef → abcdef
9	phosphoglucomutase	G1P ↔ G6P	abcdef ↔ abcdef

* For each compound carbon atoms are identified using lower case letters to represent successive carbon atoms of each compound.

Table 3.1 Continued. Stoichiometry and atom transformations for gluconeogenesis model in Fig. 3.5.

No.	Enzyme	Stoichiometry	Atom transformations*
Glycerol metabolism			
10	glycerol kinase	Glyc → Glyc3P	abc → abc
11	glycerol 3-phosphate dehydrogenase	Glyc3P ↔ DHAP + NADH	abc ↔ abc C2-H ↔ NADH
Lower gluconeogenesis			
12	glyceraldehyde 3-phosphate dehydrogenase	BPG + NADH ↔ GAP	abc ↔ abc NADH ↔ C1-H
13	phosphoglycerate kinase	3PG ↔ BPG	abc ↔ abc
14	phosphoglycerate mutase	2PG ↔ 3PG	abc ↔ abc
15	enolase	PEP + H ↔ 2PG	abc ↔ abc H ↔ C2-H
16	phosphoenolpyruvate carboxykinase	OAC → PEP + CO2	abcd → abc + d
Hydrogen incorporation into oxaloacetate and NADH from endogenous sources			
17		OAC + H → OAC + H	abcd → abcd C3-H^{proS} + H ↔ H + C3-H^{proS}
18		OAC + H → OAC + H	abcd → abcd C3-H^{proR} + H ↔ H + C3-H^{proR}
19		H → NADH	H → NADH
20		unlabeled → NADH	$H^{unlabeled}$ → NADH
21		NADH → other	NADH → H^{other}

* For each compound carbon atoms are identified using lower case letters to represent successive carbon atoms of each compound.

known to have the opposite stereochemistry, i.e. PMI specifically abstracts the pro-S hydrogen. Furthermore, no intramolecular hydrogen transfer has been observed for this reaction, and thus the hydrogen at C-2 of mannose 6-phosphate (M6P) always originates from the medium. Table 3.1 summarizes the assumed stereochemistry for all reactions in our model.

3.2.14 Estimation of Intracellular Fluxes

Metabolic fluxes and their confidence intervals were determined by simultaneous fitting of mass isotopomer abundances of glucose fragments to a detailed metabolic network model of hepatocytes using the software Metran (Maciek Antoniewicz, manuscript submitted). In short, Metran estimates fluxes by minimizing the difference between the observed and simulated measurements using an iterative least-squares minimization procedure. The objective of this routine is to evaluate a set of feasible fluxes that best accounts for the observed isotopomer and extracellular flux measurements. After metabolic fluxes were calculated, statistical analysis was automatically performed to obtain accurate standard deviations and 95% confidence intervals of fluxes by evaluating the sensitivity of the objective function with respect to fluxes as described in (Maciek Antoniewicz, manuscript submitted). Flux validation was accomplished by a statistical test for the goodness-of-fit based on the chi-square test for model adequacy (Maciek Antoniewicz, manuscript submitted). To ensure a global solution, flux estimation was repeated at least four times starting with random initial values. All computations were performed with Matlab 6.5 using Matlab Optimization Toolbox (Mathworks Inc.).

3.2.15 Statistics

Glycogen deposition and glucose production data were analyzed using a Student's *t* test (Microsoft Excel) to compare the means from experimental groups. $P < 0.05$ was considered statistically significant. In cases where multiple groups were all compared to a single group, the Dunnett's test for multiple comparisons was applied (57).

Besides fluxes, Metran also generates the standard deviations for the relative intracellular fluxes estimated. The standard deviation of the absolute intracellular flux (c) was calculated by combining the standard deviation of the relative intracellular flux (b) and the glucose production measurement (a) according to the following equation:

$$c = C\sqrt{\left(\frac{a}{A}\right)^2 + \left(\frac{b}{B}\right)^2}$$

where $(A \pm a) \times (B \pm b) / 100 = (C \pm c)$ and $A \times B / 100 = C$.

The correlational analysis of the absolute intracellular flux maps examined the possible relationship of glucose production to each absolute intracellular flux. Each data set consisted of 32 pairs of data each comprising an intracellular flux along with the corresponding glucose production for the various conditions examined. The exception was the glycerol uptake flux (flux 3 in Fig. 6.1), for which only 16 pairs of data were obtained. A weighted linear regression was performed for each glucose production-intracellular flux pairing using all the data points for each of the 5 intracellular fluxes as independent variables and the glucose production as the dependent variable, as shown by Press et al. (145). The data points were weighted by the standard deviations in the glucose production, which had an average coefficient of variation (COV) of 10.3%. The error in the absolute intracellular fluxes was ignored because the average COV in the

relative flux data was 2.1%. The standard deviations for the slope and the intercept of the best-fit line were also calculated.

Once the best-fit line for each flux/glucose production combination was found, we tested the hypothesis that breaking the data into two different groups would lower the weighted sum of squared residuals significantly. The groupings were chosen according to glucose level in the Preincubation medium, insulin or glucagon treatment in the Assay medium, and presence of glycerol in the Assay medium. We did not break the data into smaller groups because we felt the sample size for regression would be too small. To accept the two-group regression over the single-group regression, the following criterion had to be fulfilled for both subgroups:

$$\frac{SS_{all}}{SS_{subgroup}} \geq F(df_{num}, df_{denom}, 0.95)$$

where SS_{all} is the weighted sum of squared residuals for the regression with all the data points, $SS_{subgroup}$ is the weighted sum of squared residuals for the regression with the subgroup, and F is the F-statistic for the degrees of freedom specified in the numerator (df_{num}) and denominator (df_{denom}) and a confidence interval of 95%. The df_{num} was 30 because there were 32 data points and 2 parameters in the linear regression. The df_{denom} was 14 because there were 16 data points and 2 parameters in the linear regression. For these parameters, the F-statistic was 2.31. Therefore, when the data set of 32 points was broken into two sets of 16 data points, the decrease in the weighted sum of squared residuals was required to be a factor of 2.31 for both data sets in order to accept the two-group regression over the single group regression. The R^2 metric for each best-fit line was calculated as follows:

$$R^2 = 1 - \frac{SS_{res}}{SS_{total}}$$

where $SS_{res} = SS_{subgroup} = SS_{all}$ was the weighted sum of squared residuals calculated from the observed data to the regression line and SS_{total} was the weighted sum of squared residuals calculated from the observed data to a horizontal line situated at the mean of the dependent variable values.

Appendix

Hepatocyte Media Formulation

Block et al., J Cell Biol (1996) 132(6):1133-1149

This medium is DMEM powder base with sodium bicarbonate added. Then more components are added to make it more like Williams Medium E.

Base Medium

DMEM, no glucose, no sodium pyruvate, no glutamine, no phenol red; Sigma D-5030;

Stock Solutions

1. 200 g/L L-Ornithine. 50 ml ddH_2O, 10 g L-Ornithine (Sigma O-6503). 0.5 ml aliquot.
2. 305 g/L Niacinimide. 200 ml ddH_2O, 61 g Niacinimide (Sigma N-0636). 1 ml aliquot.
3. Trace Metals solution

    1.088 g/L $ZnCl_2$ → 0.0544 g $ZnCl_2$ (Sigma Z-0152)
    1.500 g/L $ZnSO_4 \cdot 7H_2O$ → 0.075 g $ZnSO_4 \cdot 7H_2O$ (Sigma Z-0251)
    0.400 g/L $CuSO_4 \cdot 5H_2O$ → 0.020 g $CuSO_4 \cdot 5H_2O$ (Sigma C-8027)
    0.050 g/L $MnSO_4$ → 0.0025 g $MnSO_4$ (Sigma M-7634)

    Dissolve in 50 ml 1× PBS. 0.5 ml aliquot.
4. Aliquot Penicillin/Streptomycin into 10 ml aliquots (Sigma P-0781).
5. 2 μM Bovine Insulin. Weigh out 10 mg insulin (Sigma I-6634). Add 1.5 ml sterile water. Add glacial acetic acid until insulin dissolves (~ 140 μl). Add more water to make the volume 2 ml. Add the 2 ml to 85.2 ml water to make a 20 μM solution. Dilute 4 ml of that solution in 36 ml water to make 2 μM solution. 1 ml aliquot.
6. 0.127 mM Dexamethasone. Dissolve 1 mg dexamethasone (Sigma D-8893) in 1 ml ethanol using sterile syringe and needle. After powder is dissolved, add 19 ml PBS, mix thoroughly. 800 μl aliquot. Expires 3 months from date of reconstitution.

Formulate 0 mM glucose Hepatocyte Growth Medium Base

1. Add 680 ml of ddH_2O to 1 bottle of powdered DMEM base (Sigma D-5030).
2. While stirring the DMEM base solution, add 3.7 g of sodium bicarbonate.
3. Add stock solutions:

    0.5 ml of 60 g/L L-Proline
    0.5 ml of 200 g/L L-Ornithine
    2.0 ml of 305 g/L Niacinimide
    0.5 ml of Trace Metals solution
4. Add 0.146 g Glutamine (Sigma G-8540).
5. Add 2 g Bovine Serum Albumin (Sigma A-9647).
6. Add 10 ml Penicillin/Streptomycin.
7. Adjust medium pH to 7.35 with 10 M HCl.
8. Sterile filter the medium and dispense 40 ml aliquots. Store at –20°C.
9. Add components according to media spreadsheet.

Collagen Coating Protocol

1) Dilute Type I collagen with 0.1% acetic acid to 200 μg/ml. Sterile filter. Start with 100% acetic acid. Dilute 200 μl in 200 ml ddH_2O.
2) Dispense into tissue culture dishes 40 μL/cm^2.

6-well plate	9.61 cm^2	384.4 μl	~ 400 μl
12-well plate	3.8 cm^2	152 μl	~ 150 μl
24-well plate	2.0 cm^2	80.0 μl	~ 75 μl
96-well plate	0.32 cm^2	12.8 μl	~ 30 μl (to cover well)
35 mm dish	9.62 cm^2	384.8 μl	~ 400 μl
60 mm dish	28.27 cm^2	1,130.8 μl	~ 1200 μl
T12.5 flask	12.5 cm^2	500 μl	~ 500 μl
T25 flask	25 cm^2	1000 μl	~ 1000 μl

3) Shake the plates to ensure full coverage of all wells.
4) Shake plates again to ensure coverage. Aspirate any extra liquid.
5) Air-dry dishes at RT in the biosafety cabinet overnight (no UV).
6) When dry, seal dishes in plastic bags and store at RT. Good for 3 months.

This procedure gives a coating of about 4-8 μg collagen/cm^2.

Cell Attachment and Preincubation Protocol

1) Seed cells on type I collagen-coated substrates in correct volume of Attachment Medium (1.5 × the correct amount for flask/plate).

T25 flask	4.0×10^6 cells	2.65 ml ~ 4.0 ml
T12.5 flask	2.0×10^6 cells	1.32 ml ~ 2.0 ml
6-well plate	1.5×10^6 cells	1.02 ml ~ 1.5 ml
12-well plate	6.1×10^5 cells	403 μl ~ 600 μl
24-well plate	3.2×10^5 cells	187 μl ~ 300 μl
96-well plate	5.1×10^4 cells	34 μl ~ 60 μl

2) Wait 40-60 minutes, and then aspirate medium.
3) Wash with PBS.
4) Dispense specified amount of Maintenance Medium and incubate overnight.

T25 flask	4.0×10^6 cells	2.65 ml ~ 2.6 ml
T12.5 flask	2.0×10^6 cells	1.32 ml ~ 1.3 ml
6-well plate	1.5×10^6 cells	1.02 ml ~ 1.0 ml
12-well plate	6.1×10^5 cells	403 μl ~ 400 μl
24-well plate	3.2×10^5 cells	187 μl ~ 200 μl
96-well plate	5.1×10^4 cells	34 μl ~ 40 μl

GC/MS Compound List with TMS derivatization

	Compound	*Pure*	*Extract*	*Ions*
1	Pyruvate	5.67	5.48	158, **174**, 189
2	Lactate	5.76	5.63	147, **191**, 219, 234
3	Alanine	6.79	6.83	147, 174, **190**, 218, 233
4	Butanoic Acid		8.75	147, 191, **233**
5	Valine	10.31	10.32	147, 203, **218**, 24, 262
6	Urea		11.67	147, **189**
7	Leucine		12.18	147, 158, **232**, 275
8	Proline	12.69	12.69	147, 170, **216**, 244, 260
9	Isoleucine		12.75	73, **158**, 218, 232, 260, 275
10	Glycine		13.05	147, 174, 211, **248**, 276, 291
11	Succinate*	13.58	13.53	147, 226, **247**
12	Fumarate*	14.66	14.62	147, 217, **245**, 324
13	Serine		14.85	147, 188, 204, **218**, 278, 306, 321
14	Threonine		15.53	147, 218, **291**, 335
15	β-Alanine		16.55	147, 174, **248**, 290, 305
16	Oxaloacetate	17.76		147, 202, 230, 261, 290, 378, 452
17	Malate*	18.39	18.37	233, 265, 307, **335**, 423
18	Methionine		18.89	128, **176**, 219, 250, 293
19	Glutamine	18.92	18.92	147, 156, **230**, 258, 346
20	Aspartate		19.14	147, 188, **232**, 306, 334, 349
21	Cysteine		19.88	147, 218, **220**, 294, 322, 337
22	α-Ketoglutarate*	20.60	20.55	147, 170, **198**, 288, 304, 320
23	Asparagin	20.95		147, **188**, 216, 305, 331, 405, 420
24	PEP*	21.12	21.06	147, 211, 299, **369**, 384
25	Phenylalanine		21.43	147, 192, **218**, 266, 294, 309
26	Glutamate	21.49	21.50	156, 230, **246**, 348, 363
27	Gluconate		22.19	147, 204, 291, 420, 583
28	Asparagine	22.62		147, 188, **231**, 258, 333, 348
29	Ribitol*	23.93	23.92	147, 217, 243, **319**, 395, 422
30	G3P	24.00	24.09	147, **211**, 253, 299, 328, 341, 384, 400, 415
31	Glucose-1P*	24.84, 28.38, 35.25	24.84	**217**, 232, 305, 450
32	UDP-Glucose*	24.84, 28.38	24.84	**217**, 232, 305, 450
33	Ornithine		25.79	174, 187, 200, 216, 258, 315, 330, **420**
34	3PG	25.87	25.80	147, 227, 299, 357, **387**, 431, 459, 474
35	GlucN-1P	25.9	25.9	172, 189, **217**, 232, 316, 434, 450
36	Citrate*	26.05	26.02	273, 309, 347, **375**, 436, 465
37	UDP-GlcNAc*	26.15	26.14	147, 173, 203, 217, 299, **329**, 404, 420
38	GlcNAc-1P*	26.15	26.14	147, 173, 203, 217, 299, **329**, 404, 420
39	Fructose	27.35	27.04, 27.25	217, **307**, 364
40	Glucose	27.68	27.61	157, 217, 274, 291, **319**, 374, 415, 464
41	Lysine	27.96	28.00	**156**, 174, 230, 329, 419, 434
42	Gluconic Acid		28.70	147, 205, 217, 292, 333, 433
43	Glucosamine	28.26, 28.44		205, 242, 273, 291, 304, **319**, 357, 447
44	Tyrosine		28.39	147, 179, **218**, 280, 330, 354
45	Myoinositol		29.80	189, 221, 255, **318**, 345, 362
46	Inositol		30.21	147, 217, **318**, 393, 432
47	GlucNAc*	31.0, 31.09	31.11	147, 171, 202, 243, 274, **319**, 333, 359, 417
48	Ribose-5P	31.73	31.79	217, 299, **315**, 357, 403, 459, 604, 619

49	Ribulose-5P	32.07	32.07	147, 217, 275, 299, 315, **357**, 387, 604, 619
50	Tryptophan		33.43	202, 218, **291**
51	Inositol-P		34.45	318, 434
52	Fructose-6P*	35.23	35.31	217, 299, **315**, 357, 373, 387, 403, 433, 459
53	Glucose-6P*	35.45, 35.70	35.51, 35.67	147, 191, 217, 299, 357, **387**, 721
54	GlucN-6P*	36.0, 36.07	36.12	195, 217, 241, 285, 299, 315, **387**, 403, 429
55	6P-Gluconate	37.04	36.93	217, 244, 271, 299, 315, 333, 357, **387**, 461
56	GlcNAc-6P*	37.73, 37.96, 38.33	37.73, 37.96, 38.33	299, 315, 357, **387**, 404, 433, 459

Mouse Hepatocyte Isolation Protocol (Developed by Matthew Wong)

The 2-step collagenase perfusion procedure by Seglen (Seglen, 1976), either *in situ* or *ex vivo*, is recommended. Blanching of the liver should be almost complete within a few seconds of perfusing with the first buffer. Otherwise, the liver should be discarded. For mouse, the perfusion times should be 15 minutes with the first buffer and 10 minutes with the second buffer should be enough. The liver should be swollen and sufficiently softened. The temperature of the liver should be maintained at 37°C throughout the perfusion. After excision of the liver, the cell suspension should be kept at 0–4°C until the cells are seeded in culture. A minimum viability of 85% and a minimum yield of at least 1.5 x 10^6 cells/gram mouse is recommended. Avertin can be used for anesthesia.

A good reference is:
Pertoft H. and Smedsrod B. 1987. Separation and Characterization of Liver Cells, in: Cell Separation: Methods and Selected Applications, vol. 4, Academic Press.

Solutions:

Perfusion Buffer Concentrate (PBC)

1) Make 300 ml of 1 M NaOH (12 g NaOH).
2) Dissolve NaCl (103.75 g), KCl (6.25 g), and HEPES (28.7 g) in H_2O (350 ml) while stirring. When all have been dissolved, add 75 ml of 1 M NaOH. Add H_2O to a total volume of 500 ml.
3) Sterile filter (0.2 μm) the solution and divide into 20 ml portions.

Collagenase Buffer Concentrate (CBC)

1) Solution A: dissolve HEPES (72 g), NaCl (12 g), and KCl (1.5 g) in 1 M NaOH (198 ml).
2) Solution B: dissolve $CaCl_2 \cdot 2H_2O$ (2.1 g) in H_2O to a total volume of 30 ml.
3) Mix solution A and B while stirring. Be careful to add B drop by drop.
4) Add H_2O to a total volume of 300 ml.
5) Sterile filter (0.2 μm) and freeze the solution in portions of 20 ml.

Avertin Stock Solution

1) Mix 1 g tribromoethanol (Sigma #90710) with 0.63 ml Tert amyl alcohol (Sigma #24048-6).
2) Store stock in a dark glass container with no plastics in the cover at 4°C for up to a year. Avertin can dissolve some plastics.

1) Preparation 1 day before

- Autoclave 1 L of ddH_2O for 30 minutes fluid at 121°C.
- Autoclave surgical tools, a slotted incubator shelf, two 250 ml Pyrex bottles, and a 1 L Pyrex bottle for 30 minutes with 40 of dry time at 121°C.

2) Preparation on the day of isolation

- Thaw 1 tube of PBC (20 ml) and 1 tube of CBC (20 ml).

- Go get 2 mice.
- Perfusion buffer: add 480 ml sterile ddH_2O to 20 ml of PBC. Pour 250 ml into sterile bottle. Add 0.5 ml of 0.5 M EDTA for final concentration of 1 mM EDTA.
- Preservation buffer: mix 250 ml of perfusion buffer with 675 mg glucose (15 mM) and 2.5 g BSA. Let BSA dissolve for 5-10 minutes with occasional mixing.
- Collagenase buffer: add 180 ml ddH_2O for a total volume of 200 ml. Add 20,000 units of collagenase enzyme activity.
- Percoll solution: Add 1.3 ml of 10× Hank's Buffered Saline Solution to 11.7 ml of Percoll.
- Check pH of all four solutions and adjust to pH 7.4 with 10 M HCl or 5 M NaOH.
- Sterile filter all solutions except the Percoll and dispense into sterile bottles.
- Dilute 24 µl Avertin stock in a polypropylene tube with 2.0 ml sterile water.
- Run 10 ml 70% EtOH through perfusion apparatus to waste at 1 ml/min.
- Empty tubing by letting air pass through for 5 minutes.
- Run 20 ml sterile ddH_2O through perfusion apparatus to waste at 1 ml/min.
- Empty tubing by letting air pass through for 5 minutes.
- Prepare the sterile hood with a petri dish, cell filters, cell lifter, and three 50 ml tubes.
- Prepare waste basin, incubator shelf, tools, and magnifying glass.
- Prewarm perfusion buffer in 40°C bath and let the buffer circulate at 1ml/min.
- Prewarm the collagenase buffer as well.
- Pipet 25 ml preservation buffer into 100 mm Petri dish. Keep dish and bottle of preservation buffer on ice.

3) Anesthesia

- The animal should not be excessively distressed prior to anesthetization. Get the animal from its cage, place into chamber, and weigh the animal.
- Bring the animal (in the chamber) over to the hood. Put a dash of Halothane onto a piece of gauze and place it in the chamber with the animal. Close the chamber. Allow the animal to succumb to the anesthesia and lay still for 5 seconds. Quickly remove the animal from the chamber and administer general anesthetic.
- The general anesthetic administered is tribromoethanol (Avertin). Use 0.025 ml/gm + 0.05 ml. Inject into the IP cavity with an insulin syringe at a 45° angle.

22.8 g = 0.62 ml	26.4 g = 0.71 ml	30.0 g = 0.80 ml
23.2 g = 0.63 ml	26.8 g = 0.72 ml	30.4 g = 0.81 ml
23.6 g = 0.64 ml	27.2 g = 0.73 ml	30.8 g = 0.82 ml
24.0 g = 0.65 ml	27.4 g = 0.74 ml	31.2 g = 0.83 ml
24.4 g = 0.66 ml	28.0 g = 0.75 ml	31.6 g = 0.84 ml
24.8 g = 0.67 ml	28.4 g = 0.76 ml	32.0 g = 0.85 ml
25.2 g = 0.68 ml	28.8 g = 0.77 ml	32.4 g = 0.86 ml
25.6 g = 0.69 ml	29.2 g = 0.78 ml	32.8 g = 0.87 ml
26.0 g = 0.70 ml	29.6 g = 0.79 ml	33.2 g = 0.88 ml

- Place the animal on hood surface. Allow the animal up to 2 minutes to become anesthetized. Observe the animal during this period. Good anesthesia will be effected in most animals. Some may require more. If by 2 minutes the anesthesia is not sufficient, administer an extra 0.05 or 0.10 ml of Avertin.
- Make sure that the animal's breathing stays strong (1 breath/sec), and that the extremities and the nose remain pink. If the animal stops breathing, gentle chest compressions often will produce a sound rhythm. Perform anesthesia with the second animal.
- Place the animals in the supine position. Extend the extremities. They should move without significant resistance. The foot may be squeezed. Absence of reflex, including respiratory spasm, indicates good anesthesia.
- The animals may now be moved to the operating area. Place them in the supine position. The extremities are extended away from the body, and secured to the table with tape. Check the right rear leg reflex.
- Spray the abdomens with 70% ethanol and wipe to prep surgical area.

4) Surgical procedure (laparatomy)

- Grasp the skin of the upper right quadrant of the animal with rat-tooth tweezers, and retract gently upwards. Identify the xiphoid process and the beginning of the pubic bone.
- An incision is made through the skin, immediately inferior to the xiphoid process to superior to the pubic bone. Take care to minimize trauma to the abdominal muscle.
- Use the scissors and divide the abdominal muscle along the midline from the pubic bone to the xiphoid process.
- Make two incisions laterally from the midpoint of the abdomen down to the operating table.
- Using a fine-nosed hemostat, grasp the free corner of one of the abdominal flaps, lock the hemostat, and lay the hemostat on the table to retract the flap away from the body. Repeat with the remaining 3 flaps.
- At this point, if the anesthesia appears insufficient, as evidenced by rapid breathing or muscular movement, spray the remainder of the injection over the viscera. If needed, use the second injection, again in doses.

5) Surgical procedure – Cannulation

- Use a sterile cotton-tipped swab to displace the intestines to the animal's left side.
- Divide ligaments connecting the large right lobe to the stomach, the small bottom left lobe to the IVC, and the small right lobe to the stomach.
- Move the mouse under the magnifying glass for the best view.
- Cannulate the portal vein with the needle and carefully push the catheter/needle into the vein. Remove the needle. Do the cannulation as far away from the liver as possible so as not to push the catheter into the liver. Allow the catheter to fill with blood.

- With the pump on (7 ml/min), carefully measure the length/angle of tubing needed. Tape the tubing to the incubator shelf to secure it, and insert tubing into catheter. The liver swells and blanches. As soon as possible, cut the IVC to let buffer out. The liver should now blanch completely. Cut the diaphragm, and the mouse will die.
- Occlude the IVC with an applicator for ~ 5 seconds and allow the liver to swell moderately. Repeat 2 more times. Continue perfusion for 15 minutes.
- Move the tube to the collagenase buffer. Wait for 1 minute. Occlude the IVC with an applicator for ~ 5 seconds and allow the liver to swell. Repeat 2 more times. Perfuse for 10 minutes.
- As the perfusion nears 8 minutes, remove the gall bladder carefully. Also, divide the ligaments that connect the liver to the diaphragm. Be careful not to sever the IVC.

6) Surgical procedure – Dissection
- Take out catheter and stop the pump. Note the time.
- Tilt the lobes up and grab the white fibrous connective tissue with the forceps. Cut the portal vein connection and start pulling the liver gently away from the mouse. Cut any ligaments that are still connected to the liver.
- Put the liver in a 100 mm Petri dish with 25 ml preservation buffer. Keep on ice.

7) Purification
- Change gloves. Use fine forceps to gash the liver sac. Agitate to get some cells to release from liver. Scrape off cells that remain attached to the liver sac with the cell lifter. Use as few strokes as possible to minimize cell damage.
- Filter cells through 100 μm mesh into a 50 ml tube. Wash petri dish with 20 ml preservation buffer and filter. Pass the 45 ml through a 70 μm filter into a 50 ml tube.
- Spin cells at 50 × g for 3 minutes (420 rpm in Cooney lab).
- Suck off media and resuspend pellet in 25 ml preservation buffer.
- Put 12.5 ml cell suspension in two 50 ml tubes and add 6 ml Percoll solution to each.
- Spin cells at 50 × g for 5 minutes (420 rpm in Cooney lab).
- Suck off layer of dead cells and rest of Percoll solution.
- Resuspend pellets in 22.5 ml preservation buffer each, and combine the tubes.
- Spin cells at 50 × g for 3 minutes (420 rpm in Cooney lab).
- Suck off media and dissolve in 11 ml Hepatocyte Attachment Media.
- In an Eppendorf tube, add 50 μl cell suspension and 200 μl Trypan blue.
- Count cells in 5 squares. 1.5×10^6 cells/g mouse is good.

8) Cleanup
- Rinse perfusion apparatus with 10 ml 70% ethanol. Let air pass through.
- Wrap up the mouse in a black bag. Throw the applicators and gauze in biohazard waste. Bring the mouse carcasses to the 8th floor fridge in the necropsy room.

- Wash all instruments and Pyrex bottles with water. Dry instruments.

Item	Cat#	Vendor	Quant	Cost
Waterbath (41°C)	---	---	---	---
Masterflex Pump	---	---	---	---
Silicone tubing (plat. cured)	96410-13	Cole Parmer	25 ft	$36.00
15 ml Falcon tube	---	VWR Stockroom	1	---
BD Needles 16G x 1.5"	---	VWR Stockroom	2	---
Pyrex bottles, 250 ml	---	VWR Stockroom	2	---

Item	Cat#	Vendor	Quant	Cost
Tissue forceps, 4.5"	25601-080	VWR	1	$1.91
Dissecting scissors, 6"	25608-316	VWR	1	$11.27
Castro-Viejo scissors, 4"	25608-575	VWR	1	$52.14
Mosquito hemostats, 5"	25607-302	VWR	4	$54.68
Blunt-tipped fine forceps	25601-008	VWR	2	$4.44
Scalpel holder	25607-925	VWR	1	$5.59
Scalpel (#10)	25608-065	VWR	100	$26.65
Cell lifter	29442-200	VWR	100	$61.29
Angio catheter 24G	---	MIT Surgical	1	$2.03
Halothane chamber (Tupperware)	---	VWR Stockroom	1	---
Nylon mesh filter, 70 um	21008-952	VWR	50	$73.23
Nylon mesh filter, 100 um	21008-950	VWR	50	$73.23
Slotted incubator shelf	---	---	1	---
Insulin syringe 28Gx1"	BD-309309	VWR	200	$45.83
Surgical instrument tray	62687-027	VWR	1	$18.42
Autoclave bags, 12"x18"	58753-194	VWR	250	$165.95
Autoclave paper, 36"x36"	58752-964	VWR	100	$73.30
Cotton-tipped applicators	10806-005	VWR	1000	$10.35
Gauze	---	MIT Surgical	---	---
Waste basin (surgery)	---	VWR Stockroom	1	---

Item	Cat#	Vendor	Quant	Cost
KCl	P3911	Sigma	500 g	$27.95
HEPES (free acid)	---	VWR Stockroom	---	---
NaCl	S7653	Sigma	1 kg	$46.15
Collagenase (Type IV)	C-5138	Sigma	1 g	$198.85
$CaCl_2 \bullet 2H_2O$	C5080	Sigma	500 g	$41.75
D-Glucose	---	VWR Stockroom	---	---
BSA, fract. V	A4503	Sigma	50 g	$128.00
Tribromoethanol	90710	Sigma	10 g	$27.25
Tert Amyl Alcohol	24048-6	Sigma	5 ml	$27.00
EDTA	E7889	Sigma	100 ml	$23.58
Percoll	P1644	Sigma	100 ml	$57.20

4 Hepatoma Response To Glutamine Oscillations

4.1 Introduction

Advances in Physiological Genomics require connecting changes in gene sequence or gene transcription to function. A first approach to the global investigation of these relationships is to perturb the physiology of an organism and observe time-dependent changes in gene expression. Transcriptional profiling studies of this type have begun to identify groups of coexpressed and interrelated genes constituting transcriptional regulatory networks (20, 77, 181). To complement this transcriptional or horizontal level of organization, a second vertical category of networks may be considered that investigates responses to perturbations in physiology over time, but includes data from the transcriptional level and the level of cell function. This second category, which we term "physiological regulatory networks", provides a structure for directly incorporating changes in physiology in the development of regulatory networks. As a prototype for mammalian cell physiological regulatory networks, we have examined the time-dependent response of confluent cultured mouse hepatoma cells to changes in the glutamine concentration of the medium. Using this model, we report quantitative changes in gene expression, metabolic fluxes, and metabolite levels for pathways directly involving glutamine and its metabolites.

Most mammalian cells in culture require super-physiological levels of glutamine for optimal growth. High rates of glutamine consumption are commonly observed in tumor cell lines, hybridomas, and other rapidly proliferating cells (129). The importance of glutamine is further demonstrated by the observation that changes in the extracellular glutamine concentration cause metabolic shifts in mammalian cell culture (109, 121). For example, in continuous hybridoma cultures, a step change from approximately 0 to 0.9 mM extracellular glutamine (with excess glucose present) produced a marked increase in the consumption of glucose, glutamine, and oxygen, and the production of ammonium, alanine, and lactate (121). This observation that glutamine is required for high rates of glycolysis has been observed in a variety of mammalian cells. Rat lymphocytes increased the consumption of glucose when glutamine was in the medium (6). C6 rat glioma cells increased glucose consumption by 60% when transferred from glutamine-free medium to 4 mM glutamine (140). When both glucose and glutamine are available, glutamine provides a significant fraction of the cellular energy requirements, calculated as 40% for normal diploid fibroblast cells (215) and Chinese hamster cells (46) and as high as 70% for HeLa cells (150). This capacity for elevated glutamine consumption may be a consequence of a distinct high capacity glutamine transport system, which has been documented for human hepatoma cells (18). Once inside the cell, glutamine carbon has several fates. It may enter the TCA cycle at oxaloacetate, but, for each molecule entering the cycle, one four- or five-carbon moiety must exit to maintain steady state. The flux of glutamine carbon to purine biosynthesis is an example of one such biosynthetic exit path. A second pathway is exit from the TCA cycle via malic enzyme to pyruvate, which can either be converted to lactate or acetyl-CoA. Both

of these paths allow the cell to maintain steady state TCA cycle metabolite levels, and the latter pathway is required for complete oxidation of glutamine. Finally, glutamine can be converted to citrate via reductive carboxylation where isocitrate dehydrogenase carries flux in reverse of the TCA cycle direction. This last pathway contributes significantly to *de novo* lipogenesis in rat hepatoma (71) and to gluconeogenesis in normal perfused rat liver (45).

To develop a prototype for physiological regulatory networks, we chose Hepa1-6 cells, a mouse hepatoma cell line. This cell line arose from a C57/L mouse and retains many liver-specific phenotypes, including the secretion of several serum proteins (38). However, it does not store glycogen and has a low activity of glucose 6-phosphatase (183), suggesting an absence of glucose production. We designed studies to simultaneously probe the changes in metabolic function and gene expression following removal of glutamine from the medium for 24 h followed by 24 h of 4 mM glutamine. This glutamine depletion/repletion protocol provided the basis for investigating both metabolic physiology and gene expression under well-controlled conditions.

4.2 Results

4.2.1 Metabolic Alterations During Glutamine Oscillations

The effect of glutamine depletion/repletion on the glycolytic flux was examined using ^3H_2O release from [2-^{3}H] and [3-^{3}H] glucose as described in Methods (Fig. 4.1). The glycolytic flux at time 0 was 0.30 ± 0.03 nmol/h per 10^4 cells and did not differ for the two ^{3}H tracers. This indicates that the flux through triose phosphate isomerase did not differ from that through hexose phosphate isomerase. This agreement is expected in

view of the high glycolytic rate in the absence of significant glucose-6-phosphatase activity reported in Hepa1-6 cells (183). Removal of glutamine from the medium led to a gradual decline in the glycolytic rate to values approximately 50% of the control. Restoring glutamine to the medium returned the rates to near the starting values after a delay of approximately 12 h (Fig. 4.1), demonstrating a reversible change in flux upon glutamine depletion and repletion.

To monitor the fate of glucose further into the oxidative pathway, $^{14}CO_2$ production from ^{14}C-labeled glucose tracers was examined (Figs. 4.2 and 4.3). The flux through PDH estimated with [3,4-^{14}C] glucose at time 0 was 0.10 ± 0.01 nmol/h per 10^4 cells. The flux through PDH declined by 70% in the absence of glutamine. For a more direct estimate of the effect of glutamine on TCA cycle flux, $^{14}CO_2$ production from [6-^{14}C] glucose was examined at 0, 24, and 48 h of the protocol (Fig. 4.3). The oxidation of glucose estimated with [6-^{14}C] glucose at time 0 was 0.07 ± 0.01 nmol/h per 10^4 cells. The TCA cycle activity measured by this indicator declined 70% during glutamine depletion at 24 h and returned to control values by 48 h (Fig. 4.3). Taken together, these flux indicator assays demonstrate a reversible decline in glycolytic and TCA cycle fluxes induced by glutamine depletion and repletion.

In addition to lactate and the TCA cycle, a significant fate of glucose and glutamine carbon is polymerization in the lipogenic pathway. The effect of glutamine depletion/repletion on the total rate of lipogenesis was investigated by measuring the rate of incorporation of ^3H_2O into lipid-soluble compounds. The lipogenic flux at time 0 was 142 ± 20 pmol fatty acid/h per 10^6 cells. Following the trend of the other flux indicators,

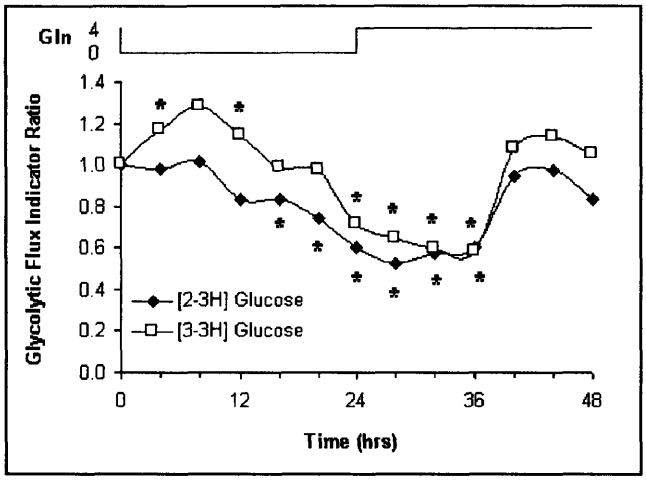

Figure 4.1. Effect of glutamine depletion/repletion on the glycolytic flux indicator ratios. The average experimental glycolytic flux indicator was normalized by a 12-h averaged control glycolytic flux indicator to yield the ratio. The hexose isomerase indicator assay used [2-^{3}H] glucose. The triose phosphate isomerase
□□□□□□□□□□□□□□□□□□□□ÿ□ÿ□ÿ□ÿ□□□□□□
□□□□□□□□□□□□□□ÿ□ÿ□ÿ□ÿ□□□□□□□□□□□□
oints where the average experimental value was significantly different from the average control value

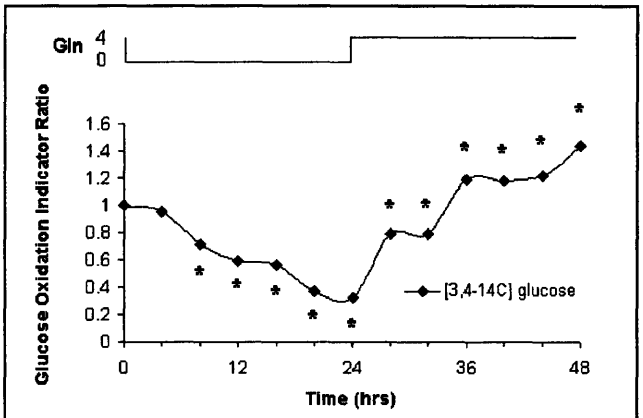

Figure 4.2. Effect of glutamine depletion/repletion on glucose oxidation indicator ratios. The average experimental glucose oxidation indicator was normalized by a 12-h averaged control glucose oxidation indicator to yield the ratio. The pyruvate dehydrogenase indicator assay used [3,4-^{14}C] □□□□□□□□□¿□0□□□□□□□ÿ□□□□□□□□ □□□□□□□□□□□□□□□□□□□□□□□□□□□□□□ □□□□□□□□□□□□□□□□□□□□□□□□□□□□□□ ficantly different from the average control value (n =

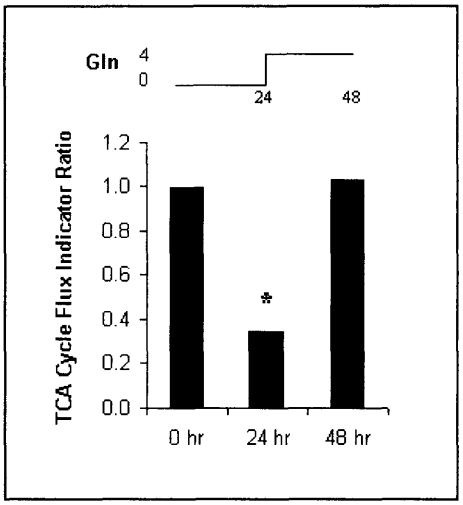

Figure 4.3. Effect of glutamine depletion/repletion on TCA cycle flux indicator ratios. The average experimental TCA cycle flux indicator was normalized by the control TCA cycle flux indicator to yield the ratio. The TCA cycle flux indicator assay used [6-^{14}C] glucose. The * denotes time points where the average experimental value was significantly different from the average control value ($n = 6$, $p < 0.05$).

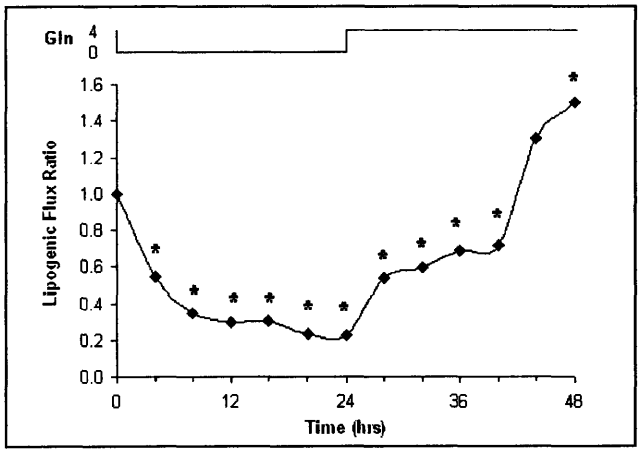

Figure 4.4. Effect of glutamine depletion/repletion of the rate of lipogenesis determined by ^3H_2O incorporation. The average experimental lipogenic flux was normalized by a 12-h averaged control lipogenic flux to yield the ratio. The * denotes time points where the average experimental value was significantly different from the average control value ($n = 3$, $p < 0.05$).

the rate of lipogenesis fell by 80% when glutamine was removed from the medium and slowly increased when it was replenished (Fig. 4.4). To quantify the sources of carbon for *de novo* lipogenesis, ISA was employed as described in the Methods. ISA estimated the fractional contribution of glucose and glutamine to the lipogenic acetyl-CoA pool (D) and the fraction of newly synthesized fatty acid in esterified lipid after a 24-h incubation (g(24 h)) (Table 4.1). In control medium, both glucose and glutamine were major contributors to the lipogenic acetyl-CoA pool. Together, they accounted for 70% of the lipogenic carbon. This indicates that 30% of the lipogenic carbons were either from endogenous compounds or from compounds in the medium other than glucose and glutamine. ISA estimated the fractional synthesis of new palmitate in 24 h as approximately 26% of the total cellular esterified pool in control conditions. These results contrasted with the findings in glutamine-depleted medium, where glucose accounted for only 19% of lipogenic carbon and the fractional synthesis of new palmitate was only 8.5% of the total. These findings indicate that glutamine depletion significantly reduced the flux of glucose carbon into lipogenic pathways. The total esterified palmitate for the two conditions following the 24-h tracer study was similar (Table 4.1), suggesting that esterified palmitate turnover was greater in the presence of glutamine.

To examine whether changes in intracellular metabolites played a role in the observed changes in glycolytic and TCA cycle rate, levels of key TCA cycle intermediates and related amino acids were monitored during glutamine depletion/repletion (Fig. 4.5). These data indicate that, with the exception of succinate, which did not change over the course of treatment, the metabolite concentrations declined rapidly when glutamine was removed from the medium, and returned to basal levels

Table 4.1. *Isotopomer spectral analysis of glucose and glutamine utilization in palmitate synthesis*

Sample	Glc	Gln	U-^{13}C	D	g (24 h)	Palmitate
Control	25 mM	4 mM	Glc	0.37 ± 0.02	0.23 ± 0.01	10 ± 1.5
Control	25 mM	4 mM	Gln	0.33 ± 0.01	0.28 ± 0.03	10 ± 1.5
Expt	25 mM	0 mM	Glc	0.19 ± 0.01	0.09 ± 0.01*	8.9 ± 0.9

Values are means ± SD. D, fractional contribution of labeled substrate to the lipogenic acetyl-CoA pool; g (24 h), fraction of newly synthesized fatty acid after 24-h incubation. *Difference between control and experimental (Expt) is significant ($P < 0.05$). Palmitate measurements are in terms of $\mu g/10^6$ cells.

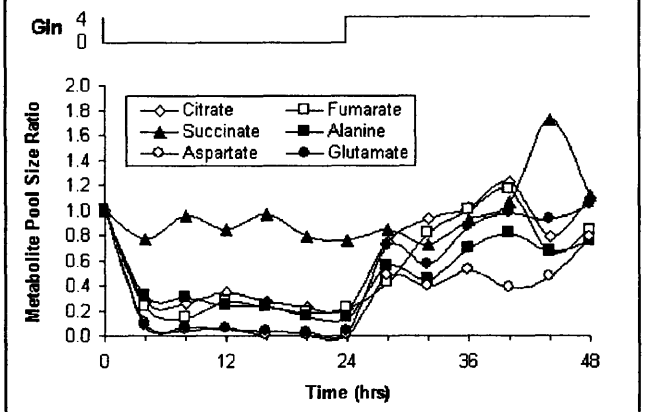

Figure 4.5. Effect of glutamine depletion/repletion on the metabolite pool sizes. The experimental metabolite pool size was normalized by the control metabolite pool size at each time point to yield the ratio.

when glutamine was repleted. This finding supports the anaplerotic role of glutamine carbon in replenishing the TCA cycle and the role of glutamate transaminases in maintaining amino acid levels. In summary, the analysis of key metabolite levels indicated that observed changes are consistent with flux changes, and thus metabolite changes could play a key role in altering flux in this model.

4.2.2 Role of Gene Expression in Flux Alterations

Changes in metabolic fluxes may be the consequence of changes occurring at the transcriptional level. To evaluate the significance of new mRNA synthesis, the flux measurements were repeated in the presence of actinomycin D (a DNA intercalator). Cells were treated with actinomycin D for 24 h beginning either at t = 0 when glutamine was depleted from the medium or at t = 24 h when glutamine was repleted. One-hour flux assays were conducted at t = 24 or 48 h, following the 24-h actinomycin D exposure. Assays measured glycolytic flux (^3H_2O production from [2-^{3}H] glucose), PDH flux ($^{14}CO_2$ production from [3,4-^{14}C] glucose), TCA cycle flux ($^{14}CO_2$ production from [6-^{14}C] glucose), and lipogenesis (^3H_2O incorporation into lipids). Each of these assays indicated that the observed changes in flux produced by glutamine depletion and repletion were altered in the presence of actinomycin D. Three specific patterns are illustrated in Figures 4.6, 4.7, and 4.8. In the presence of actinomycin D, the glycolytic flux did not decline during glutamine depletion (Fig. 4.6A) and did not recover completely during glutamine repletion (Fig. 4.6B). This indicates that *de novo* mRNA synthesis was necessary to allow the glycolytic rate to fall when glutamine was depleted (Fig. 4.6A) and to allow it to return to normal values when glutamine is repleted (Fig.

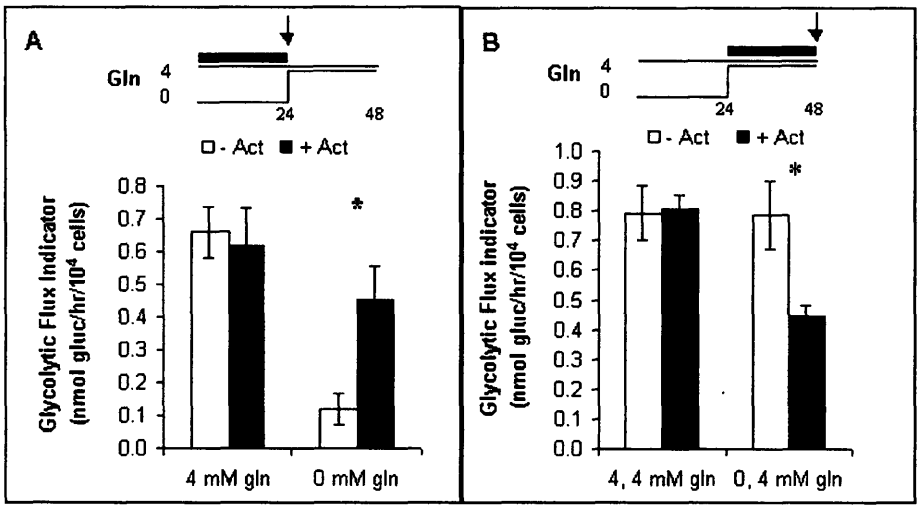

Figure 4.6. Effect of actinomycin D on glycolytic flux estimated using [2-^{3}H] glucose over the course of glutamine depletion/repletion. Actinomycin D was added to control and experimental groups in the first 24 h (A) or in the second 24 h (B) as indicated by a black bar. Arrow denotes time of flux assay. In comparisons between cells in the absence (open bars) or presence (solid bars) of actinomycin D for each glutamine treatment ($n = 6, \pm$ SD), * denotes a significant difference ($p < 0.05$).

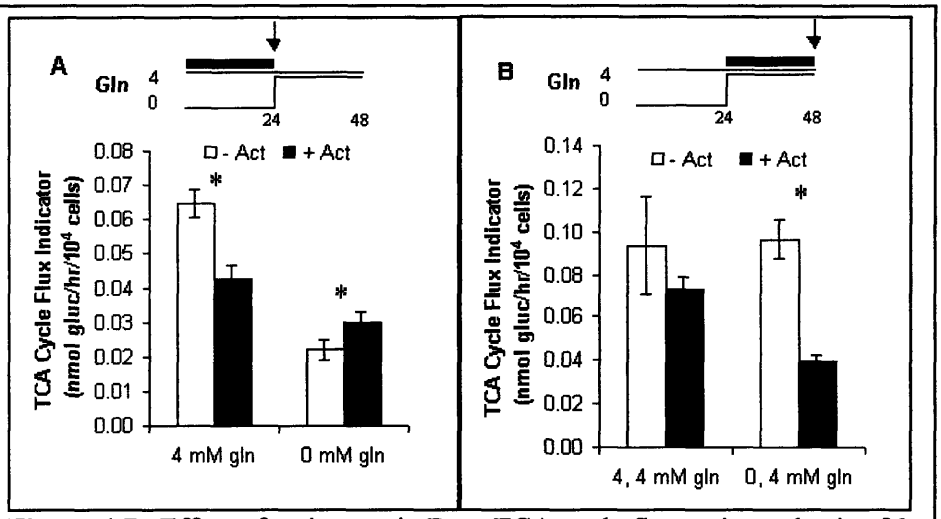

Figure 4.7. Effect of actinomycin D on TCA cycle flux estimated using [6-^{14}C] glucose over the course of glutamine depletion/repletion. Actinomycin D was added to control and experimental groups in the first 24 h (A) or in the second 24 h (B) as indicated by a black bar. Arrow denotes time of flux assay. In comparisons between cells in the absence (open bars) or presence (solid bars) of actinomycin D for each glutamine treatment (n = 6, ± SD), * denotes a significant difference ($p < 0.05$).

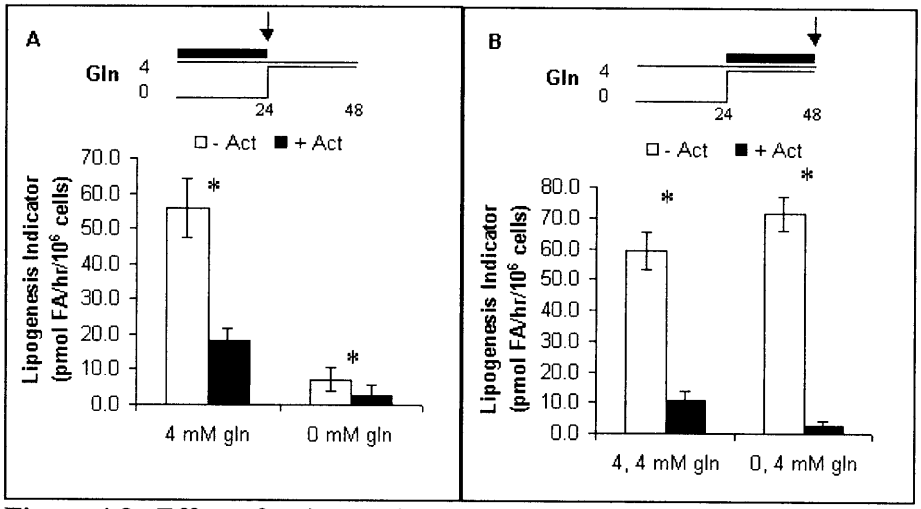

Figure 4.8. Effect of actinomycin D on lipogenic flux estimated using ^3H_2O over the course of glutamine depletion/repletion. Actinomycin D was added to control and experimental groups in the first 24 h (A) or in the second 24 h (B) as indicated by a black bar. Arrow denotes time of flux assay. In comparisons between cells in the absence (open bars) or presence (solid bars) of actinomycin D for each glutamine treatment (n = 6, ± SD), * denotes a significant difference ($p < 0.05$).

4.6B). However, the maintenance of glycolytic flux in control cells over a 24-h period did not require *de novo* mRNA synthesis. The glycolytic flux indicator value at time = 0 was 0.47 ± 0.04 nmol/h per 10^4 cells. A similar, but less pronounced pattern was seen in the TCA cycle flux (Fig. 4.7). The TCA cycle flux indicator value at time = 0 was 0.07 ± 0.01 nmol/h per 10^4 cells. A different pattern was found when the lipogenic flux was monitored with ^3H_2O incorporation (Fig. 4.8). Here, *de novo* mRNA synthesis was required to maintain the normal lipogenic flux over 24 h in control medium, but mRNA synthesis was not required for decreased lipogenesis produced by glutamine depletions (Fig. 4.8A). *De novo* mRNA synthesis was also required for cells to respond to glutamine repletion (Fig. 4.8B). The lipogenic flux indicator value at time = 0 was 99.5 ± 7.9 pmol FA/h per 10^6 cells.

4.2.3. Microarray Analysis of Gene Expression

DNA microarray studies were conducted at specified intervals across the glutamine depletion/repletion protocol, as described in the Methods. The gene expression data for duplicate microarrays were merged and averaged to create a union data set. Genes were retained in the union set only if data were available for each of the 7 time points. Analysis of this data indicated that 3,185 of the 17,280 genes were expressed at every time point during the glutamine depletion/repletion protocol. To capture genes with significant changes in gene expression, the data were filtered to eliminate genes that did not have at least one time point with a log2 ratio greater than 0.6 or less than –0.6. Of the 3,185 genes, 950 genes were considered unchanged at every time point and condition by this criterion. The remaining 2,235 genes were examined to

determine if genes associated with the observed flux changes were altered significantly and to determine if any of the 2,235 genes were highly correlated with the glycolytic flux indicator or with the glutamine level in the medium. To investigate the behavior of genes in the pathways affected by glutamine depletion/repletion, expression values for treated cells were compared to controls at the end of glutamine depletion (24 h) and after 12 h of glutamine repletion (36 h) (Table 4.2). Lipid synthesis increased upon glutamine repletion and a gene catalyzing a highly regulated step in cholesterol synthesis, HMG-CoA reductase, was found to increase upon glutamine repletion. However, fatty acid synthase, whose expression is often found to correlate with fatty acid synthesis, was not found to change in this study. Genes catalyzing early steps of fatty acid oxidation, acyl-CoA synthetase and acyl-CoA dehydrogenase, increased during glutamine depletion and decreased during the glutamine repletion. These findings are consistent with the fact that lipid oxidation is suppressed when lipogenesis is elevated, due to the actions of malonyl-CoA. Glycolysis increased upon glutamine repletion. Several glycolytic genes increased upon glutamine repletion, including 6-phosphofructo-2-kinase/fructose-2,6-bisphosphatase 2, phosphofructokinase, and glucose phosphate isomerase 1 complex. It should be noted that many metabolic genes involved in the pathways affected by glutamine did not change significantly. Among the 950 unchanged genes were citrate synthase, PDH-β, pyruvate kinase, lactate dehydrogenase 1, triosephosphate isomerase, and ATP-citrate lyase (data not shown). Acetyl-CoA carboxylase (94) and PEPCK (149) have previously been found to be affected by glutamine oscillations, but did not qualify for our 3,185-gene data set. Taken together, our results indicate that the dramatic flux changes associated with glutamine depletion and repletion are accompanied by large

Table 4.2. *Expression response of genes in central carbon and lipid metabolism to glutamine repletion.*

Gene Name	T = 24 h	T = 36 h	Response
Acyl-CoA Synthetase	1.68	−0.42	Decrease
Acyl-CoA Dehydrogenase	2.08	−0.90	Decrease
Glutamate Dehydrogenase	0.69	−1.04	Decrease
Pyruvate Carboxylase	0.68	0.51	Decrease
Fatty Acid Synthase	0.36	0.12	Unchanged
6-Phosphofructo-2-kinase/Fructose2,6-bisphosphatase 2	1.07	1.92	Increase
HMG-CoA Reductase	−0.69	2.44	Increase
Phosphofructokinase	−1.56	2.13	Increase
Glucose Phosphate Isomerase 1 Complex	0.08	2.31	Increase
β-actin	0.40	1.22	Increase

'T = 24 h' values reflect the log2 ratio comparing experimental and control cells at the 24-h time point with the glutamine concentration at 0 mM. 'T = 36 h' values reflect the log2 ratio comparing experimental and control cells at the 36-h time point, 12 h after glutamine repletion to 4 mM.

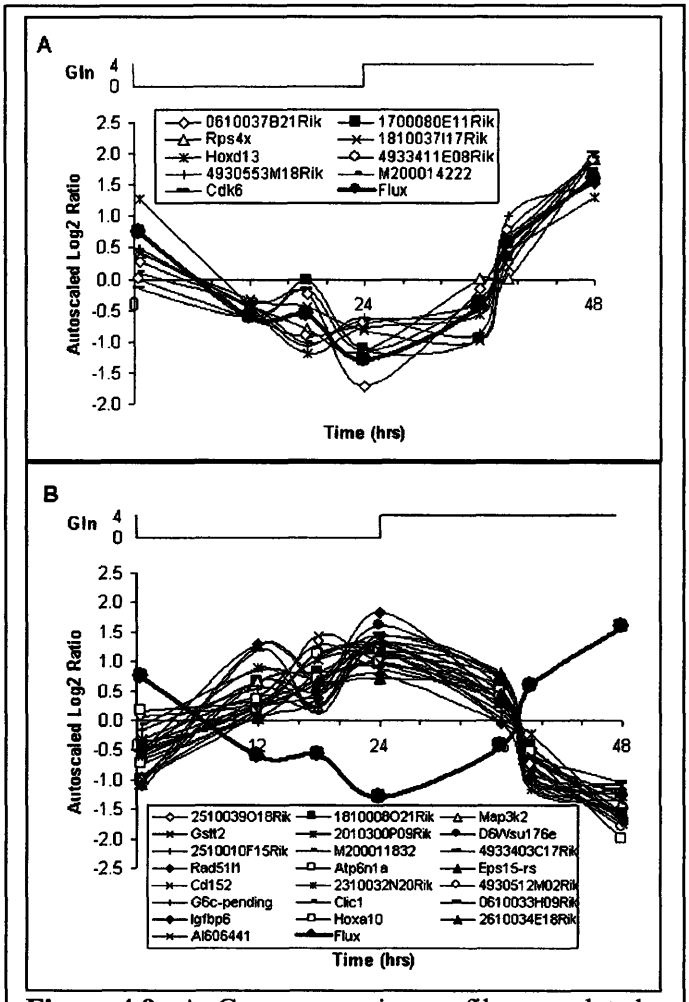

Figure 4.9. A: Gene expression profiles correlated to hexose isomerase flux indicator with a correlation coefficient ≥ 0.90. B: Gene expression profiles anti-correlated to hexose isomerase flux indicator with a correlation coefficient ≤ –0.90.

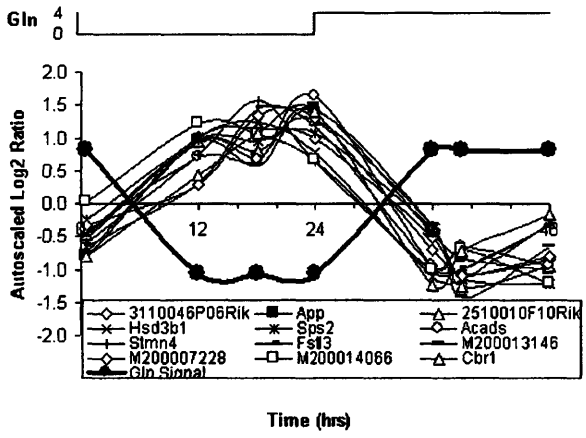

Figure 4.10. Gene expression profiles anti-correlated to autoscaled glutamine concentration with a correlation coefficient ≤ –0.90.

changes in only a few of the many enzymes catalyzing the reactions in these pathways. Finally, Table 4.2 lists the increased expression of β-actin upon glutamine repletion, consistent with the findings of Husson et al. (75). In addition to characterizing the behavior of genes known to be involved in the pathways affected by glutamine, we used correlational analysis to identify genes whose expression patterns correlated with the observed fluxes. The correlational analysis revealed a larger number of genes that were anti-correlated with glutamine and fluxes than those that were correlated. For example, correlational analysis of the glycolysis flux detected 9 correlated genes with a correlation coefficient ≥ 0.90 (Fig. 4.9A). However, 22 anti-correlated genes were detected with a correlation coefficient ≤ -0.90 (Fig. 4.9B). Analysis of gene expression data with the autoscaled glutamine input signal found 16 anti-correlated genes with a correlation coefficient less than –0.90 (Fig. 4.10). Yet, no correlated genes were found with a correlation coefficient greater than 0.90. Finally, the gene expression data were analyzed by a pattern discovery algorithm, Teiresias (151). The data set of log2 ratios at time points was converted into a binary data set of positive or negative derivatives between time points. Teiresias was then used to discover patterns within this binary data set. Twelve genes were found to have the pattern of 3 positive derivatives followed by 3 negative derivatives (Fig. 4.11). Using the same criteria, Teiresias did not detect any genes exhibiting the expression pattern of 3 negative derivatives followed by 3 positive derivatives.

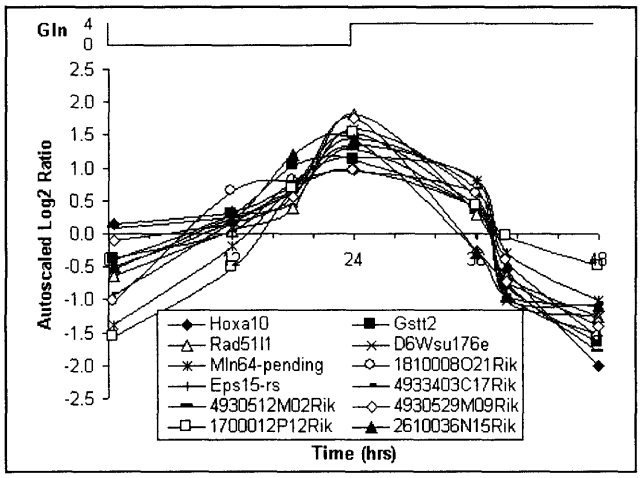

Figure 4.11. Gene expression profiles discovered by Teiresias to have a pattern of 3 positive derivatives followed by 3 negative derivatives.

4.3 Discussion

With the completion of the mouse genome sequence and the development of protocols for generating transgenic animals, mouse models are providing important insights into human diseases. The glutamine depletion/repletion protocol described here demonstrated that changes in fluxes could be evaluated in a mouse hepatic cell model at short time intervals over a 48-h period. This was facilitated by the development of 1-h flux assays specifically for this project. The observed flux changes could then be combined with data for metabolite levels and gene expression, providing a prototype for simultaneous monitoring of fluxes, metabolite levels, and gene expression. While previous studies with mouse hepatoma cell lines have recorded distinct enzyme expression patterns characteristic of these cells (38), quantitative analysis of fluxes comparable to those in human and rat hepatoma cell lines have been lacking. The present study demonstrated that mouse Hepa1-6 cells share metabolic flux characteristics with other transformed cell lines with regard to glutamine metabolism. Consistent with previous findings (6, 140), glutamine is required for high rates of glycolytic flux (Fig. 4.1). Glutamine is also a major source of carbon for *de novo* lipogenesis (Table 4.1), as found with rat hepatoma cells (71). Thus, the Hepa1-6 mouse cell line is well suited for the investigation of physiological regulatory networks that integrate gene expression and functional data.

The glutamine depletion/repletion protocol provided a mechanism for examining changes in metabolic flux in terms of two key sites of controlling flux: control via changes in the levels of substrates and other metabolites, and control via changes in the level of mRNA mediated by transcription. Flux measurements following incubation in

actinomycin D provided a tool for examining the necessity of transcriptional changes in this model. The glycolytic flux response observed in response to actinomycin D demonstrated that, in the absence of a change in glutamine, *de novo* mRNA synthesis was not critical to maintaining flux (Fig. 4.6). This suggests that the mRNA and/or its protein products required for maintenance of the glycolytic flux are relatively stable, a pattern characteristic of a pathway that is not regulated at the transcriptional level in the short term. The TCA cycle may also be an example of a pathway that is not transcriptionally regulated in the short term. Citrate synthase and pyruvate dehydrogenase beta were among the 950 genes with no significant gene expression changes during glutamine depletion/repletion. In place of transcriptional changes, alterations in fluxes in these pathways may be the result of control at the enzyme activity or metabolite level, a form of regulation that allows rapid response to changing conditions. The finding that the concentrations of five of the six metabolites correlated with the flux changes (Fig. 4.5) provides a mechanism for changes in flux as a result of changes in substrate concentration. Although maintenance of glycolytic flux did not require *de novo* mRNA synthesis, the requirement for mRNA synthesis to effect the changes in flux during glutamine depletion/repletion clearly indicates a role for *de novo* mRNA synthesis in regulating these fluxes (Fig. 4.6). The effect of actinomycin D on the lipogenic flux demonstrated that *de novo* mRNA synthesis was critical to maintaining flux. The lipogenic mRNA and/or its protein products are less stable than glycolytic mRNA, and may exert some control over the lipogenic flux at the transcriptional level in the short term. Thus, in developing a more complete description of flux control in this model, the quantitative importance both of metabolite changes and gene expression will be required.

The use of actinomycin D in conjunction with the glutamine depletion/repletion protocol provides a model for the analysis of the time course of transcriptional changes modulating metabolic flux.

Changes in gene expression monitored with DNA microarrays indicated activation of gene expression accompanied the decline in metabolic fluxes observed upon glutamine depletion (Figs. 4.9 and 4.10). This finding brings into focus the fact that increased transcription of some genes was required to allow cells to respond to the new metabolic conditions created by removing glutamine from the medium. Activation of gene expression in the absence of glutamine was also supported by the finding that actinomycin D prevented, at least partially, the expected decline in glycolytic flux during glutamine depletion as discussed above. Most of the genes found to be activated or anti-correlated with glutamine levels or flux are not known to be directly connected to intermediary metabolism. They were retained following a filter that required a substantial change in gene expression and eliminated most genes due to either to poor signal or small changes in expression. The Teiresias algorithm provided another method other than correlation to identify genes of interest. Out of the 12 genes identified with the correct 3-up/3-down pattern, 8 were also found on the list of genes from the glycolytic flux anti-correlational analysis. In other words, 8 of the genes identified by Teiresias also had correlation coefficients to the glycolytic flux ≤ -0.90. The other 4 genes had correlation coefficients between -0.71 and -0.89. Teiresias sought out genes that had a desirable pattern, but were not necessarily highly correlated with the flux signal. While the role of the genes detected here in modulating flux has not been resolved, the ability of this model to examine the relationship between genes and fluxes may be an important

tool for future studies. Another finding of note in the analysis of microarray data was that most relevant metabolic genes did not display significant expression changes. Thus, this study demonstrates the importance of a physiological approach combining metabolite data and gene expression data to understand regulatory networks controlling flux. We propose the glutamine depletion/repletion model as a prototype for developing physiological regulatory models in integrative systems biology.

5 Modulation Of Liver Insulin Action By The Hexosamine Biosynthetic Pathway

5.1 Introduction

Development of insulin resistance is the primary pathophysiological event of Type 2 diabetes, and many models have been developed to study the pathophysiology of insulin resistance. Prolonged hyperglycemia is one such model and is known to induce insulin resistance in animal and cell culture systems. In 1991, Marshall et al. discovered that prolonged hyperglycemia enhanced flux through the hexosamine biosynthesis pathway (HBP) and induced insulin resistance in the adipocyte glucose transport system (111). It was postulated that under conditions of hyperglycemia, approximately 1 to 3% of the glucose flux through glycolysis was shunted into the HBP (111, 112). The increased generation of hexosamine metabolites apparently enhanced the glycosylation of proteins with *N*-acetylglucosamine (GlcNAc) moieties, negatively impacting insulin signaling and yielding insulin resistance. Numerous studies *in vitro* and *in vivo* have provided evidence supporting the involvement of the HBP in inducing insulin resistance in adipose, muscle, and other tissue types (21, 116, 117, 132, 157, 197, 212). In examining the HBP's mechanism of action, Patti et al. found that insulin receptor substrate-1 and 2 had decreased phosphorylation in conjunction with increased glycosylation (138). Park et al. reported that insulin receptor substrate-1 and Akt2 had

increased glycosylation and decreased phosphorylation after treatment with PUGNAc, which inhibits the removal of GlcNAc units from proteins (135). Spampinato et al. found that glucosamine infusion into rats decreased insulin-stimulated insulin receptor autophosphorylation in skeletal muscle (173). Insulin-stimulated glycogen synthase activity in 3T3-L1 adipocytes was decreased by glycosylation (137). In total, there is ample evidence that enhanced HBP activity interrupts insulin signaling through protein glycosylation with HBP products, and enhanced HBP activity may be one mechanism of hyperglycemia-induced insulin resistance. Because the liver is also an insulin-sensitive tissue, we hypothesized that the HBP activity affected insulin sensitivity in a similar manner in the liver.

Based on previous literature, we chose to use pharmacological agents to modulate the HBP activity (Fig. 5.1). Alloxan, a uracil analog, was shown to inhibit *O*-GlcNAc transferase in isolated pancreatic islets (91), limiting HBP activity. Glucosamine is rapidly transported into hepatocytes through glucose transporters and undergoes direct phosphorylation to glucosamine-6-phosphate (111, 113), increasing HBP activity. Glucosamine bypasses the first and rate-limiting enzyme of this pathway, glutamine:fructose-6-P amidotransferase (GFAT), circumventing the allosteric feedback inhibition of GFAT by glucosamine-6P (24) and uridine diphosphate-*N*-acetyl glucosamine (UDP-GlcNAc) (92). This allows artificially high levels of UDP-GlcNAc. Glucosamine is also a competitor of glucose for glucokinase (11) and the glucose transporter. Azaserine, a glutamine analog, was shown to restore insulin sensitivity to the glucose uptake system in adipocytes (111). It was postulated that azaserine reduced HBP

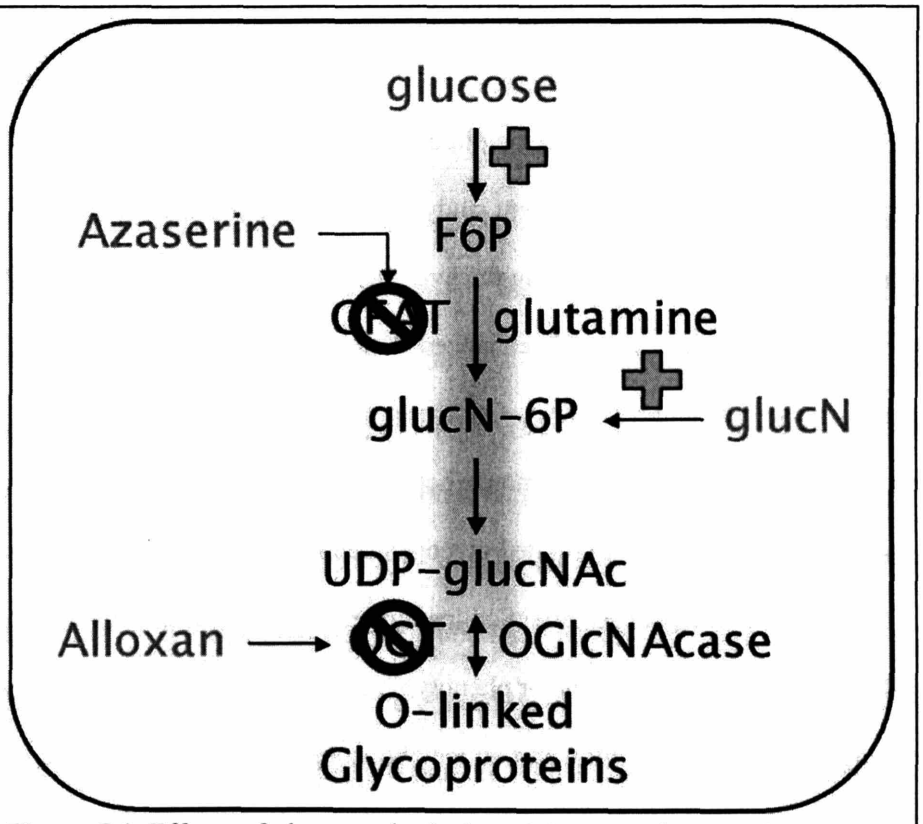

Figure 5.1. Effects of pharmacological modulators on hexosamine biosynthetic pathway activity. Glucose and glucosamine increase HBP activity by providing more substrate. Azaserine and alloxan decrease HBP activity by inhibiting enzymes in the HBP.

activity by competitively inhibiting GFAT. We used both single modulator treatments and combination treatments to study the effect of HBP activity on insulin sensitivity.

Previous data indicated that the HBP activity might influence insulin sensitivity in the liver. Virkamaki et al. found that infusion of glucosamine into rats abolished insulin- and glucose-stimulated glycogen deposition by ~100-fold (193). However, these data were taken in an animal model, in which the direct effect of glucosamine infusion on the liver was not known in detail. In the current study, we set out to test our hypotheses in mouse hepatocytes. We focused on testing the hypotheses that 1) modulation of HBP activity affects insulin sensitivity, and 2) enhanced HBP activity is one mechanism of hyperglycemia-induced insulin resistance. Our experimental approach involved modulating the HBP activity in cultured mouse hepatocytes by various pharmacological agents and measuring the insulin-stimulated glycogen deposition and insulin suppression of glucose production to quantify the effect on insulin sensitivity. We also investigated the intracellular events behind these major phenotypic changes by profiling the relative levels of various metabolites in central carbon metabolism and the HBP.

The results support the hypothesis that modulation of the HBP activity affects insulin sensitivity, and that enhanced HBP activity is a mechanism for hyperglycemia-induced insulin resistance. Metabolite profiling data showed that hyperglycemia increased the pools of hexose-phosphates and hexosamine intermediates. The assumed reduction or enhancement of HBP activity by pharmacological agents correlated with the corresponding effect on insulin sensitivity, and was also reflected in the metabolite levels. Taken together, we postulate that the HBP activity is one of the factors regulating insulin sensitivity in the liver.

5.2 Results

5.2.1 Insulin-Stimulated Glycogen Synthesis

We examined first the effects of treating hepatocytes with glucosamine, azaserine, and alloxan on insulin-stimulated glycogen deposition. The exposure of the hepatocytes to a series of glucosamine concentrations in 5 mM glucose Preincubation medium is shown in Fig. 5.2. The effect of glucosamine, which was to decrease insulin sensitivity and blunt insulin-stimulated glycogen synthesis, decreased in a dose-dependent manner and was negligible at or below 0.1 mM. The most effective concentration of glucosamine was 1 mM, which decreased the glucose to glycogen flux by 36%. The glucosamine treatments did not have an effect on the groups without insulin.

The effect of alloxan alone and in combination with glucosamine was examined during treatment with 5 mM glucose Preincubation medium (Fig. 5.3). In Figure 5.3A, treatment with 1 mM glucosamine again reduced insulin-stimulated glucose to glycogen flux by 40%, as compared to Control. Treatment with alloxan and glucosamine reduced insulin-stimulated glucose to glycogen flux by only 18%. The increase in insulin-stimulated glucose to glycogen flux caused by the addition of alloxan to glucosamine was significant, indicating that alloxan partially restored insulin stimulation of glycogen deposition. Addition of alloxan alone to the Preincubation medium (Fig. 5.3B) did not change the insulin-stimulated glucose to glycogen flux. The different treatments in Figure 5.3 caused significant changes to the groups without insulin stimulation, but the magnitudes of the changes were quite small. In both Figs. 5.3A and 5.3B, the Control groups showed the highest insulin sensitivity, as measured by the glycogen deposition.

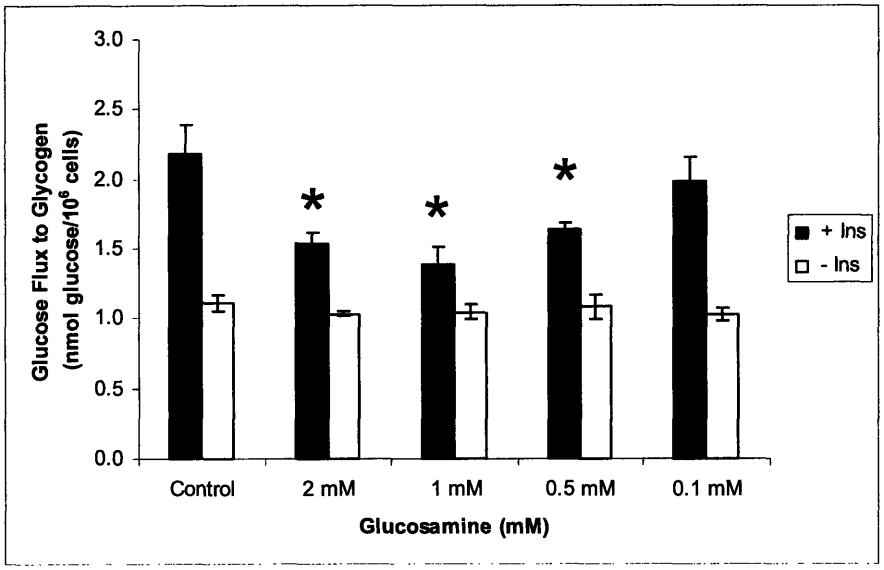

Figure 5.2. Insulin-stimulated glycogen deposition response to glucosamine treatment. Cells were incubated with different doses of glucosamine in the 5 mM glucose Preincubation medium. * = significant difference between "+ ins" groups and their control ($P < 0.05$, $n = 3$ to 6). Dunnett's t test was used for all comparisons.

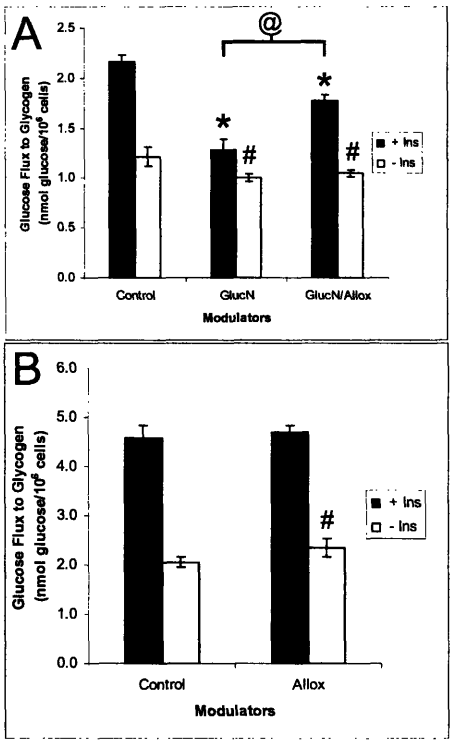

Figure 5.3. Insulin-stimulated glycogen deposition response to 1 mM glucosamine and/or 3 mM alloxan treatment. Cells were incubated with doses of glucosamine/alloxan in the 5 mM glucose Preincubation medium. * = significant difference between "+ ins" groups and their control ($P < 0.05$, $n = 3$ to 4). # = significant difference between "- ins" groups and their control ($P < 0.05$, $n = 3$ to 4). @ = significant different between indicated groups ($P < 0.05$, $n = 3$ to 4). Dunnett's t test was used for comparison in panel A, while Student's t test was used for panel B.

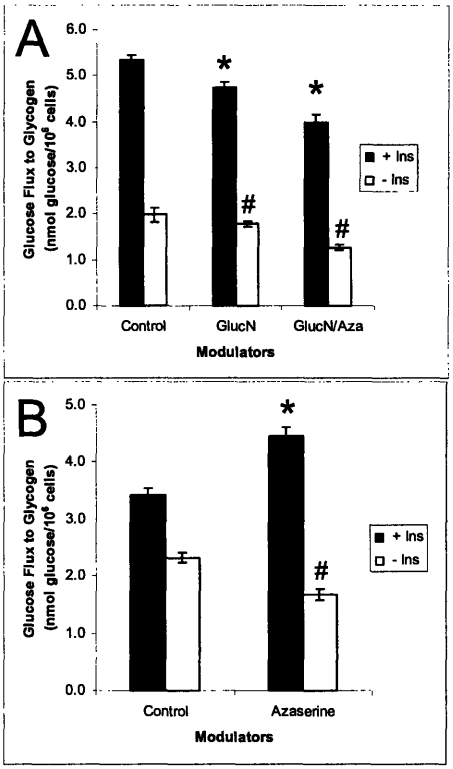

Figure 5.4. Insulin-stimulated glycogen deposition response to 1 mM glucosamine and/or 10 μM azaserine treatment. Cells were incubated with doses of glucosamine/azaserine in the 20 mM glucose Preincubation medium. * = significant difference between "+ ins" groups and their control ($P < 0.05$, n = 4 to 6). # = significant difference between "- ins" groups and their control ($P < 0.05$, n = 4 to 6). Dunnett's t test was used for panel A, while Student's t test was used for panel B.

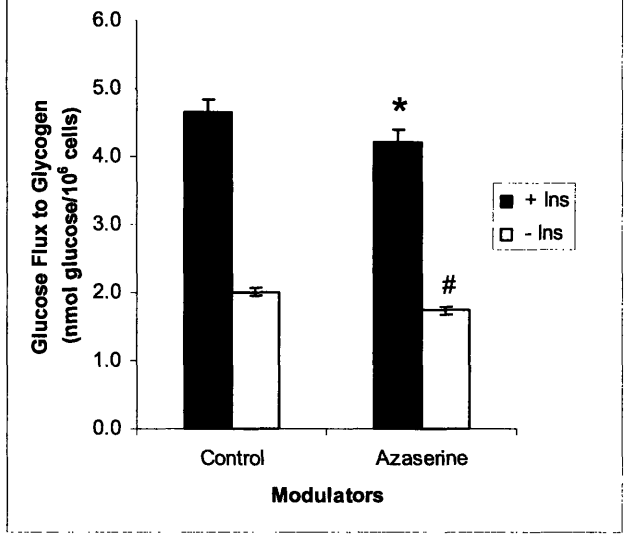

Figure 5.5. Insulin-stimulated glycogen deposition response to azaserine treatment. Cells were incubated with 10 μM azaserine in the 5 mM glucose Preincubation medium. * = significant difference between "+ ins" groups and their control ($P < 0.05$, $n = 4$ to 5). # = significant difference between "- ins" groups and their control ($P < 0.05$, $n = 4$). Student's t test was used.

Next, we examined the effect of glucosamine and azaserine at high concentrations of glucose (20 mM) in the Preincubation medium (Fig. 5.4). Addition of glucosamine (Fig. 5.4A) reduced insulin-stimulated glucose to glycogen flux by 11% from Control, which was much less than the reduction in the 5 mM glucose Preincubation case. Addition of glucosamine and azaserine reduced the insulin-stimulated glucose to glycogen flux further (25% from Control). These effects were contrasted with preincubation with azaserine (Fig. 5.4B), which led to a 30% increase in insulin-stimulated glucose to glycogen flux over Control.

Azaserine was tested for its effect in the presence of 5 mM glucose Preincubation medium (Fig. 5.5). There was a significant decrease in insulin sensitivity in the azaserine-treated cells, but the change was small (10%). This result was in contrast to azaserine's effect in the 20 mM glucose Preincubation treatment.

5.2.2 Insulin Suppression of Glucose Production

We next explored the effect of the different modulators on glucose production under insulin suppression and glucagon stimulation. The effect of glucosamine and/or alloxan with 5 mM glucose Preincubation medium was examined first (Fig. 5.6). Panel A shows the results with lactate/pyruvate in the Assay medium. The addition of glucosamine had significant effects on both the insulin treatment (24% increase in glucose production) and the glucagon treatment (22% decrease in glucose production). These effects showed glucosamine-induced resistance to both insulin and glucagon. Alloxan by itself had little effect on insulin sensitivity, but adding alloxan to glucosamine improved insulin sensitivity and nearly reduced glucose production back to Control level.

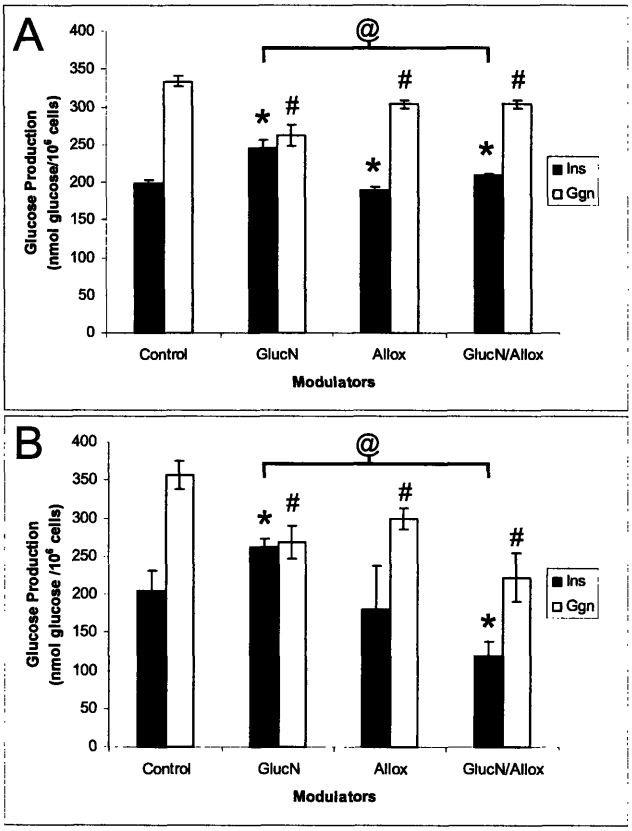

Figure 5.6. Glucose production response to 1 mM glucosamine and/or 3 mM alloxan treatment. Cells were incubated with doses of glucosamine/alloxan in the 5 mM glucose Preincubation medium. A: Assay medium with lactate/pyruvate. B: Assay medium with lactate/pyruvate and glycerol.
* = significant difference between "Ins" groups and their control ($P < 0.05$, n = 3 to 5). # = significant difference between "Ggn" groups and their control ($P < 0.05$, n = 3 to 5). @ = significant difference between indicated groups ($P < 0.05$, n = 3 to 5). Dunnett's t test was used for all comparisons. Ggn = glucagon.

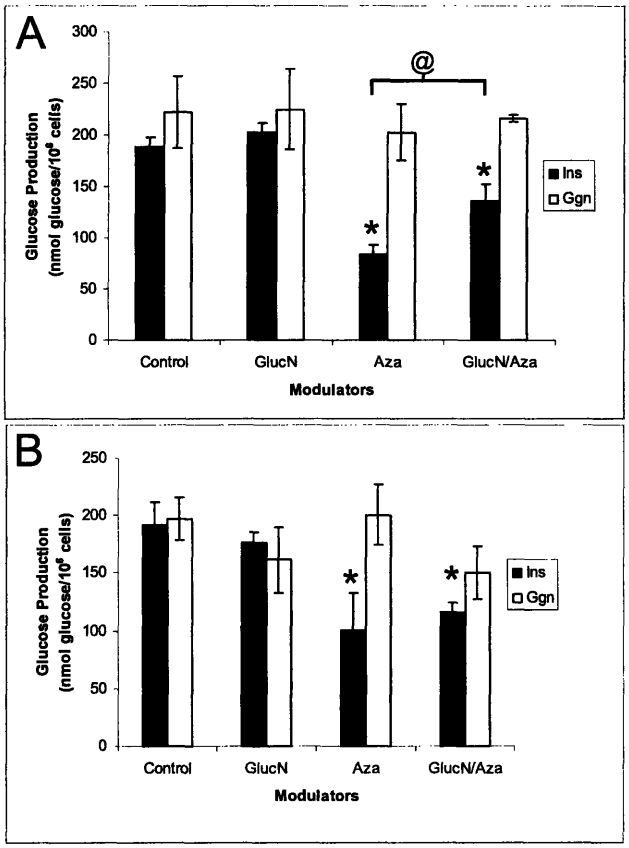

Figure 5.7. Glucose production response to 1 mM glucosamine and/or 10 μM azaserine treatment. Cells were incubated with glucosamine/azaserine in the 20 mM glucose Preincubation medium. A: Assay medium with lactate/pyruvate. B: Assay medium with lactate/pyruvate and glycerol. * = significant difference between "Ins" groups and their control ($P < 0.05$, n = 3 to 4). Dunnett's t test was used for all comparisons.

The glucose production experiments were repeated with 1.5 mM glycerol as an additional gluconeogenic substrate in the Assay medium (Fig. 5.6B). The Control group displayed very similar glucose production to the Control group in panel 5.6A despite the addition of glycerol. When 1 mM glucosamine was added to the Preincubation medium, glucose production in the presence of insulin was increased by 29% and glucose production in the presence of glucagon was decreased by 25%, as compared to Control. Again, the cells had decreased insulin and glucagon sensitivity. Addition of 3 mM alloxan did not have a significant effect on insulin suppression of glucose production. But when added with glucosamine, alloxan suppressed glucose production by 42% when compared with Control and 55% when compared with the GlucN treatment. These results with glycerol in the Assay medium were very similar to the results without glycerol, indicating that glycerol did not have a significant impact on the metabolism.

Next, the effect of glucosamine and/or azaserine was tested in the presence of 20 mM glucose Preincubation medium (Fig. 5.7). Panel A shows the results from adding lactate/pyruvate to the Assay medium. In contrast to 5 mM glucose Preincubation medium, the Control group in 20 mM glucose Preincubation medium had the highest glucose production, therefore was the least sensitive to insulin. Hyperglycemia had reduced insulin sensitivity, mirroring the results in glycogen deposition. There was no change in glucose production when 1 mM glucosamine was added. The addition of azaserine, on the other hand, increased the sensitivity of the cells to insulin, and glucose production was suppressed by 56% compared to the Control group with insulin. When both azaserine and glucosamine were added to the hepatocytes, the insulin suppression was not as effective. The addition of glucosamine increased glucose production by 62%

as compared to the treatment of azaserine alone. All treatments seemed to have no effect on the glucagon sensitivity.

The effect of glucosamine and/or azaserine was tested in the presence of 20 mM glucose Preincubation medium (Fig. 5.7B) with glycerol added to the Assay medium. Hyperglycemia reduced insulin sensitivity, and addition of 1 mM glucosamine to the Preincubation medium left the insulin suppression of glucose production unchanged. The addition of azaserine increased the sensitivity of the cells to insulin, and glucose production was suppressed by 47% when compared to the Control group with insulin. Addition of glucosamine and azaserine did not significantly change glucose production as compared to azaserine alone, but glucose production was still significantly below the Control level. These results largely agreed with the results obtained without glycerol in the Assay medium (Fig. 5.7A).

5.2.3 Metabolite Level Quantification

We further explored the intracellular effects of the different treatments by quantifying the relative changes in metabolite levels in response to the changes in glucose level and the addition of pharmacological agents. In all experiments, metabolite levels in a particular treatment were normalized to that same metabolite's level in a reference treatment (1 mM glucose Preincubation medium with no modulators), as mentioned in Materials and Methods. As such, all metabolites for the reference treatment would have relative metabolite levels of 1.0.

We first examined the hepatocytes with 5 mM glucose Preincubation medium (Table 5.1). The Control treatment showed that 5 mM glucose caused a mild buildup of

glycolytic and HBP intermediates in comparison to the reference state. GlucN treatment further increased glucose-6P levels, and drastically boosted all four HBP intermediates. Alloxan treatment made significant increases to upper glycolytic intermediates glucose-6P, fructose-6P, and PEP. However, it only increased the upper three HBP intermediates, and left the UDP-GlucNAc-1P pool unchanged. The combination of glucosamine and alloxan in the GlucN/Allox group produced an synergistic effect. Glucose-6P and fructose-6P were increased beyond what either single modulator had achieved. All four HBP intermediates were also increased in a synergistic fashion, ranging from 2× to 6× the amount in the Control group. In all four treatments, the TCA cycle intermediate levels were not perturbed from the reference state.

We then profiled the metabolites in several treatments with 20 mM glucose in the Preincubation medium (Table 5.2). In the Control group, the levels of glucose-6P, fructose-6P, and UDP-glucose-1P were higher than they were with 5 mM glucose. The upper three HBP intermediates were also increased over the 5 mM glucose treatment. When glucosamine was added to 20 mM glucose, the UDP-GlucNAc-1P pool was increased by almost 4×, and the citrate pool was decreased by nearly 40%. The addition of azaserine only increased the GlucNAc-6P pool over the Control group. The GlucN/Aza treatment resulted in a mild increase of GlucNAc and a 7× increase of UDP-GlucNAc-1P.

Table 5.1. Metabolite levels after treatment with 5 mM glucose Preincubation medium.

Pathway	Control	GlucN	Alloxan	GlucN/Allox
Glycolysis				
G6P	3.7 ± 0.5	4.9 ± 0.8	8.1 ± 1.1	12.6 ± 1.6
F6P	1.6 ± 0.1	1.7 ± 0.4	2.5 ± 0.3	3.7 ± 0.4
PEP	2.1 ± 0.4	2.1 ± 0.6	2.9 ± 0.6	2.9 ± 0.3
PYR	1.2 ± 0.2	0.9 ± 0.1	1.0 ± 0.2	0.8 ± 0.1
UDP-Gluc-1P	0.9 ± 0.1	0.8 ± 0.1	0.9 ± 0.2	1.0 ± 0.2
HBP				
GlucN6P	3.3 ± 0.3	4.8 ± 0.5	8.0 ± 0.9	12.0 ± 1.2
GlucNAc6P	2.2 ± 0.5	3.6 ± 0.6	3.7 ± 0.4	4.5 ± 0.6
GlucNAc	2.3 ± 0.3	3.3 ± 0.2	4.0 ± 0.5	4.9 ± 0.5
UDP-GlucNAc-1P	1.1 ± 0.2	4.9 ± 0.7	1.4 ± 0.2	6.5 ± 0.5
TCA Cycle				
Citrate	1.2 ± 0.2	0.8 ± 0.2	1.4 ± 0.2	1.2 ± 0.2
α-KG	1.1 ± 0.1	1.0 ± 0.1	1.2 ± 0.1	1.1 ± 0.1
Succinate	0.9 ± 0.1	0.9 ± 0.1	0.7 ± 0.1	0.8 ± 0.1
Fumarate	1.0 ± 0.1	0.8 ± 0.1	1.0 ± 0.1	0.9 ± 0.1
Malate	1.1 ± 0.1	0.9 ± 0.1	1.1 ± 0.1	0.9 ± 0.0

Values are means ± SD of n = 3 to 5 replicates. The values represent the ratio of the pool size of a particular metabolite in the indicated treatment with the pool size of the same metabolite in a reference treatment of 1 mM glucose and no modulators. Control, treatment with no modulators; GlucN, treatment with 1 mM glucosamine; Alloxan, treatment with 3 mM alloxan; Both, treatment with 1 mM glucosamine and 3 mM alloxan; UDP-Gluc-1P, combined pools of glucose-1P and UDP-glucose; UDP-GlucNAc-1P, combined pools of glucNAc-1P and UDP-glucNAc. All groups have 5 mM glucose.

Table 5.2. Metabolite levels after treatment with 20 mM glucose Preincubation medium.

Pathway	Control	GlucN	Azaserine	GlucN/Aza
Glycolysis				
G6P	7.6 ± 0.4	6.6 ± 0.7	7.2 ± 0.8	6.8 ± 0.7
F6P	7.1 ± 0.7	6.8 ± 0.6	7.3 ± 0.3	6.5 ± 0.6
PEP	1.3 ± 0.3	1.1 ± 0.2	1.8 ± 0.4	1.7 ± 0.3
PYR	1.4 ± 0.2	1.2 ± 0.2	1.6 ± 0.1	1.4 ± 0.2
UDP-Gluc-1P	1.9 ± 0.2	1.4 ± 0.2	2.5 ± 0.3	2.3 ± 0.3
HBP				
GlucN6P	8.4 ± 0.9	8.1 ± 0.5	8.4 ± 0.8	7.8 ± 0.7
GlucNAc6P	5.3 ± 0.2	4.0 ± 0.2	7.7 ± 0.6	5.5 ± 0.4
GlucNAc	3.8 ± 0.3	4.0 ± 0.4	4.2 ± 0.3	5.3 ± 0.2
UDP-GlucNAc-1P	1.2 ± 0.2	4.4 ± 0.3	1.6 ± 0.2	8.5 ± 0.4
TCA Cycle				
Citrate	1.6 ± 0.3	1.0 ± 0.1	1.7 ± 0.1	1.4 ± 0.2
α-KG	0.6 ± 0.1	0.6 ± 0.1	0.6 ± 0.1	0.6 ± 0.1
Succinate	0.9 ± 0.1	0.8 ± 0.0	1.0 ± 0.1	1.0 ± 0.1
Fumarate	1.3 ± 0.2	1.0 ± 0.0	1.4 ± 0.2	1.1 ± 0.1
Malate	1.4 ± 0.1	1.0 ± 0.1	1.5 ± 0.1	1.2 ± 0.1

Values are means ± SD of n = 3 to 5 replicates. The values represent the ratio of the pool size of a particular metabolite in the indicated treatment with the pool size of the same metabolite in a reference treatment of 1 mM glucose and no modulators. Control, treatment with no modulators; GlucN, treatment with 1 mM glucosamine; Azaserine, treatment with 10 μM azaserine; Both, treatment with 1 mM glucosamine and 10 μM azaserine; UDP-Gluc-1P, combined pools of glucose-1P and UDP-glucose; UDP-GlucNAc-1P, combined pools of glucNAc-1P and UDP-glucNAc. All groups have 20 mM glucose.

5.3 Discussion

Hyperglycemia is a main characteristic of Type 2 diabetes mellitus that stems from insulin resistance. It also contributes to disease pathogenesis by impairing both insulin sensitivity and insulin secretion (85, 95, 170, 209). Thus, hyperglycemia is not only a symptom of diabetes, but also a driving force that can sustain or worsen the diabetic state. A strong hypothesis for a cellular mechanism of hyperglycemia is its effect on the HBP. The elevated glucose concentration shunts carbon flux towards the HBP, increasing the generation of hexosamine intermediates. The latter, in turn, increase protein glycosylation and ultimately deactivate insulin signaling proteins (among other proteins), which induces further insulin resistance.

In the liver tissue, insulin action has the dual role of inducing glycogen synthesis and suppressing glucose production. The glycogen synthesis assay was only concerned with the activation of glycogen synthase by insulin (43, 97, 98). Insulin and glucagon affect glucose production by regulating several important enzymes in hepatic glucose production, which is the sum of glycogenolysis and gluconeogenesis. Insulin activates glycogen synthesis and glycolysis, while glucagon activates glycogenolysis and gluconeogenesis. Insulin activates glycogen synthase (43, 97, 98), glucokinase (79), and pyruvate kinase (17). Insulin antagonizes the activation of glycogen phosphorylase (78), PEPCK (12), G6Pase (12), pyruvate carboxylase (80). Glucagon exerts a repressive effect on glucokinase (79), pyruvate kinase (17), and glycogen synthase (51). Glucagon activates glycogen phosphorylase (78) and the key gluconeogenic enzymes PEPCK, G6Pase (12), and pyruvate carboxylase (80). Given the evidence that enhanced HBP

activity impairs insulin signaling (135, 138, 173), it follows that modulation of HBP activity may influence insulin regulation of glycogen deposition and glucose production.

5.3.1 Correlation of HBP Activity and Insulin Sensitivity

Previous investigators have used glucosamine to artificially increase HBP activity (10, 113-115, 137, 138, 154, 193). These experiments have shown that addition of glucosamine to cells or infusion of glucosamine into animals blunts the insulin-stimulated glucose uptake of muscle and adipose tissue. Our experiments showed that glucosamine decreased insulin sensitivity in mouse hepatocytes under the low glucose Preincubation treatment. Insulin stimulation of glycogen deposition and insulin suppression of glucose production were diminished by glucosamine. This suggested that the HBP activity in the low glucose Preincubation treatment was minimal and the addition of glucosamine increased it substantially, resulting in reduced insulin sensitivity. In contrast, the addition of glucosamine to high glucose Preincubation treatments had little effect on insulin sensitivity in terms of glucose production and glycogen deposition. So unlike the low glucose treatments, the HBP activity in the high glucose state was assumed to be near saturation, and glucosamine increased HBP activity only incrementally. Insulin sensitivity was therefore expected to be unchanged, and these data were consistent with the negative correlation between HBP activity and insulin sensitivity.

Regarding the inhibitory effect of glucosamine on glucose transport and phosphorylation, we examined the effect of glucosamine on the treatments without insulin. Glucosamine is phosphorylated to glucosamine-6-phosphate by glucokinase, and is therefore a competitive inhibitor of glucokinase with respect to glucose (11). This

inhibition of glucokinase and the use of the GLUT2 glucose transporter by glucosamine were possible contributors to insulin resistance outside of HBP effects. However, the glucosamine treatments were much less effective at reducing glycogen deposition without the presence of insulin. In the glucose production experiments, glucosamine had either no effect or decreased glucose production in the presence of glucagon, instead of increasing the glucose production as it did in the presence of insulin. These results indicate that the effects of glucosamine outside of the HBP were negligible in our system. The combination treatment of glucosamine with alloxan also provides key evidence that the insulin desensitizing effect of glucosamine was mainly due to increasing HBP activity. The treatment of the hepatocytes with alloxan alone did not affect insulin sensitivity at low or high Preincubation glucose (data not shown for alloxan treatments with high glucose incubation) for glycogen deposition or glucose production, making the case against alloxan affecting glucokinase activity or GLUT2 capacity by itself. However, when alloxan and glucosamine were added in combination at low glucose, alloxan improved insulin sensitivity in comparison to glucosamine alone, suggesting that alloxan stemmed the increase in HBP activity from glucosamine. Previous investigators have shown that alloxan was able to abolish the increase in glycosylation caused by glucosamine (91). Since it is unlikely that alloxan affected glucokinase activity or GLUT2 capacity, these data support the hypothesis that alloxan and glucosamine exerted an effect on insulin sensitivity by modulating HBP activity, and by extension, protein glycosylation. It is interesting to note that alloxan did not increase insulin sensitivity at high glucose Preincubation. One possible explanation is that glucose also generated aminosugars other than GlucNAc that affected insulin sensitivity, and alloxan was only

able to inhibit the *O*-GlcNAc transferase. The situation with alloxan is to be contrasted with azaserine, which was able to restore insulin sensitivity by inhibiting HBP activity further up in the pathway. Precluding glucose carbon from even entering the hexosamine metabolism seemed to be more effective than merely preventing *O*-GlcNAc transfer. From the behavior of these two inhibitors, it is plausible that aminosugars other than glucosamines, such as mannosamines and galactosamines, may also play a role in insulin sensitivity.

Azaserine has been used previously to increase the insulin sensitivity of glucose transport in primary adipocytes (111). Azaserine was theorized to increase insulin sensitivity by decreasing HBP activity through GFAT inhibition. Our data showed that azaserine had little effect on insulin action in the low glucose Preincubation treatment, and had a large positive effect in high glucose Preincubation treatment for both glycogen synthesis and glucose production. It was expected that azaserine would have a minimal, or perhaps detrimental, effect at low glucose because the activity of the HBP would be relatively small. The presence of high glucose provided a large carbon flux into the HBP that would distinguish between the presence and absence of azaserine. We saw that azaserine enhanced insulin sensitivity in glucose production as compared to the Control treatment, suggesting that hyperglycemia reduced insulin sensitivity through enhanced HBP activity. The combination of glucosamine with azaserine neutralized the increase in action provided by azaserine alone, both for glycogen deposition and glucose production. We hypothesize that glucosamine increased HBP activity in the presence of azaserine by entering the HBP downstream of GFAT (azaserine's inhibition target). Taken together, the data suggest that azaserine increased insulin sensitivity by decreasing HBP activity.

In total, the glycogen deposition and glucose production data suggest that the HBP activity correlated negatively with insulin sensitivity, and that the HBP was one mechanism by which prolonged hyperglycemia caused insulin resistance.

5.3.2 Modulator Mechanisms by Metabolite Profiling

We used metabolite profiling (53) to gain insight into the intracellular effects of increasing glucose from 5 mM to 20 mM and adding pharmacological agents to the medium. Raising the glucose level from 5 mM to 20 mM predictably raised hexose phosphates and most of the HBP intermediates, and yet, lower glycolytic intermediates such as phosphoenolpyruvate (PEP) and pyruvate were unchanged. These results are consistent with the hypothesis that excess fructose-6P was shunted into the HBP.

Addition of glucosamine to the 5 mM glucose Preincubation treatment increased all intermediates in the HBP, whereas the effect was much smaller in the 20 mM glucose Preincubation treatment. This is consistent with the previous result that glucosamine had a detrimental effect on insulin sensitivity at low glucose, but no effect at high glucose. We hypothesize that the activity of the HBP was enhanced by glucosamine at 5 mM glucose, whereas the HBP activity was already near its maximum at 20 mM glucose. Another interesting point was the differing levels of the UDP-GlcNAc/GlcNAc-1P pool between the high glucose treatments with and without glucosamine. It is known that GFAT is feedback inhibited by glucosamine-6P (24) and UDP-GlcNAc (60), and the addition of glucosamine seemed to bypass this inhibition. However, due to the measurement of the combined pool, we cannot say for certain this is the case. The addition of glucosamine to 5 mM glucose Preincubation medium did not decrease the

levels of glycolytic intermediates, indicating that inhibition of glucokinase may not have been significant.

The results of the alloxan treatment were consistent with the previously reported inhibition of *O*-GlcNAc transferase (91). HBP intermediates were greatly increased, and the effect extended to the hexose phosphates. Given their modes of action, it was not surprising to see that glucosamine and alloxan had synergistic effects on hexose phosphate and HBP intermediate levels. These results were consistent with the hypothesis that alloxan countered glucosamine's effects on insulin sensitivity by decreasing flow of HBP intermediates to protein glycosylation, corresponding to alloxan's restorative action in the insulin sensitivity experiments.

The inhibition of GFAT by azaserine was not apparent from the metabolite profiling data. It was expected that azaserine would decrease the concentration of HBP intermediates, but azaserine seemed to actually increase GlcNAc-6P. Since azaserine is a glutamine analog, it was possible that it could inhibit entry of glutamine into the TCA cycle. Our metabolite profiling data showed that the levels of α-ketoglutarate and other TCA cycle intermediates did not change with the addition of azaserine, suggesting that azaserine did not have an impact on the TCA cycle.

We were concerned with possible "side effects" of the metabolite level changes brought on by alloxan and glucosamine in the 5 mM Preincubation medium. Alloxan and glucosamine induced large changes in metabolite pools, which could have had some unintended effects on glycogen synthesis and glucose production. The dramatic increases in the G6P metabolite pool were of particular concern because G6P is an important substrate for the ensuing glycogen deposition and glucose production assays. However,

we noted that there was no effect on glycogen deposition in the absence of insulin when glucosamine was added. Addition of alloxan did not increase glycogen deposition or glucose production in the presence of insulin despite the doubling of G6P. Finally, addition of glucosamine and alloxan together cancelled out glucosamine's effects for glycogen deposition and glucose production. The sensitivity phenotypes of the hepatocytes in glycogen deposition and glucose production were the same with no modulators as with both modulators present even though the metabolite profiles were wildly different. It is possible that the washing step and the change to the Assay medium eliminated any differences in intracellular metabolite levels. These observations led us to conclude that the pharmacological side effects did not play a major role in insulin sensitivity.

5.3.3 Conclusions

Elucidation of the pathophysiology of Type 2 diabetes and the etiology of hyperglycemia-mediated diabetic complications is essential to the development of potential treatment strategies. We presented evidence that the HBP activity is negatively correlated with liver insulin sensitivity, and that the HBP is a mechanism for hyperglycemia-induced insulin resistance in primary hepatocytes. To our knowledge, these are the only data showing the effect of HBP activity on hepatocytes and on glucose production. Consequently, we now have evidence that the HBP plays a key role in sensing hyperglycemic conditions in all 3 peripheral insulin targets: liver, muscle, and adipose tissue. We postulate that this pathway, under chronic hyperglycemia, triggers a cascade of responses that lead to impaired insulin signaling and insulin resistance. The

data here and in previous HBP literature underline the increasingly important role of the HBP in regulating insulin sensitivity and energy homeostasis. A dysfunctional HBP may contribute to the pathophysiology of Type 2 diabetes.

Further studies are needed to confirm the role of the HBP in hepatic insulin resistance. In addition to the phenotypic and metabolite profiling data provided here, more detailed studies of the molecular actions of the HBP, similar to ones in muscle and adipose tissue, are needed. It is imperative that the assumed events between manipulation of HBP activity and the affected glycogen deposition or glucose production are consistent with our hypothesis that the HBP is modulating insulin sensitivity. That is, the glycosylation and phosphorylation states of insulin signaling proteins should correlate with the metabolic data, as should activity or transcription of metabolic enzymes in the glycogenesis or gluconeogenesis pathways.

6 Bioreaction Network Analysis Of Hepatic Glucose Production

6.1 Introduction

Hyperglycemia is both a common feature of Type 2 diabetes and a known inducer of insulin resistance in animal and cell culture models (111). Whole body studies in humans using the glucose clamp suggest that increased hepatic glucose production (HGP) is a major contributor to the hyperglycemia observed in Type 2 diabetes (122, 182). Despite differences in etiology in animal models of Type 2 diabetes (genetic, diet, or surgical), abnormalities in the control of HGP appear to be a common feature. With regard to the source of the excess HGP, there is evidence that increased gluconeogenesis is responsible for the elevated HGP observed in Type 2 diabetes (32). To better understand the factors regulating HGP, we examined the response of the HGP bioreaction network in cultured mouse hepatocytes to a set of systematic perturbations in order to gain insight into the physiology underlying the control of HGP.

We used an array of perturbations to gather a diverse set of data that represented many different glucose production phenotypes, as well as many configurations of the glucose production network. One set of perturbations was the use of insulin and glucagon to treat the hepatocytes. As shown in Fig. 2.4, insulin and glucagon affect glucose production by regulating several important enzymes in hepatic glucose

production, which is the sum of glycogenolysis and gluconeogenesis. Insulin activates glycogen synthesis and glycolysis, while glucagon activates glycogenolysis and gluconeogenesis (12, 17, 43, 51, 78-80, 97, 98).

Another perturbation was the preincubation of hepatocytes in hyperglycemic conditions. Prolonged hyperglycemia is known to induce insulin resistance in animal and cell culture systems (111), apparently through the increased generation of hexosamine metabolites and subsequent glycosylation of proteins with *N*-acetylglucosamine (GlcNAc) (135, 137, 138, 173). It was postulated that under conditions of hyperglycemia, approximately 1 to 3% of the glucose flux through glycolysis was shunted into the hexosamine biosynthetic pathway (HBP) (111, 112). In addition to hyperglycemia, we also chose to use pharmacological agents to modulate HBP activity. Alloxan (91) and azaserine (111) were used to limit HBP activity. Glucosamine (111, 113) was used to increase HBP activity. Thus, hyperglycemia and HBP activity seem to be connected and both seem to affect insulin sensitivity.

The final type of perturbation varied the gluconeogenic substrate availability with the presence and absence of glycerol in the Assay medium. The presence of glycerol gave the cells a gluconeogenic substrate that was unaffected by PEPCK activity, which became important in elucidating the control structure of the glucose production network.

The results revealed some of the principles determining the glucose production phenotype and the configuration of the bioreaction network. Hyperglycemia led to a greater contribution of glycogenolysis to glucose production, and the composition of the gluconeogenic flux was dependent on the available substrates. Perturbations in hyperglycemia, hormones, and HBP activity affected overall glucose production.

Gluconeogenesis was much larger than glycogenolysis, and therefore regulation of gluconeogenesis determined the glucose production phenotype. The prominence of gluconeogenesis agreed with results found in Type 2 diabetes patients and other animal models. G6Pase was identified as the enzyme in gluconeogenesis controlling the glucose production phenotype, whereas PEPCK played a secondary role.

6.2 Results

6.2.1 Relative Intracellular Flux Measurements

We estimated some of the intracellular fluxes that contributed to glucose production under different treatments. The glucose production data already showed that the absolute amount of glucose produced varied with different treatments, and subsequently we examined the changes in the central carbon flux map (Fig. 6.1) during the different treatments. Flux 1 represents the flux from glycogenolysis to G6P. Flux 2 represents the flux from gluconeogenesis to G6P. Flux 3 represents the flux from glycerol to gluconeogenesis. Flux 4 represents the net flux from DHAP to GAP, and flux 5 represents the flux from amino acids, lactate, and pyruvate to gluconeogenesis.

First, we labeled the Assay medium with 10% D_2O, leaving all other pre-assay conditions identical to those of the original glucose production experiments. These labeling experiments probed the glucose production results shown in Figs. 5.6A and 5.7A. As mentioned in the Methods, the isotopic labeling information allowed Metran to estimate fluxes 1, 2, 4, and 5 (Tables 6.1 and 6.2). Since there was no glycerol in the Assay medium, the lower gluconeogenic flux provided all of the gluconeogenic carbon.

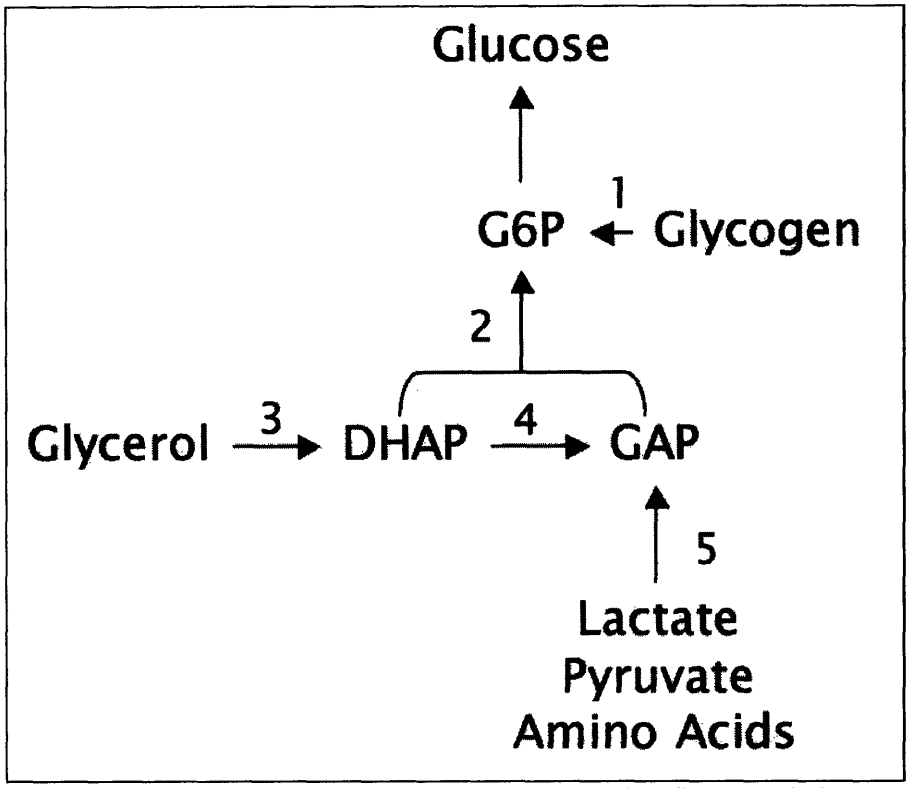

Figure 6.1. Metabolic network for glucose production flux calculations. 1, flux from glycogenolysis; 2, flux from gluconeogenesis; 3, gluconeogenic flux from glycerol to DHAP; 4, net flux from DHAP to GAP; 5, gluconeogenic flux from lactate, pyruvate, and amino acids.

Table 6.1. Relative glycogenolysis and gluconeogenesis fluxes assayed with D_2O labeling.

Glucose Level	Modulator	Hormone	Glycogenolysis	Gluconeogenesis
Low Glucose	Control	Ins	6.9 ± 1.3	93.1 ± 1.3
		Ggn	9.0 ± 1.3	91.0 ± 1.3
	GlucN	Ins	10.5 ± 1.3	89.5 ± 1.3
		Ggn	10.1 ± 1.3	89.9 ± 1.3
	Allox	Ins	10.4 ± 1.3	89.6 ± 1.3
		Ggn	9.2 ± 1.3	90.8 ± 1.3
	Both	Ins	10.3 ± 1.3	89.7 ± 1.3
		Ggn	11.7 ± 1.3	88.3 ± 1.3
High Glucose	Control	Ins	24.0 ± 0.7	76.0 ± 0.7
		Ggn	23.5 ± 0.6	76.5 ± 0.6
	GlucN	Ins	23.9 ± 0.6	76.1 ± 0.6
		Ggn	25.1 ± 0.6	74.9 ± 0.6
	Aza	Ins	29.5 ± 0.6	70.5 ± 0.6
		Ggn	27.3 ± 0.6	72.7 ± 0.6
	Both	Ins	28.5 ± 0.6	71.5 ± 0.6
		Ggn	22.8 ± 1.1	77.2 ± 1.1

Values are the optimal fluxes calculated by Metran to fit glucose isotopomer data, ± SD. The values represent the contribution of glycogenolysis (Flux 1) and gluconeogenesis (Flux 2) to glucose production (normalized to 100). Control, treatment with no modulators; GlucN, treatment with 1 mM glucosamine; Aza, treatment with 10 μM azaserine; Allox, treatment with 3 mM alloxan; Both, treatment with both modulators used in glucose group.

Table 6.2. Relative fluxes contributing to gluconeogenesis assayed with D_2O labeling

Glucose Level	Mod	Hormone	Low to GAP	DHAP to GAP
Low Glucose	Control	Ins	186.2 ± 2.7	-93.1 ± 1.3
		Ggn	182.0 ± 2.7	-91.0 ± 1.3
	GlucN	Ins	179.0 ± 2.6	-89.5 ± 1.3
		Ggn	179.8 ± 2.7	-89.9 ± 1.3
	Allox	Ins	179.2 ± 2.7	-89.6 ± 1.3
		Ggn	181.6 ± 2.7	-90.8 ± 1.3
	Both	Ins	179.4 ± 2.7	-89.7 ± 1.3
		Ggn	176.6 ± 2.7	-88.3 ± 1.3
High Glucose	Control	Ins	152.0 ± 1.4	-76.0 ± 0.7
		Ggn	153.0 ± 1.3	-76.5 ± 0.6
	GlucN	Ins	152.2 ± 1.3	-76.1 ± 0.7
		Ggn	149.8 ± 1.3	-74.9 ± 0.6
	Aza	Ins	141.0 ± 1.3	-70.5 ± 0.6
		Ggn	145.4 ± 1.3	-72.7 ± 0.6
	Both	Ins	143.0 ± 1.3	-71.5 ± 0.6
		Ggn	154.4 ± 2.7	-77.2 ± 1.4

Values are the optimal fluxes calculated by Metran to fit glucose isotopomer data, ± SD. The values represent the contribution of net DHAP → GAP (Flux 4) lower gluconeogenesis (Flux 5) to the gluconeogenesis (Flux 2) values shown in Table 6.1. Low to GAP = flux of lactate, pyruvate, and amino acids to GAP; DHAP to GAP = net flux from DHAP to GAP; Control, treatment with no modulators; GlucN, treatment with 1 mM glucosamine; Aza, treatment with 10 μM azaserine; Both, treatment with both modulators used in specific glucose group.

Table 6.3. Relative glycogenolysis and gluconeogenesis fluxes assayed with [U-^{13}C] glycerol labeling

Glucose Level	Modulator	Hormone	Glycogenolysis	Gluconeogenesis
Low Glucose	Control	Ins	10.4 ± 0.4	89.6 ± 0.4
		Ggn	11.2 ± 0.4	88.8 ± 0.4
	GlucN	Ins	11.7 ± 0.4	88.3 ± 0.4
		Ggn	10.9 ± 0.5	89.1 ± 0.5
	Allox	Ins	11.4 ± 0.4	88.6 ± 0.4
		Ggn	9.8 ± 0.4	90.2 ± 0.4
	Both	Ins	10.0 ± 0.3	90.0 ± 0.3
		Ggn	10.7 ± 0.4	89.3 ± 0.4
High Glucose	Control	Ins	18.3 ± 0.3	81.7 ± 0.3
		Ggn	17.9 ± 0.5	82.1 ± 0.5
	GlucN	Ins	18.4 ± 0.4	81.6 ± 0.4
		Ggn	17.4 ± 0.5	82.6 ± 0.5
	Aza	Ins	16.1 ± 0.4	83.9 ± 0.4
		Ggn	20.6 ± 0.5	79.4 ± 0.5
	Both	Ins	18.1 ± 0.4	81.9 ± 0.4
		Ggn	18.2 ± 0.4	81.8 ± 0.4

Values are the optimal fluxes calculated by Metran to fit glucose isotopomer data, ± SD. The values represent the contribution of glycogenolysis (Flux 1) and gluconeogenesis (Flux 2) to glucose production (normalized to 100). Control, treatment with no modulators; GlucN, treatment with 1 mM glucosamine; Aza, treatment with 10 μM azaserine; Allox, treatment with 3 mM alloxan; Both, treatment with both modulators used in specific glucose group.

Table 6.4. Relative fluxes contributing to gluconeogenesis assayed with [U-^{13}C] glycerol labeling

Glucose Level	Mod	Horm	Glyc to DHAP	Low to GAP	DHAP to GAP
Low Glucose	Control	Ins	91.2 ± 0.2	87.9 ± 0.9	1.6 ± 0.5
		Ggn	86.7 ± 0.2	90.9 ± 0.8	-2.1 ± 0.5
	GlucN	Ins	93.3 ± 0.2	83.3 ± 0.8	5.0 ± 0.5
		Ggn	87.6 ± 0.2	90.6 ± 1.0	-1.5 ± 0.5
	Allox	Ins	92.5 ± 0.2	84.7 ± 0.9	3.9 ± 0.5
		Ggn	88.1 ± 0.2	92.3 ± 0.8	-2.1 ± 0.5
	Both	Ins	93.4 ± 0.2	86.6 ± 0.7	3.4 ± 0.4
		Ggn	86.9 ± 0.2	91.7 ± 0.8	-2.4 ± 0.5
High Glucose	Control	Ins	84.4 ± 0.2	79.0 ± 0.7	2.7 ± 0.4
		Ggn	78.3 ± 0.2	85.9 ± 1.0	-3.8 ± 0.6
	GlucN	Ins	85.6 ± 0.2	77.6 ± 0.8	4.0 ± 0.5
		Ggn	81.8 ± 0.2	83.4 ± 1.0	-0.8 ± 0.5
	Aza	Ins	87.8 ± 0.2	80.0 ± 0.8	3.9 ± 0.5
		Ggn	79.3 ± 0.2	79.5 ± 0.9	-0.1 ± 0.5
	Both	Ins	87.6 ± 0.2	76.2 ± 0.8	5.7 ± 0.4
		Ggn	82.6 ± 0.2	81.1 ± 0.9	0.8 ± 0.5

Values are the optimal fluxes calculated by Metran to fit glucose isotopomer data, ± SD. The values represent the contributions of glycerol (Flux 3), net DHAP → GAP flux (Flux 4), and lower gluconeogenesis (Flux 5) to the gluconeogenesis values (Flux 2) shown in Table 6.3. Glyc to DHAP = flux of glycerol to DHAP; Low to GAP = flux of lactate, pyruvate, and amino acids to GAP; DHAP to GAP = net flux from DHAP to GAP; Control, treatment with no modulators; GlucN, treatment with 1 mM glucosamine; Aza, treatment with 10 μM azaserine; Both, treatment with both modulators used in specific glucose group.

Thus, its flux was not independent and was always double the gluconeogenic flux. The carbon from lower gluconeogenesis was split evenly between DHAP and GAP.

In another experiment, we added 1.5 mM [U-^{13}C] glycerol as the labeled substrate to the Assay medium. With the addition of glycerol, the assay conditions now corresponded to the glucose production results shown in Figs. 5.6B and 5.7B. This labeling strategy allowed the estimation of fluxes 1, 2, 3, 4, and 5 (Tables 6.3 and 6.4). As outlined in the Methods, these relative intracellular flux maps were the basis for calculating the absolute flux maps.

6.2.2 Absolute Intracellular Flux Measurements

The absolute fluxes for the D_2O labeling scheme are shown in Tables 6.5 and 6.6, and those for [U-^{13}C] glycerol labeling scheme are shown in Tables 6.7 and 6.8. Examination of the overall glucose production rates revealed that addition of glycerol to the Assay medium did not change the results significantly. However, changing the Preincubation glucose level had a large effect. Focusing on the Control groups, it was observed that high glucose Preincubation treatment reduced the glucose production significantly in the glucagon-treated Controls, but not insulin-treated Controls. The reduction in the glucagon-treated Control illustrated the suppression of glucose production by hyperglycemia *per se*. When azaserine was added, insulin suppression of glucose production was restored, and it was apparent that the high glucose Control group was insulin resistant. The glucose production in the insulin-treated high glucose Control group was significantly lower than that in the insulin-treated Control group with low

Table 6.5. Absolute glycogenolysis and gluconeogenesis fluxes assayed with D_2O labeling.

Glucose Level	Mod	Horm	Glycogenolysis	Gluconeogenesis	Total
Low Glucose	Control	Ins	13.8 ± 2.7	187.5 ± 4.6	201.3 ± 4.0[#]
		Ggn	29.5 ± 4.5	296.6 ± 11.8	326.1 ± 12.1
	GlucN	Ins	25.5 ± 3.5	216.1 ± 11.3	241.6 ± 12.1
		Ggn	26.8 ± 3.8	239.0 ± 13.2	265.7 ± 14.1
	Allox	Ins	19.9 ± 2.6	171.3 ± 6.0	191.2 ± 6.0
		Ggn	27.5 ± 4.1	272.4 ± 10.0	299.9 ± 10.1
	Both	Ins	21.7 ± 2.9	189.6 ± 4.6	211.4 ± 4.0
		Ggn	35.2 ± 4.2	264.7 ± 9.7	299.9 ± 10.1
High Glucose	Control	Ins	44.1 ± 2.9	139.3 ± 8.5	183.4 ± 11.0
		Ggn	52.1 ± 8.3	169.8 ± 26.7	221.9 ± 34.8*
	GlucN	Ins	48.3 ± 2.6	153.5 ± 7.1	201.7 ± 9.2
		Ggn	56.5 ± 9.8	169.0 ± 28.9	225.6 ± 38.5
	Aza	Ins	24.9 ± 2.8	59.5 ± 6.5	84.4 ± 9.2
		Ggn	55.5 ± 7.6	148.1 ± 20.0	203.6 ± 27.5
	Both	Ins	44.4 ± 6.9	111.5 ± 17.1	155.9 ± 23.8
		Ggn	46.5 ± 6.3	157.1 ± 19.9	203.6 ± 25.7

Values are the means ± SD (nmol/10^6 cells). Control, treatment with no modulators; GlucN, treatment with 1 mM glucosamine; Aza, treatment with 10 μM azaserine; Allox, treatment with 3 mM alloxan; Both, treatment with both modulators used in glucose group.

* denotes a significant difference when compared to Low Glucose-Control-Ggn treatment. $P < 0.05$.

[#] denotes a significant difference when compared to High Glucose-Aza-Ins treatment. $P < 0.05$.

Table 6.6. Absolute fluxes contributing to gluconeogenesis assayed with D_2O labeling

Glucose Level	Modulator	Hormone	Low to GAP	DHAP to GAP
Low Glucose	Control	Ins	374.8 ± 9.2	-187.4 ± 4.6
		Ggn	593.5 ± 23.6	-296.8 ± 11.8
	GlucN	Ins	432.4 ± 22.5	-216.2 ± 11.3
		Ggn	477.8 ± 26.3	-239.0 ± 13.2
	Allox	Ins	342.6 ± 12.0	-171.3 ± 6.0
		Ggn	544.7 ± 19.9	-272.5 ± 10.0
	Both	Ins	379.2 ± 9.2	-189.7 ± 4.6
		Ggn	529.7 ± 19.5	-264.8 ± 9.7
High Glucose	Control	Ins	278.8 ± 16.9	-139.4 ± 8.5
		Ggn	339.5 ± 53.4	-169.8 ± 26.7
	GlucN	Ins	307.0 ± 14.2	-153.5 ± 7.1
		Ggn	337.9 ± 57.8	-169.0 ± 28.9
	Aza	Ins	119.0 ± 13.0	-59.5 ± 6.5
		Ggn	296.0 ± 40.1	-148.0 ± 20.0
	Both	Ins	222.9 ± 34.2	-111.5 ± 17.1
		Ggn	314.3 ± 40.0	-157.2 ± 20.0

Values are the means ± SD (nmol/10^6 cells). Low to GAP = flux of lactate, pyruvate, and amino acids to GAP; DHAP to GAP = net flux from DHAP to GAP; Control, treatment with no modulators; GlucN, treatment with 1 mM glucosamine; Aza, treatment with 10 μM azaserine; Both, treatment with both modulators used in specific glucose group.

Table 6.7. Absolute glycogenolysis and gluconeogenesis fluxes assayed with [U-^{13}C] glycerol labeling

Glucose Level	Mod	Horm	Glycogenolysis	Gluconeogenesis	Total
Low Glucose	Control	Ins	21.3 ± 2.9	182.7 ± 23.8	204.0 ± 26.5#
		Ggn	37.1 ± 3.7	293.3 ± 27.2	330.5 ± 30.6
	GlucN	Ins	29.8 ± 1.1	225.2 ± 2.1	255.0 ± 2.0
		Ggn	28.5 ± 2.2	232.6 ± 14.6	261.1 ± 16.3
	Allox	Ins	20.5 ± 6.6	159.0 ± 50.6	179.5 ± 57.1
		Ggn	29.2 ± 1.8	268.7 ± 12.9	297.8 ± 14.3
	Both	Ins	11.8 ± 2.1	106.5 ± 18.4	118.3 ± 20.4
		Ggn	21.6 ± 2.1	180.4 ± 16.4	202.0 ± 18.4
High Glucose	Control	Ins	35.2 ± 3.6	156.7 ± 15.7	191.9 ± 19.2
		Ggn	35.3 ± 3.6	162.3 ± 15.8	197.7 ± 19.2*
	GlucN	Ins	30.4 ± 3.3	134.6 ± 14.1	165.0 ± 17.3
		Ggn	26.0 ± 4.1	123.7 ± 19.0	149.7 ± 23.0
	Aza	Ins	16.3 ± 5.3	85.4 ± 27.4	101.7 ± 32.6
		Ggn	41.5 ± 5.6	160.0 ± 21.4	201.5 ± 26.9
	Both	Ins	21.2 ± 1.5	95.8 ± 6.3	117.1 ± 7.7
		Ggn	27.2 ± 4.2	122.4 ± 18.8	149.7 ± 23.0

Values are the means ± SD (nmol/10^6 cells). Control, treatment with no modulators; GlucN, treatment with 1 mM glucosamine; Aza, treatment with 10 μM azaserine; Allox, treatment with 3 mM alloxan; Both, treatment with both modulators used in glucose group.

* denotes a significant difference when compared to Low Glucose-Control-Ggn treatment. $P < 0.05$.

# denotes a significant difference when compared to High Glucose-Aza-Ins treatment. $P < 0.05$.

Table 6.8. Absolute fluxes contributing to gluconeogenesis assayed with [U-^{13}C] glycerol labeling

Glucose Level	Modulator	Horm	Glyc to DHAP	Low to GAP	DHAP to GAP
Low Glucose	Control	Ins	186.1 ± 24.2	179.3 ± 23.4	3.3 ± 1.1
		Ggn	286.5 ± 26.5	300.4 ± 28.0	-6.9 ± 1.7
	GlucN	Ins	237.9 ± 2.0	212.4 ± 2.7	12.7 ± 1.2
		Ggn	228.7 ± 14.3	236.5 ± 15.0	-3.9 ± 1.4
	Allox	Ins	166.1 ± 52.8	152.1 ± 48.4	6.9 ± 2.4
		Ggn	262.5 ± 12.6	274.9 ± 13.4	-6.2 ± 1.4
	Both	Ins	110.5 ± 19.0	102.5 ± 17.7	4.0 ± 0.8
		Ggn	175.4 ± 16.0	185.3 ± 16.9	-4.8 ± 1.1
High Glucose	Control	Ins	162.0 ± 16.2	151.6 ± 15.2	5.2 ± 1.0
		Ggn	154.8 ± 15.0	169.8 ± 16.6	-7.5 ± 1.3
	GlucN	Ins	141.3 ± 14.8	128.1 ± 13.5	6.7 ± 1.0
		Ggn	122.5 ± 18.8	124.9 ± 19.3	-1.2 ± 0.8
	Aza	Ins	89.3 ± 28.6	81.4 ± 26.1	4.0 ± 1.4
		Ggn	159.8 ± 21.3	160.2 ± 21.4	-0.2 ± 1.0
	Both	Ins	102.5 ± 6.7	89.2 ± 5.9	6.6 ± 0.7
		Ggn	123.6 ± 19.0	121.3 ± 18.7	1.1 ± 0.8

Values are the means ± SD (nmol/10^6 cells). Glyc to DHAP = flux of glycerol to DHAP; Low to GAP = flux of lactate, pyruvate, and amino acids to GAP; DHAP to GAP = net flux from DHAP to GAP; Control, treatment with no modulators; GlucN, treatment with 1 mM glucosamine; Aza, treatment with 10 μM azaserine; Allox, treatment with 3 mM alloxan; Both, treatment with both modulators used in glucose group.

glucose preincubation, which again illustrated the suppression of glucose production by hyperglycemia *per se*.

We also observed that gluconeogenesis was a significantly larger flux than glycogenolysis in all treatments. Changes in the gluconeogenic flux largely, positive or negative, determined the glucose production phenotype, a result that was confirmed in the correlational analysis.

6.2.3 Correlational Analysis

The patterns in the data generated by the intracellular flux analysis were further analyzed by examining the possible correlations between each of the intracellular fluxes and the overall glucose production. Additionally, we created judicious data subsets and regressed each subset with the glucose production to search for a significant improvement in the correlations, as described in Methods. All parameters for the correlational analysis are listed in Table 6.9.

Figures 6.2 and 6.3 show the correlation of the glycogenolysis flux with glucose production with the data points as a single set (6.2) and after splitting the data set into Preincubation medium treatments with low and high glucose (6.3). Analysis of the residuals validated the two-group approach. It was apparent that the Preincubation glucose level indeed impacted the way glycogenolysis was used in glucose production. Splitting the glycogenolysis data according to other perturbations did not yield significant improvement in the residuals. We observed that the best-fit line for the low glucose data had a higher slope than the high glucose, which was reflective of the lower contribution of glycogenolysis to glucose production in the low glucose incubations. The difference

Table 6.9. Parameters for the best-fit lines in the correlational analysis.

Flux	Division	Slope	Intercept	SS_{all}	SS_{total}
Fluxes as single data sets					
1	--	2.15 ± 0.18	171.03 ± 5.08	935.7	1307.6
2	--	1.04 ± 0.03	19.67 ± 6.61	28.8	1307.6
3	--	1.00 ± 0.05	19.14 ± 10.62	7.1	1085.6
4	--	0.06 ± 0.01	232.56 ± 1.77	1053.4	1289.2
5	--	0.11 ± 0.01	196.95 ± 3.82	993.2	1289.2
Fluxes split into 2 sets				$SS_{subgroup}$	SS_{total}
1	High Glucose	3.46 ± 0.33	35.17 ± 11.73	32.7	171.6
	Low Glucose	4.48 ± 0.24	124.97 ± 6.44	123.6	464.4
2	High Glucose	1.26 ± 0.11	3.41 ± 13.12	3.4	171.6
	Low Glucose	1.18 ± 0.06	-12.64 ± 11.95	6.4	464.4
4	No Glycerol	-0.98 ± 0.05	26.6 ± 8.79	23.2	507.0
	Glycerol	6.47 ± 0.81	207.11 ± 4.71	396.3	1085.6
5	No Glycerol	0.49 ± 0.02	26.63 ± 8.79	23.0	507.0
	Glycerol	1.10 ± 0.05	20.68 ± 10.56	7.9	1085.6

Fluxes are numbered as in Fig. 6.1. "Division" indicates how the data set was split. "High Glucose" denotes 20 mM glucose Preincubation treatment. "Low Glucose" denotes 5 mM glucose Preincubation treatment. "No Glycerol" denotes no glycerol in the Assay medium. "Glycerol" denotes 1.5 mM glycerol in the Assay medium.

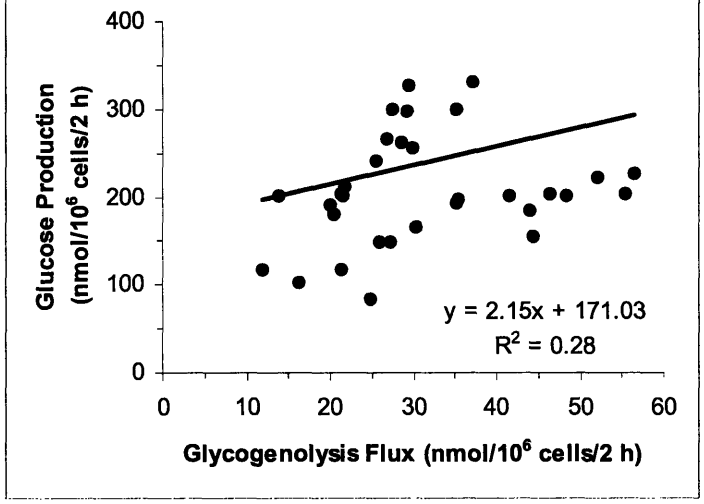

Figure 6.2. Correlation of glycogenolysis flux to glucose production with a single regression. Data points included were all 32 glycogenolysis and glucose production flux measurements from the D_2O and [U-^{13}C] glycerol labeling schemes.

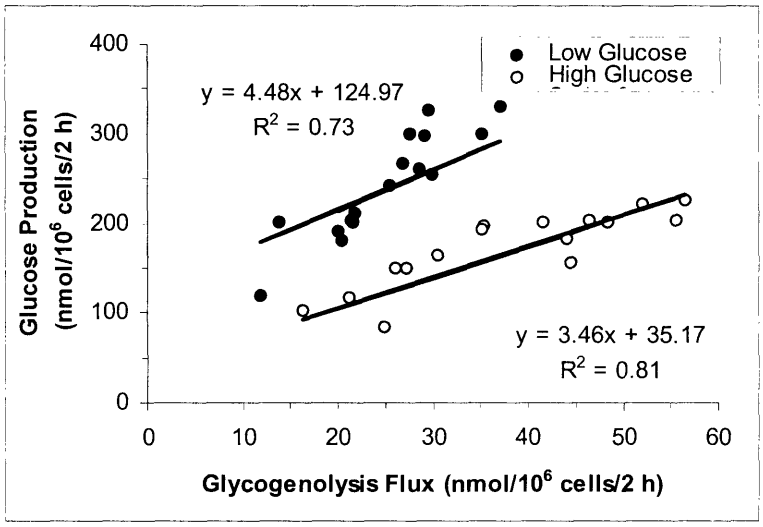

Figure 6.3. Correlation of glycogenolysis flux to glucose production after regressing low and high glucose Preincubation treatments separately. Data points included were all 32 glycogenolysis and glucose production flux measurements from the D_2O and [U-^{13}C] glycerol labeling schemes.

in the y-intercepts was also reflective of the larger contribution of glycogenolysis glucose production in the high glucose Preincubation treatment. We hypothesized that the relationship between glycogenolysis and glucose production varied with the amount of glycogen stored, assuming that high glucose preincubation resulted in a larger glycogen store. After the high glucose Preincubation treatment, the hepatocytes apparently utilized glycogen in a more aggressive manner to produce glucose.

Figures 6.4 and 6.5 show the correlation of the gluconeogenesis flux with glucose production as a single data set (6.4) and after splitting the data set into Preincubation medium treatments with low and high glucose (6.5). Analysis of the residuals validated the two-group approach, although the improvement was not as large as in the glycogenolysis case. We again concluded that the Preincubation glucose level impacted the way gluconeogenesis was used in glucose production, but not to the extent as in glycogenolysis. Splitting the gluconeogenesis data according to other perturbations did not yield significant improvement in the residuals. In both regressions, the slopes of the best-fit lines were near 1.0 and the y-intercepts were near 0, reflecting the dominating contribution of gluconeogenesis to glucose production. The large contribution of gluconeogenesis combined with the higher R^2 coefficients for gluconeogenesis suggested that gluconeogenesis contributed to glucose production in a more profound, perhaps even more controlling manner relative to glycogenolysis under all perturbations – hormones, Preincubation glucose level, glycerol availability, and HBP activity.

Next, we correlated the glycerol uptake to glucose production (Fig. 6.6). The data points included here were the 16 conditions from the [U-^{13}C] glycerol labeling experiment. Glycerol uptake correlated very well with glucose production and, by

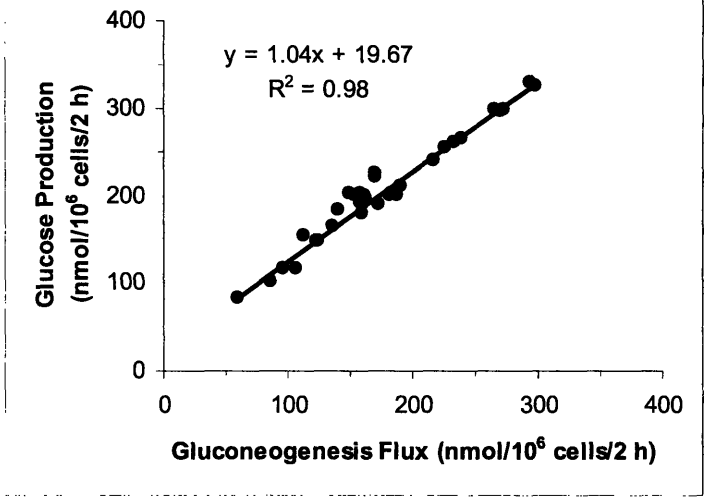

Figure 6.4. Correlation of gluconeogenesis flux to glucose production with a single regression. Data points included were all 32 gluconeogenesis and glucose production flux measurements from both D_2O and [U-^{13}C] glycerol labeling schemes.

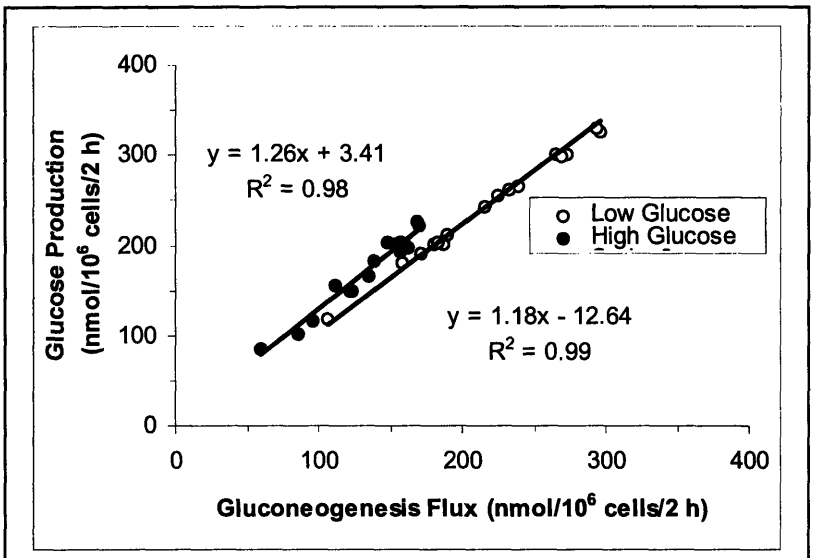

Figure 6.5. Correlation of gluconeogenesis flux to glucose production after regressing low and high glucose Preincubation treatments separately. Data points included were all 32 gluconeogenesis and glucose production flux measurements from the D_2O and [U-^{13}C] glycerol labeling schemes.

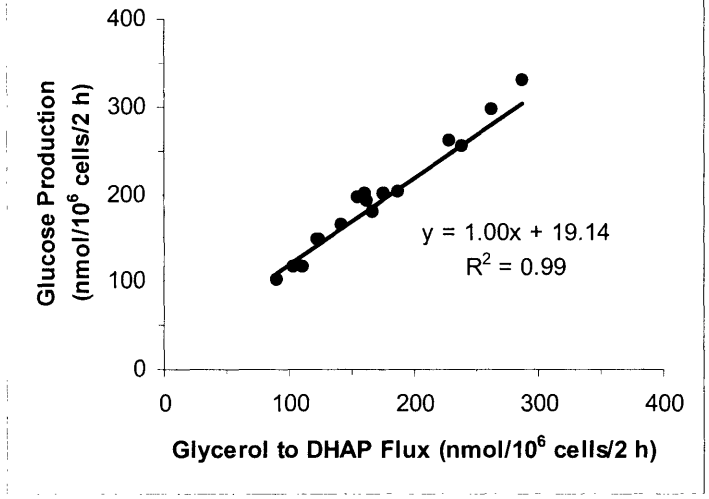

Figure 6.6. Correlation of glycerol to DHAP flux to glucose production. Data points included were all 16 glycerol to DHAP and glucose production flux measurements from the [U-^{13}C] glycerol labeling scheme.

association, total gluconeogenesis. The slope of the best-fit line was ~1, which corresponded to glycerol contributing half the 3-carbon units going towards gluconeogenesis.

Figures 6.7 and 6.8 show the correlation of the net DHAP → GAP flux to glucose production as a single data set (6.7) and after splitting the data set into Assay medium incubations with and without glycerol (6.8). Analysis of the residuals showed that the two-group regression was appropriate, and the net DHAP → GAP flux behavior depended on the availability of gluconeogenic substrates. The net DHAP → GAP flux was dependent on the gluconeogenic flux in the no glycerol case, and so it was expected to be well correlated to glucose production. The case with glycerol showed a weak correlation with glucose production, as well as a small magnitude.

Figures 6.9 and 6.10 show the correlation of the lower gluconeogenic flux to glucose production in a single data set (6.9) and after splitting the data set into Assay medium incubations with and without glycerol (6.10). Analysis of the residuals validated the two-group approach. Splitting the lower gluconeogenesis data according to other perturbations did not yield significant improvement in the residuals. We observed that the availability of glycerol changed the manner in which lower gluconeogenesis was used to supply 3-carbon units for gluconeogenesis. In the case without glycerol, the slope of the best-fit line was ~ 0.5 because lower gluconeogenesis provided all of the 3-carbon units for glucose production. With glycerol, the slope of the best-fit line was ~ 1 because lower gluconeogenesis only provided half of the 3-carbon units for glucose production. This behavior of the lower gluconeogenesis pathway indicated that its utilization for

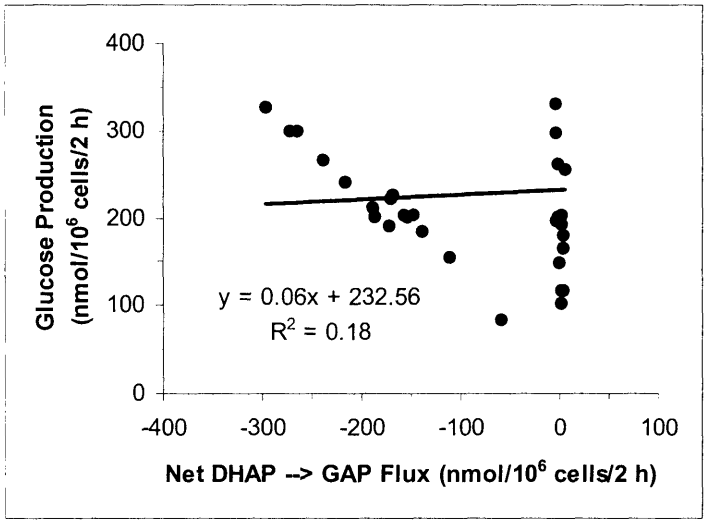

Figure 6.7. Correlation of net DHAP → GAP flux to glucose production with a single regression. Data points included were all 32 net DHAP → GAP and glucose production flux measurements from the D_2O and [U-^{13}C] glycerol labeling schemes.

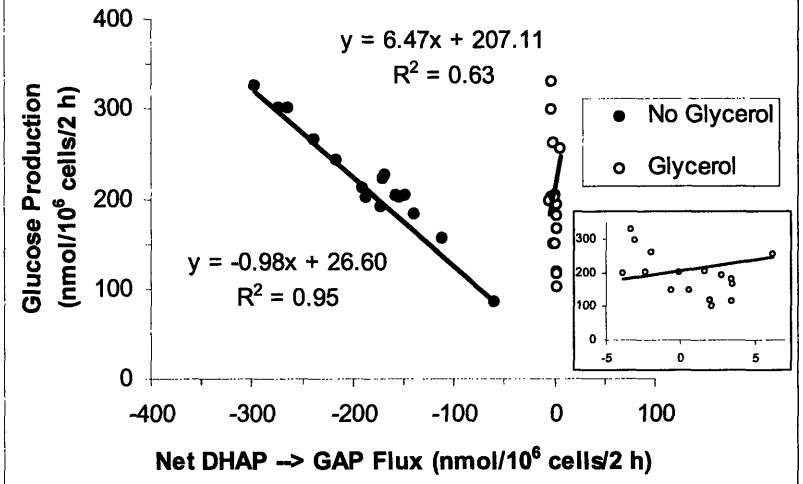

Figure 6.8. Correlation of net DHAP → GAP flux to glucose production after regressing Assay medium incubations with and without glycerol separately. Data points included were all 32 net DHAP → GAP and glucose production flux measurements from the D_2O and [U-^{13}C] glycerol labeling schemes. The inset graph shows data from the [U-^{13}C] glycerol labeling on a more appropriate scale.

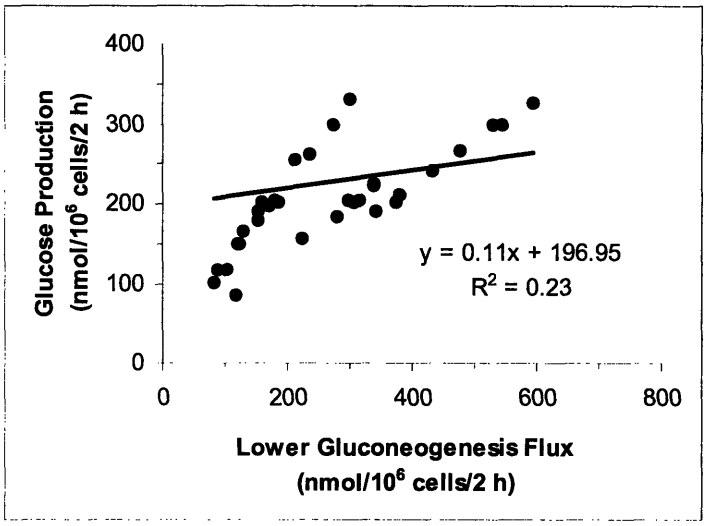

Figure 6.9. Correlation of lower gluconeogenesis flux to glucose production with a single regression. Data points included were all 32 lower gluconeogenesis and glucose production flux measurements from the D_2O and [U-^{13}C] glycerol labeling schemes.

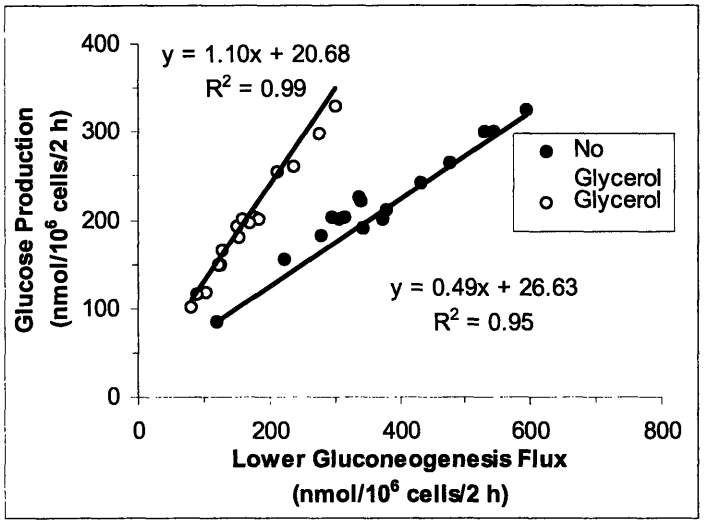

Figure 6.10. Correlation of lower gluconeogenesis flux to glucose production after regressing Assay medium incubations with and without glycerol separately. Data points included were all 32 lower gluconeogenesis and glucose production flux measurements from the D_2O and [U-^{13}C] glycerol labeling schemes.

glucose production was dependent on the availability of gluconeogenic substrates. The presence of glycerol greatly reduced the use of lactate, which was the largest initial extracellular substrate pool in lower gluconeogenesis.

6.3 Discussion

6.3.1 Control of Glucose Production Network

We combined the glucose production data, absolute flux maps, and correlational analysis to gain insight into the structure of the glucose production network and the control of the glucose production phenotype. We found that perturbations in the Preincubation glucose level led to changes in the configuration of the G6P node and in the overall glucose production. First, the Preincubation glucose level defined the interaction of glycogenolysis and gluconeogenesis at the G6P node, as shown in the correlational analysis. In both interaction regimes, the gluconeogenic flux was the dominant factor in determining glucose production. Second, the Preincubation glucose level also affected overall glucose production in a two-fold manner. High glucose Preincubation treatment blunted glucose production in the glucagon-treated Control groups. This inhibition of glucose production by hyperglycemia *per se* was in agreement with previous literature (1, 16, 52, 58, 162, 168, 169, 172). Hyperglycemic preincubation also induced insulin resistance, which was corrected by addition of azaserine. The dominant role of gluconeogenesis during these phenotypic changes suggested that the regulation and dysregulation of HGP was dependent on gluconeogenesis.

Changes in glycerol availability had effects that were limited to the reconfiguration of the pathways contributing to gluconeogenesis. Besides the obvious changes to glycerol uptake and net DHAP → GAP flux, the availability of glycerol also revealed the flexibility of the lower gluconeogenesis branch. Without glycerol, lower gluconeogenesis carried a very high flux (exactly double that of overall gluconeogenesis), which we assumed to originate largely from lactate/pyruvate. With glycerol in the Assay medium, that flux was approximately halved, and yet the total gluconeogenic flux and overall glucose production stayed approximately the same. Since all other conditions were identical, it was likely that there was excess lower gluconeogenic capacity when glycerol was available. Therefore, *within a given gluconeogenic substrate environment*, the lower gluconeogenesis flux was very well correlated with glucose production. But *across different substrate availabilities*, the lower gluconeogenesis flux changed drastically without affecting the glucose production phenotype. It was clear from this behavior that the fluxes from glycerol and lower gluconeogenesis were coordinated to fulfill the demand for gluconeogenic substrates to produce G6P. We think it would be interesting to test if other gluconeogenic substrates such as alanine, aspartate, and acetate act with a similar coordination.

In contrast to the perturbations of Preincubation glucose level and Assay medium glycerol, the different treatments of hormones and HBP activity modulation modified the overall glucose production without reconfiguring the network. The intracellular fluxes moved in concert along the best-fit line that related them to glucose production. In general, glucagon increased glucose production, and insulin decreased it. Two-group regressions split according to hormone treatment were not statistically accepted. This

result indicates that hormone treatments acted through similar mechanisms, which is consistent with the knowledge that glucagon and insulin affect the same enzymes in glucose production. Modulation of glucose production through HBP activity may have come about by modifying hormone action (25).

On the basis of these observations, we hypothesize the control structure of the glucose production network to be as follows. G6Pase consumption of G6P sets the demand for G6P production. Depending on the glycogen store size, glycogenolysis and gluconeogenesis fulfilled the G6P production in a coordinated manner, with higher glycogen content (i.e., high glucose preincubation) increasing the contribution of glycogenolysis. Gluconeogenesis was always a much larger flux and less random, and so the regulation or dysregulation of gluconeogenesis dominated the glucose production phenotype. The pathways supplying 3-carbon units for gluconeogenesis were then coordinated according to the availability of gluconeogenic substrates. In this hierarchy, we concluded that the driving force that determined the glucose production phenotype was the G6Pase activity. PEPCK activity was normally secondary in hierarchy, but gained importance when there was no glycerol available and lactate/pyruvate was the only significant gluconeogenic substrate in the Assay medium. It is our hypothesis, then, that G6Pase activity determined the glucose production phenotype, and that dysregulation of G6Pase can lead to insulin resistant phenotypes.

The association of G6Pase and PEPCK dysregulation with Type 2 diabetes is consistent with our conclusion about the importance of gluconeogenesis in insulin resistant glucose production phenotypes. Normally, gluconeogenesis is responsible for the sustained production of glucose in fasting animals (86, 96), but it is inappropriately

active in the diabetic state. In the liver, dysfunctional regulation of PEPCK and G6Pase gene promoters was associated with the pathophysiology of Type 2 diabetes (13, 156, 184, 187). In individuals with Type 2 diabetes, altered rates of gluconeogenesis were responsible for increased hepatic glucose production and the observed chronic hyperglycemia (31, 32, 41, 105). In diabetic rats, Rossetti et al. found a marked increase in hepatic glucose production (~2-fold), glucose cycling (2.7-fold), and gluconeogenesis (2.7-fold), while the rate of hepatic glycogenolysis was similar to that in control animals. Furthermore, the increment in hepatic glucose production above control levels could be accounted for entirely by the marked increase in gluconeogenic flux (158). Our hypothesis regarding the dominant role of G6Pase in gluconeogenesis may add to our understanding of the dysregulation of HGP in Type 2 diabetes.

6.3.2 Conclusions

Elucidation of the pathophysiology of Type 2 diabetes and the etiology of hyperglycemia-mediated diabetic complications is paramount in the development of a treatment strategy. With that goal in mind, our study examined the structure of the glucose production network in hepatocytes. Through intracellular flux maps and correlational analysis, we found that the dysregulation of gluconeogenesis was mainly responsible for the insulin resistance seen in hepatocytes under prolonged hyperglycemia. Perturbations in hormones and HBP activity affected overall glucose production, while perturbations in glycerol availability affected the configuration of the glucose production network. Perturbations in the glucose preincubation level affected both. Taking all the data into account, we concluded that G6Pase was the most important enzyme in

determining the glucose production phenotype. Although PEPCK was also an important enzyme in gluconeogenesis, its importance was secondary to G6Pase in the control hierarchy, except when lower gluconeogenesis provided all the gluconeogenic carbon.

We think it would be very useful in future studies to assay the mRNA expression of G6Pase under insulin regulation after perturbing the system with Preincubation glucose level, hormones, and HBP activity. Further efforts must also be put forth to characterize the regulation of this complex, multifunctional enzyme by insulin and glucagon, with the goal of understanding its possible dysregulation in Type 2 diabetes.

7 Conclusions And Recommendations

7.1 Conclusions

It was demonstrated in this thesis that the integration of gene expression data and different types of metabolic data can provide valuable insight into the physiology of a cellular system. The overall phenotype characterization provided by radioisotope-incorporation/release flux measurements or biochemical assays give the researcher a simple, coarse-grain picture of the metabolism to evaluate the overall response of the system. Correlation with gene expression data can suggest interesting candidates for the drivers of that response at the expression level. Then, metabolite profiling and stable isotope flux calculations can be done to explore the details behind the overall phenotype and increase the understanding of the phenomena leading to the cellular response. If these calculations can be detailed enough to be evaluated in the background of previous biological knowledge about the regulation of metabolism, then the integration of knowledge makes the conclusions that can be drawn much more valuable.

The method presented in this thesis for functional genomics is an alternative to what has been published previously in the field. The use of a metabolic flux pattern for correlation to gene expression profiles provided a more specific functional endpoint for the coregulated gene clusters in question. The use of the pattern discovery tool Teiresias was also shown. This body of work is in need of validation to confirm the actual function

of the gene clusters that were found. The more expedient method may be to take the genes that were anticorrelated with the glycolytic flux, and suppress them by RNAi. Then the cells could be assayed to confirm that expression of these genes was necessary for the reduction of the glycolytic flux.

This thesis also presented data showing the HBP as a causal mechanism for hyperglycemia-induced insulin resistance. The activity of the HBP was negatively correlated with liver insulin sensitivity. These data agree with literature showing HBP-induced insulin resistance in muscle and adipose tissue, completing the analysis of the major peripheral insulin-sensitive tissues. These studies make it increasingly likely that HBP is a major player in the exacerbation of the insulin resistant state in Type 2 diabetes, as well as a primary factor in the development of insulin resistance.

Finally, the analysis of the glucose production bioreaction network revealed several features of the network. The intracellular flux data and correlational analysis presented revealed that dysregulation of gluconeogenesis was responsible for the loss of insulin sensitivity in glucose production. It was also found that the gluconeogenic enzyme G6Pase was ultimately responsible for the glucose production phenotype. Thus, the regulation of G6Pase and gluconeogenesis are of utmost concern in controlling hepatic glucose overproduction in Type 2 diabetes.

7.2 Recommendations

In this context, I propose that future work in the area of HBP research concentrate on these goals:

- Identification of molecular events in hyperglycemia-induced insulin resistance in hepatocytes
- Identification of targets of HBP regulation
- Characterization of effects of HBP activity on G6Pase/PEPCK mRNA expression
- Correlation of HBP activity and insulin resistance in humans
- Identification of polymorphisms in HBP enzymes associated with insulin resistance in humans.

The first three points suggest research that will be done in animals or cells, and the last two points will be researched in humans. These thrusts will define the scope of HBP regulation of energy homeostasis and define the impact of the HBP on human insulin resistance and Type 2 diabetes.

As mentioned in Chapter 5, the metabolic effects described provide the impetus for molecular studies. The progression of research in muscle and adipose tissue advanced in the same fashion: metabolic studies to identify the gross effect of hyperglycemia, and then molecular studies to flesh out the events in between. The hepatocyte studies are starting later, but will likely follow the same trajectory as the other tissues. The timeline will probably be shorter, as the hepatocyte studies will be guided by the preceding studies in the other two tissues.

The work on the identification of the targets of HBP regulation is progressing steadily. The regulation of targets by the HBP is carried out by reversible glycosylation by *O*-GlcNAc residues on target proteins. This regulation is akin to the mechanism of phosphorylation. As mentioned in Chapter 5, several insulin signaling intermediates

have been shown to be regulated by *O*-GlcNAc glycosylation. It has been demonstrated that glycosylation of insulin signaling proteins inhibited their phosphorylation. This presents a very strong model for the HBP disruption of glucose uptake in muscle and adipose, glycogen synthesis in muscle and liver, and suppression of glucose production in liver. However, it is known that *O*-GlcNAc glycosylation affects many other pathways. Beyond insulin signaling, increased HBP flux was shown to increase leptin production in 3T3-L1 adipocytes through transcriptional mechanisms (213). Gronning et al. showed that hyperglycemia increased the levels of transcription repressor Id2 through the HBP (61). Id2 is a protein that indirectly regulates gene expression by sequestering certain transcription factors and preventing them from forming functional dimers. Id2 targets include the class-A bHLH transcription factors and the sterol regulatory element binding protein 1 (SREBP-1). Id2 blocked the SREBP1 induced induction of hormone sensitive lipase promoter activity. Rumberger et al. showed that increased HBP flux upregulated mRNA transcription of fatty acid synthase, acetyl-CoA carboxylase, and glycerol-3-phosphate dehydrogenase (161). Such regulation may connect the HBP with the Type 2 diabetes characteristic of dyslipidemia. These results show that the domain of HBP regulation goes far beyond glucose metabolism. The HBP truly has a role in overall energy homeostasis.

The next logical step after identifying HBP glycosylation targets is to check the on expression of target genes. In the case of insulin signaling proteins, the targets are known. Concentrating on glucose production, the main targets are G6Pase and PEPCK. Insulin signaling should normally repress the expression of these genes, and an increase in HBP flux should release the repression. To our knowledge, no group has examined

these gene expression effects. In studies in muscle and adipose tissue, the phenotypic measurement of insulin sensitivity was GLUT4 translocation for glucose uptake, which did not involve gene expression mechanisms. In this study, it seems clear that gene expression plays a role, due to the known transcriptional mechanisms of G6Pase and PEPCK regulation by insulin.

There are very few clinical studies examining the role of the HBP in human insulin resistance. Two studies using glucosamine infusions found no effects on glucose utilization during a euglycemic insulin clamp or on hepatic glucose production. Humans may be less sensitive to the insulin resistance-promoting effect of GlucN than rodents (125, 142). In two other studies, the hypothesis of a simple positive correlation between hexosamine intermediate levels in muscle or adipose tissue and insulin resistance was not supported (143, 144). However, I think the variables studied here were ambiguous. The levels of hexosamine intermediates provide no information about the flux going through the pathway to protein glycosylation. It is the protein glycosylation that is associated with insulin resistance. With more informative human studies, we will find out if the human results correspond to the results from animals and cells.

The hyperglycemia and the activity of the HBP represent the effects of the nutritional environment, and the other side of the equation is the genetic makeup of the individual. The introduction mentioned the polymorphisms studied so far that have been associated with insulin resistance and Type 2 diabetes. Since there is such a mountain of evidence regarding HBP's role as a secondary factor in exacerbating the insulin resistant state, I would not be surprised if polymorphisms in HBP enzymes turned out to be primary defects associated with insulin resistance. Indeed, some genetic studies have

uncovered polymorphisms connecting the HBP and insulin resistance. Four hundred and twelve Caucasian nondiabetic, metabolically characterized individuals were screened for expression of two single-nucleotide polymorphisms in the 5'-flanking region of GFAT. One of them (–913 G/A) was associated with a significantly higher body mass index, percent body fat, and increased intramyocellular lipid content in males but no in females (196). A recent publication reports that a single-nucleotide polymorphism in intron 10 of the gene expressing *O*-GlcNAcase is associated with Type 2 diabetes in Mexican Americans (99). Intron 10 contains an alternate stop codon and may lead to decreased expression of the 130-kDa isoforms, which is predicted to contain the *O*-GlcNAcase activity. The gene is located on chromosome 10q and overlaps a region that has been previously shown to be associated with Type 2 diabetes.

As the field of hexosamine biosynthetic pathway research matures, I think it will make a significant contribution to the understanding of insulin resistance pathophysiology. Although the role of the HBP in human insulin resistance is currently undetermined, the strong evidence in animals and the preliminary evidence in humans make it seem likely that a role for the HBP in the development of insulin resistance and Type 2 diabetes will prevail. The management of Type 2 diabetes may indeed involve therapies that attempt to decrease the activity of the HBP by inhibiting one of more of its key enzymes. Understanding the HBP's connection with insulin signaling, leptin signaling, and other energy homeostasis-related endocrinology will be important in understanding the pathogenesis of Type 2 diabetes and slowing it down.

References

1. **Ader M, Pacini G, Yang YJ, and Bergman RN.** Importance of glucose per se to intravenous glucose tolerance. Comparison of the minimal-model prediction with direct measurements. *Diabetes* 34: 1092-1103, 1985.

2. **Agius L and Alberti KG.** Regulation of flux through pyruvate dehydrogenase and pyruvate carboxylase in rat hepatocytes. Effects of fatty acids and glucagon. *Eur J Biochem* 152: 699-707, 1985.

3. **Alessi DR and Cohen P.** Mechanism of activation and function of protein kinase B. *Curr Opin Genet Dev* 8: 55-62, 1998.

4. **Alizadeh AA, Eisen MB, Davis RE, Ma C, Lossos IS, Rosenwald A, Boldrick JC, Sabet H, Tran T, Yu X, Powell JI, Yang L, Marti GE, Moore T, Hudson J, Jr., Lu L, Lewis DB, Tibshirani R, Sherlock G, Chan WC, Greiner TC, Weisenburger DD, Armitage JO, Warnke R, Levy R, Wilson W, Grever MR, Byrd JC, Botstein D, Brown PO, and Staudt LM.** Distinct types of diffuse large B-cell lymphoma identified by gene expression profiling. *Nature* 403: 503-511, 2000.

5. **Andjelkovic M, Alessi DR, Meier R, Fernandez A, Lamb NJ, Frech M, Cron P, Cohen P, Lucocq JM, and Hemmings BA.** Role of translocation in the activation and function of protein kinase B. *J Biol Chem* 272: 31515-31524, 1997.

6. **Ardawi MS and Newsholme EA.** Glutamine metabolism in lymphocytes of the rat. *Biochem J* 212: 835-842, 1983.

7. **Babadjanova G, Allolio B, Beuschlein F, Chuchalin A, and Reincke M.** Polymorphism of the glycogen synthase gene and non-insulin-dependent diabetes mellitus in the Russian population. *Metabolism* 46: 121-122, 1997.

8. **Baier LJ, Permana PA, Yang X, Pratley RE, Hanson RL, Shen GQ, Mott D, Knowler WC, Cox NJ, Horikawa Y, Oda N, Bell GI, and Bogardus C.** A calpain-10 gene polymorphism is associated with reduced muscle mRNA levels and insulin resistance. *J Clin Invest* 106: R69-73, 2000.

9. **Bailey CJ and Turner RC.** Metformin. *N Engl J Med* 334: 574-579, 1996.

10. **Bailey CJ and Turner SL.** Glucosamine-induced insulin resistance in L6 muscle cells. *Diabetes Obes Metab* 6: 293-298, 2004.

11. **Balkan B and Dunning BE.** Glucosamine inhibits glucokinase in vitro and produces a glucose-specific impairment of in vivo insulin secretion in rats. *Diabetes* 43: 1173-1179, 1994.

12. **Barthel A and Schmoll D.** Novel concepts in insulin regulation of hepatic gluconeogenesis. *Am J Physiol Endocrinol Metab* 285: E685-692, 2003.

13. **Barzilai N and Rossetti L.** Role of glucokinase and glucose-6-phosphatase in the acute and chronic regulation of hepatic glucose fluxes by insulin. *J Biol Chem* 268: 25019-25025, 1993.

14. **Baumann CA, Ribon V, Kanzaki M, Thurmond DC, Mora S, Shigematsu S, Bickel PE, Pessin JE, and Saltiel AR.** CAP defines a second signalling pathway required for insulin-stimulated glucose transport. *Nature* 407: 202-207, 2000.

15. **Baynes KC, Beeton CA, Panayotou G, Stein R, Soos M, Hansen T, Simpson H, O'Rahilly S, Shepherd PR, and Whitehead JP.** Natural variants of human p85 alpha phosphoinositide 3-kinase in severe insulin resistance: a novel variant with impaired insulin-stimulated lipid kinase activity. *Diabetologia* 43: 321-331, 2000.

16. **Bell PM, Firth RG, and Rizza RA.** Effects of hyperglycemia on glucose production and utilization in humans. Measurement with [23H]-, [33H]-, and [614C]glucose. *Diabetes* 35: 642-648, 1986.

17. **Blair JB, Cimbala MA, Foster JL, and Morgan RA.** Hepatic pyruvate kinase. Regulation by glucagon, cyclic adenosine 3'-5'-monophosphate, and insulin in the perfused rat liver. *J Biol Chem* 251: 3756-3762, 1976.

18. **Bode BP and Souba WW.** Glutamine transport and human hepatocellular transformation. *JPEN J Parenter Enteral Nutr* 23: S33-37, 1999.

19. **Bogardus C, Lillioja S, Stone K, and Mott D.** Correlation between muscle glycogen synthase activity and in vivo insulin action in man. *J Clin Invest* 73: 1185-1190, 1984.

20. **Bolouri H and Davidson EH.** Modeling transcriptional regulatory networks. *Bioessays* 24: 1118-1129, 2002.

21. **Bouche C, Serdy S, Kahn CR, and Goldfine AB.** The cellular fate of glucose and its relevance in type 2 diabetes. *Endocr Rev* 25: 807-830, 2004.

22. **Brass EP and Vetter WH.** Interleukin-6, but not tumour necrosis factor-alpha, increases lipogenesis in rat hepatocyte primary cultures. *Biochem J* 301 (Pt 1): 193-197, 1994.

23. **Broderick TL, Quinney HA, and Lopaschuk GD.** Carnitine stimulation of glucose oxidation in the fatty acid perfused isolated working rat heart. *J Biol Chem* 267: 3758-3763, 1992.

24. **Broschat KO, Gorka C, Page JD, Martin-Berger CL, Davies MS, Huang Hc HC, Gulve EA, Salsgiver WJ, and Kasten TP.** Kinetic characterization of human glutamine-fructose-6-phosphate amidotransferase I: potent feedback inhibition by glucosamine 6-phosphate. *J Biol Chem* 277: 14764-14770, 2002.

25. **Buse MG.** Hexosamines, insulin resistance, and the complications of diabetes: current status. *Am J Physiol Endocrinol Metab* 290: E1-E8, 2006.

26. **Butler M, McKay RA, Popoff IJ, Gaarde WA, Witchell D, Murray SF, Dean NM, Bhanot S, and Monia BP.** Specific inhibition of PTEN expression reverses hyperglycemia in diabetic mice. *Diabetes* 51: 1028-1034, 2002.

27. **Chiang SH, Baumann CA, Kanzaki M, Thurmond DC, Watson RT, Neudauer CL, Macara IG, Pessin JE, and Saltiel AR.** Insulin-stimulated GLUT4 translocation requires the CAP-dependent activation of TC10. *Nature* 410: 944-948, 2001.

28. **Clare A and King RD.** How well do we understand the clusters found in microarray data? *In Silico Biol* 2: 511-522, 2002.

29. **Clement S, Krause U, Desmedt F, Tanti JF, Behrends J, Pesesse X, Sasaki T, Penninger J, Doherty M, Malaisse W, Dumont JE, Le Marchand-Brustel Y, Erneux C, Hue L, and Schurmans S.** The lipid phosphatase SHIP2 controls insulin sensitivity. *Nature* 409: 92-97, 2001.

30. **Cohen P.** The role of protein phosphorylation in neural and hormonal control of cellular activity. *Nature* 296: 613-620, 1982.

31. **Consoli A and Nurjhan N.** Contribution of gluconeogenesis to overall glucose output in diabetic and nondiabetic men. *Ann Med* 22: 191-195, 1990.

32. **Consoli A, Nurjhan N, Capani F, and Gerich J.** Predominant role of gluconeogenesis in increased hepatic glucose production in NIDDM. *Diabetes* 38: 550-557, 1989.

33. **Cooper S and Shedden K.** Microarray analysis of gene expression during the cell cycle. *Cell Chromosome* 2: 1, 2003.

34. **Cox NJ.** Challenges in identifying genetic variation affecting susceptibility to type 2 diabetes: examples from studies of the calpain-10 gene. *Hum Mol Genet* 10: 2301-2305, 2001.

35. **Crook ED and McClain DA.** Regulation of glycogen synthase and protein phosphatase-1 by hexosamines. *Diabetes* 45: 322-327, 1996.

36. **Cusi K, Consoli A, and DeFronzo RA.** Metabolic effects of metformin on glucose and lactate metabolism in noninsulin-dependent diabetes mellitus. *J Clin Endocrinol Metab* 81: 4059-4067, 1996.

37. **Damsbo P, Vaag A, Hother-Nielsen O, and Beck-Nielsen H.** Reduced glycogen synthase activity in skeletal muscle from obese patients with and without type 2 (non-insulin-dependent) diabetes mellitus. *Diabetologia* 34: 239-245, 1991.

38. **Darlington GJ, Bernhard HP, Miller RA, and Ruddle FH.** Expression of liver phenotypes in cultured mouse hepatoma cells. *J Natl Cancer Inst* 64: 809-819, 1980.

39. **Decaux JF, Antoine B, and Kahn A.** Regulation of the expression of the L-type pyruvate kinase gene in adult rat hepatocytes in primary culture. *J Biol Chem* 264: 11584-11590, 1989.

40. **Deeb SS, Fajas L, Nemoto M, Pihlajamaki J, Mykkanen L, Kuusisto J, Laakso M, Fujimoto W, and Auwerx J.** A Pro12Ala substitution in PPARgamma2 associated with decreased receptor activity, lower body mass index and improved insulin sensitivity. *Nat Genet* 20: 284-287, 1998.

41. **DeFronzo RA and Ferrannini E.** Insulin resistance. A multifaceted syndrome responsible for NIDDM, obesity, hypertension, dyslipidemia, and atherosclerotic cardiovascular disease. *Diabetes Care* 14: 173-194, 1991.

42. **del Bosque-Plata L, Aguilar-Salinas CA, Tusie-Luna MT, Ramirez-Jimenez S, Rodriguez-Torres M, Auron-Gomez M, Ramirez E, Velasco-Perez ML, Ramirez-Silva A, Gomez-Perez F, Hanis CL, Tsuchiya T, Yoshiuchi I, Cox NJ, and Bell GI.** Association of the calpain-10 gene with type 2 diabetes mellitus in a Mexican population. *Mol Genet Metab* 81: 122-126, 2004.

43. **Dent P, Lavoinne A, Nakielny S, Caudwell FB, Watt P, and Cohen P.** The molecular mechanism by which insulin stimulates glycogen synthesis in mammalian skeletal muscle. *Nature* 348: 302-308, 1990.

44. **DeRisi JL, Iyer VR, and Brown PO.** Exploring the metabolic and genetic control of gene expression on a genomic scale. *Science* 278: 680-686, 1997.

45. **Des Rosiers C, Di Donato L, Comte B, Laplante A, Marcoux C, David F, Fernandez CA, and Brunengraber H.** Isotopomer analysis of citric acid cycle and gluconeogenesis in rat liver. Reversibility of isocitrate dehydrogenase and involvement of ATP-citrate lyase in gluconeogenesis. *J Biol Chem* 270: 10027-10036, 1995.

46. **Donnelly M and Scheffler IE.** Energy metabolism in respiration-deficient and wild type Chinese hamster fibroblasts in culture. *J Cell Physiol* 89: 39-51, 1976.

47. **Ek J, Andersen G, Urhammer SA, Hansen L, Carstensen B, Borch-Johnsen K, Drivsholm T, Berglund L, Hansen T, Lithell H, and Pedersen O.** Studies of the Pro12Ala polymorphism of the peroxisome proliferator-activated receptor-gamma2 (PPAR-gamma2) gene in relation to insulin sensitivity among glucose tolerant caucasians. *Diabetologia* 44: 1170-1176, 2001.

48. **Elchebly M, Payette P, Michaliszyn E, Cromlish W, Collins S, Loy AL, Normandin D, Cheng A, Himms-Hagen J, Chan CC, Ramachandran C, Gresser MJ, Tremblay ML, and Kennedy BP.** Increased insulin sensitivity and obesity resistance in mice lacking the protein tyrosine phosphatase-1B gene. *Science* 283: 1544-1548, 1999.

49. **Erion MD, van Poelje PD, Dang Q, Kasibhatla SR, Potter SC, Reddy MR, Reddy KR, Jiang T, and Lipscomb WN.** MB06322 (CS-917): A potent and selective inhibitor of fructose 1,6-bisphosphatase for controlling gluconeogenesis in type 2 diabetes. *Proc Natl Acad Sci U S A* 102: 7970-7975, 2005.

50. **Evans JC, Frayling TM, Cassell PG, Saker PJ, Hitman GA, Walker M, Levy JC, O'Rahilly S, Rao PV, Bennett AJ, Jones EC, Menzel S, Prestwich P, Simecek N, Wishart M, Dhillon R, Fletcher C, Millward A, Demaine A, Wilkin T, Horikawa Y, Cox NJ, Bell GI, Ellard S, McCarthy MI, and Hattersley AT.** Studies of association between the gene for calpain-10 and type 2 diabetes mellitus in the United Kingdom. *Am J Hum Genet* 69: 544-552, 2001.

51. **Exton JH, Blackmore PF, El-Refai MF, Dehaye JP, Strickland WG, Cherrington AD, Chan TM, Assimacopoulos-Jeannet FD, and Chrisman TD.** Mechanisms of hormonal regulation of liver metabolism. *Adv Cyclic Nucleotide Res* 14: 491-505, 1981.

52. **Ferrannini E, Locatelli L, Jequier E, and Felber JP.** Differential effects of insulin and hyperglycemia on intracellular glucose disposition in humans. *Metabolism* 38: 459-465, 1989.

53. **Fiehn O, Kopka J, Trethewey RN, and Willmitzer L.** Identification of uncommon plant metabolites based on calculation of elemental compositions using gas chromatography and quadrupole mass spectrometry. *Anal Chem* 72: 3573-3580, 2000.

54. **Friedman DL and Larner J.** Studies on Udpg-Alpha-Glucan Transglucosylase. Iii. Interconversion of Two Forms of Muscle Udpg-Alpha-Glucan Transglucosylase by a Phosphorylation-Dephosphorylation Reaction Sequence. *Biochemistry* 128: 669-675, 1963.

55. **George S, Rochford JJ, Wolfrum C, Gray SL, Schinner S, Wilson JC, Soos MA, Murgatroyd PR, Williams RM, Acerini CL, Dunger DB, Barford D, Umpleby AM, Wareham NJ, Davies HA, Schafer AJ, Stoffel M, O'Rahilly S, and Barroso I.** A family with severe insulin resistance and diabetes due to a mutation in AKT2. *Science* 304: 1325-1328, 2004.

56. **Gitzelmann R, Steinmann B, and Van Den Berghe G.** In: *The Metabolic and Molecular Basis of Inherited Disease*, edited by Scriver CR, Beaudet AL, Sly WS and Valle D. New York: McGraw-Hill, 1995, p. 905-934.

57. **Glantz SA and Slinker BK.** *Primer of Applied Regression and Analysis of Variance*. New York, NY: McGraw-Hill, Inc, 1990.

58. **Glinsmann WH, Hern EP, and Lynch A.** Intrinsic regulation of glucose output by rat liver. *Am J Physiol* 216: 698-703, 1969.

59. **Gloyn AL, Weedon MN, Owen KR, Turner MJ, Knight BA, Hitman G, Walker M, Levy JC, Sampson M, Halford S, McCarthy MI, Hattersley AT, and Frayling TM.** Large-scale association studies of variants in genes encoding the pancreatic beta-cell KATP channel subunits Kir6.2 (KCNJ11) and SUR1 (ABCC8) confirm that the KCNJ11 E23K variant is associated with type 2 diabetes. *Diabetes* 52: 568-572, 2003.

60. **Graack HR, Cinque U, and Kress H.** Functional regulation of glutamine:fructose-6-phosphate aminotransferase 1 (GFAT1) of Drosophila melanogaster in a UDP-N-acetylglucosamine and cAMP-dependent manner. *Biochem J* 360: 401-412, 2001.

61. **Gronning LM, Tingsabadh R, Hardy K, Dahlen KT, Jat PS, Gnudi L, and Shepherd PR.** Glucose induces increases in levels of the transcriptional repressor Id2 via the hexosamine pathway. *Am J Physiol Endocrinol Metab*, 2005.

62. **Groop LC, Kankuri M, Schalin-Jantti C, Ekstrand A, Nikula-Ijas P, Widen E, Kuismanen E, Eriksson J, Franssila-Kallunki A, Saloranta C, and et al.** Association between polymorphism of the glycogen synthase gene and non-insulin-dependent diabetes mellitus. *N Engl J Med* 328: 10-14, 1993.

63. **Gunther EC, Stone DJ, Gerwien RW, Bento P, and Heyes MP.** Prediction of clinical drug efficacy by classification of drug-induced genomic expression profiles in vitro. *Proc Natl Acad Sci U S A* 100: 9608-9613, 2003.

64. **Hachey DL, Parsons WR, McKay S, and Haymond MW.** Quantitation of monosaccharide isotopic enrichment in physiologic fluids by electron ionization or

negative chemical ionization GC/MS using di-O-isopropylidene derivatives. *Anal Chem* 71: 4734-4739, 1999.

65. **Hall RK, Yamasaki T, Kucera T, Waltner-Law M, O'Brien R, and Granner DK.** Regulation of phosphoenolpyruvate carboxykinase and insulin-like growth factor-binding protein-1 gene expression by insulin. The role of winged helix/forkhead proteins. *J Biol Chem* 275: 30169-30175, 2000.

66. **Hansen L, Zethelius B, Berglund L, Reneland R, Hansen T, Berne C, Lithell H, Hemmings BA, and Pedersen O.** In vitro and in vivo studies of a naturally occurring variant of the human p85alpha regulatory subunit of the phosphoinositide 3-kinase: inhibition of protein kinase B and relationships with type 2 diabetes, insulin secretion, glucose disappearance constant, and insulin sensitivity. *Diabetes* 50: 690-693, 2001.

67. **Hara A and Radin NS.** Lipid extraction of tissues with a low-toxicity solvent. *Anal Biochem* 90: 420-426, 1978.

68. **Herzig S, Long F, Jhala US, Hedrick S, Quinn R, Bauer A, Rudolph D, Schutz G, Yoon C, Puigserver P, Spiegelman B, and Montminy M.** CREB regulates hepatic gluconeogenesis through the coactivator PGC-1. *Nature* 413: 179-183, 2001.

69. **Hill MM, Andjelkovic M, Brazil DP, Ferrari S, Fabbro D, and Hemmings BA.** Insulin-stimulated protein kinase B phosphorylation on Ser-473 is independent of its activity and occurs through a staurosporine-insensitive kinase. *J Biol Chem* 276: 25643-25646, 2001.

70. **Hirota K, Daitoku H, Matsuzaki H, Araya N, Yamagata K, Asada S, Sugaya T, and Fukamizu A.** Hepatocyte nuclear factor-4 is a novel downstream target of insulin via FKHR as a signal-regulated transcriptional inhibitor. *J Biol Chem* 278: 13056-13060, 2003.

71. **Holleran AL, Briscoe DA, Fiskum G, and Kelleher JK.** Glutamine metabolism in AS-30D hepatoma cells. Evidence for its conversion into lipids via reductive carboxylation. *Mol Cell Biochem* 152: 95-101, 1995.

72. **Holleran AL, Lindenthal B, Aldaghlas TA, and Kelleher JK.** Effect of tamoxifen on cholesterol synthesis in HepG2 cells and cultured rat hepatocytes. *Metabolism* 47: 1504-1513, 1998.

73. **Horikawa Y, Oda N, Cox NJ, Li X, Orho-Melander M, Hara M, Hinokio Y, Lindner TH, Mashima H, Schwarz PE, del Bosque-Plata L, Oda Y, Yoshiuchi I, Colilla S, Polonsky KS, Wei S, Concannon P, Iwasaki N, Schulze J, Baier LJ, Bogardus C, Groop L, Boerwinkle E, Hanis CL, and Bell GI.** Genetic variation in the gene encoding calpain-10 is associated with type 2 diabetes mellitus. *Nat Genet* 26: 163-175, 2000.

74. **Hughes TR, Marton MJ, Jones AR, Roberts CJ, Stoughton R, Armour CD, Bennett HA, Coffey E, Dai H, He YD, Kidd MJ, King AM, Meyer MR, Slade D, Lum PY, Stepaniants SB, Shoemaker DD, Gachotte D, Chakraburtty K, Simon J, Bard M, and Friend SH.** Functional discovery via a compendium of expression profiles. *Cell* 102: 109-126, 2000.

75. **Husson A, Quillard M, Fairand A, Chedeville A, and Lavoinne A.** Hypoosmolarity and glutamine increased the beta-actin gene transcription in isolated rat hepatocytes. *FEBS Lett* 394: 353-355, 1996.

76. **Huxtable SJ, Saker PJ, Haddad L, Walker M, Frayling TM, Levy JC, Hitman GA, O'Rahilly S, Hattersley AT, and McCarthy MI.** Analysis of parent-offspring trios provides evidence for linkage and association between the insulin gene and type 2 diabetes mediated exclusively through paternally transmitted class III variable number tandem repeat alleles. *Diabetes* 49: 126-130, 2000.

77. **Ideker T, Thorsson V, Ranish JA, Christmas R, Buhler J, Eng JK, Bumgarner R, Goodlett DR, Aebersold R, and Hood L.** Integrated genomic and proteomic analyses of a systematically perturbed metabolic network. *Science* 292: 929-934, 2001.

78. **Ishibashi K, Fujioka T, and Ui M.** Insulin increased cAMP phosphodiesterase activity antagonizing metabolic actions of glucagon in rat hepatocytes cultured with herbimycin A. *Eur J Pharmacol* 409: 109-121, 2000.

79. **Iynedjian PB.** Mammalian glucokinase and its gene. *Biochem J* 293 (Pt 1): 1-13, 1993.

80. **Jitrapakdee S and Wallace JC.** Structure, function and regulation of pyruvate carboxylase. *Biochem J* 340 (Pt 1): 1-16, 1999.

81. **Kadowaki T, Kadowaki H, and Yazaki Y.** Polymorphism of the glycogen synthase gene and non-insulin-dependent diabetes mellitus. *N Engl J Med* 328: 1568-1569, 1993.

82. **Kaestner KH.** The hepatocyte nuclear factor 3 (HNF3 or FOXA) family in metabolism. *Trends Endocrinol Metab* 11: 281-285, 2000.

83. **Kaestner KH, Katz J, Liu Y, Drucker DJ, and Schutz G.** Inactivation of the winged helix transcription factor HNF3alpha affects glucose homeostasis and islet glucagon gene expression in vivo. *Genes Dev* 13: 495-504, 1999.

84. **Kaibori M, Kwon AH, Teshima S, Nakanishi H, Kitano T, Kamiyama Y, and Okumura T.** Hepatocyte growth factor inhibits insulin-stimulated glycogen synthesis in primary cultured hepatocytes. *J Hepatol* 38: 407-413, 2003.

85. **Karam JH.** Reversible insulin resistance in non-insulin-dependent diabetes mellitus. *Horm Metab Res* 28: 440-444, 1996.

86. **Katz J and Tayek JA.** Gluconeogenesis and the Cori cycle in 12-, 20-, and 40-h-fasted humans. *Am J Physiol* 275: E537-542, 1998.

87. **Kelleher JK and Masterson TM.** Model equations for condensation biosynthesis using stable isotopes and radioisotopes. *Am J Physiol* 262: E118-125, 1992.

88. **Kim SK, Lund J, Kiraly M, Duke K, Jiang M, Stuart JM, Eizinger A, Wylie BN, and Davidson GS.** A gene expression map for Caenorhabditis elegans. *Science* 293: 2087-2092, 2001.

89. **Knott JH.** Short History of the Discovery and Treatment of Diabetes. http://www.diabetesliving.com/basics/history.htm. June 21, 2005.

90. **Kohn AD, Summers SA, Birnbaum MJ, and Roth RA.** Expression of a constitutively active Akt Ser/Thr kinase in 3T3-L1 adipocytes stimulates glucose uptake and glucose transporter 4 translocation. *J Biol Chem* 271: 31372-31378, 1996.

91. **Konrad RJ, Zhang F, Hale JE, Knierman MD, Becker GW, and Kudlow JE.** Alloxan is an inhibitor of the enzyme O-linked N-acetylglucosamine transferase. *Biochem Biophys Res Commun* 293: 207-212, 2002.

92. **Kornfeld R.** Studies on L-glutamine D-fructose 6-phosphate amidotransferase. I. Feedback inhibition by uridine diphosphate-N-acetylglucosamine. *J Biol Chem* 242: 3135-3141, 1967.

93. **Kotani K, Ogawa W, Matsumoto M, Kitamura T, Sakaue H, Hino Y, Miyake K, Sano W, Akimoto K, Ohno S, and Kasuga M.** Requirement of atypical protein kinase clambda for insulin stimulation of glucose uptake but not for Akt activation in 3T3-L1 adipocytes. *Mol Cell Biol* 18: 6971-6982, 1998.

94. **Krause U, Bertrand L, Maisin L, Rosa M, and Hue L.** Signalling pathways and combinatory effects of insulin and amino acids in isolated rat hepatocytes. *Eur J Biochem* 269: 3742-3750, 2002.

95. **Kruszynska YT and Olefsky JM.** Cellular and molecular mechanisms of non-insulin dependent diabetes mellitus. *J Investig Med* 44: 413-428, 1996.

96. **Landau BR, Wahren J, Chandramouli V, Schumann WC, Ekberg K, and Kalhan SC.** Contributions of gluconeogenesis to glucose production in the fasted state. *J Clin Invest* 98: 378-385, 1996.

97. **Larner J.** Insulin and the stimulation of glycogen synthesis. The road from glycogen structure to glycogen synthase to cyclic AMP-dependent protein kinase to insulin mediators. *Adv Enzymol Relat Areas Mol Biol* 63: 173-231, 1990.

98. **Lawrence JC, Jr. and Zhang JN.** Control of glycogen synthase and phosphorylase by amylin in rat skeletal muscle. Hormonal effects on the phosphorylation of phosphorylase and on the distribution of phosphate in the synthase subunit. *J Biol Chem* 269: 11595-11600, 1994.

99. **Lehman DM, Fu DJ, Freeman AB, Hunt KJ, Leach RJ, Johnson-Pais T, Hamlington J, Dyer TD, Arya R, Abboud H, Goring HH, Duggirala R, Blangero J, Konrad RJ, and Stern MP.** A single nucleotide polymorphism in MGEA5 encoding O-GlcNAc-selective N-acetyl-beta-D glucosaminidase is associated with type 2 diabetes in Mexican Americans. *Diabetes* 54: 1214-1221, 2005.

100. **Liao J, Barthel A, Nakatani K, and Roth RA.** Activation of protein kinase B/Akt is sufficient to repress the glucocorticoid and cAMP induction of phosphoenolpyruvate carboxykinase gene. *J Biol Chem* 273: 27320-27324, 1998.

101. **Lock LS, Royal I, Naujokas MA, and Park M.** Identification of an atypical Grb2 carboxyl-terminal SH3 domain binding site in Gab docking proteins reveals Grb2-dependent and -independent recruitment of Gab1 to receptor tyrosine kinases. *J Biol Chem* 275: 31536-31545, 2000.

102. **Lohmueller KE, Pearce CL, Pike M, Lander ES, and Hirschhorn JN.** Meta-analysis of genetic association studies supports a contribution of common variants to susceptibility to common disease. *Nat Genet* 33: 177-182, 2003.

103. **Lowenstein JM, Brunengraber H, and Wadke M.** Measurement of rates of lipogenesis with deuterated and tritiated water. *Methods Enzymol* 35: 279-287, 1975.

104. **Ma H, Fukiage C, Kim YH, Duncan MK, Reed NA, Shih M, Azuma M, and Shearer TR.** Characterization and expression of calpain 10. A novel ubiquitous calpain with nuclear localization. *J Biol Chem* 276: 28525-28531, 2001.

105. **Magnusson I, Rothman DL, Katz LD, Shulman RG, and Shulman GI.** Increased rate of gluconeogenesis in type II diabetes mellitus. A 13C nuclear magnetic resonance study. *J Clin Invest* 90: 1323-1327, 1992.

106. **Malaisse WJ, Liemans V, Malaisse-Lagae F, Ottinger R, and Willem R.** Phosphoglucoisomerase-catalyzed interconversion of hexose phosphates. Study by 13C NMR of proton and deuteron exchange. *Mol Cell Biochem* 103: 131-140, 1991.

107. **Malaisse WJ, Malaisse-Lagae F, Liemans V, Ottinger R, and Willem R.** Phosphoglucoisomerase-catalyzed interconversion of hexose phosphates: isotopic discrimination between hydrogen and deuterium. *Mol Cell Biochem* 93: 153-165, 1990.

108. **Mamputu JC, Wiernsperger NF, and Renier G.** Antiatherogenic properties of metformin: the experimental evidence. *Diabetes Metab* 29: 6S71-76, 2003.

109. **Mancuso A, Sharfstein ST, Fernandez EJ, Clark DS, and Blanch HW.** Effect of extracellular glutamine concentration on primary and secondary metabolism of a murine hybridoma: an in vivo 13C nuclear magnetic resonance study. *Biotechnol Bioeng* 57: 172-186, 1998.

110. **Marcotte EM, Pellegrini M, Thompson MJ, Yeates TO, and Eisenberg D.** A combined algorithm for genome-wide prediction of protein function. *Nature* 402: 83-86, 1999.

111. **Marshall S, Bacote V, and Traxinger RR.** Discovery of a metabolic pathway mediating glucose-induced desensitization of the glucose transport system. Role of hexosamine biosynthesis in the induction of insulin resistance. *J Biol Chem* 266: 4706-4712, 1991.

112. **Marshall S, Garvey WT, and Traxinger RR.** New insights into the metabolic regulation of insulin action and insulin resistance: role of glucose and amino acids. *Faseb J* 5: 3031-3036, 1991.

113. **Marshall S, Nadeau O, and Yamasaki K.** Dynamic actions of glucose and glucosamine on hexosamine biosynthesis in isolated adipocytes: differential effects on glucosamine 6-phosphate, UDP-N-acetylglucosamine, and ATP levels. *J Biol Chem* 279: 35313-35319, 2004.

114. **Marshall S, Nadeau O, and Yamasaki K.** Glucosamine-induced activation of glycogen biosynthesis in isolated adipocytes. Evidence for a rapid allosteric control mechanism within the hexosamine biosynthesis pathway. *J Biol Chem* 280: 11018-11024, 2005.

115. **Marshall S, Yamasaki K, and Okuyama R.** Glucosamine induces rapid desensitization of glucose transport in isolated adipocytes by increasing GlcN-6-P levels. *Biochem Biophys Res Commun* 329: 1155-1161, 2005.

116. **McClain DA.** Hexosamines as mediators of nutrient sensing and regulation in diabetes. *J Diabetes Complications* 16: 72-80, 2002.

117. **McClain DA and Crook ED.** Hexosamines and insulin resistance. *Diabetes* 45: 1003-1009, 1996.

118. **McMillian M, Nie AY, Parker JB, Leone A, Kemmerer M, Bryant S, Herlich J, Yieh L, Bittner A, Liu X, Wan J, and Johnson MD.** Inverse gene expression patterns for macrophage activating hepatotoxicants and peroxisome proliferators in rat liver. *Biochem Pharmacol* 67: 2141-2165, 2004.

119. **Meier R, Alessi DR, Cron P, Andjelkovic M, and Hemmings BA.** Mitogenic activation, phosphorylation, and nuclear translocation of protein kinase Bbeta. *J Biol Chem* 272: 30491-30497, 1997.

120. **Meriden T.** Progress with thiazolidinediones in the management of type 2 diabetes mellitus. *Clin Ther* 26: 177-190, 2004.

121. **Miller WM, Wilke CR, and Blanch HW.** Transient responses of hybridoma cells to nutrient additions in continuous culture. 1. Glucose pulse and step changes. *Biotechnol Bioeng* 33: 477-486, 1989.

122. **Mitrakou A, Kelley D, Veneman T, Jenssen T, Pangburn T, Reilly J, and Gerich J.** Contribution of abnormal muscle and liver glucose metabolism to postprandial hyperglycemia in NIDDM. *Diabetes* 39: 1381-1390, 1990.

123. **Moller DE, Cohen O, Yamaguchi Y, Assiz R, Grigorescu F, Eberle A, Morrow LA, Moses AC, and Flier JS.** Prevalence of mutations in the insulin receptor gene in subjects with features of the type A syndrome of insulin resistance. *Diabetes* 43: 247-255, 1994.

124. **Moller DE, Yokota A, White MF, Pazianos AG, and Flier JS.** A naturally occurring mutation of insulin receptor alanine 1134 impairs tyrosine kinase function and is associated with dominantly inherited insulin resistance. *J Biol Chem* 265: 14979-14985, 1990.

125. **Monauni T, Zenti MG, Cretti A, Daniels MC, Targher G, Caruso B, Caputo M, McClain D, Del Prato S, Giaccari A, Muggeo M, Bonora E, and Bonadonna RC.** Effects of glucosamine infusion on insulin secretion and insulin action in humans. *Diabetes* 49: 926-935, 2000.

126. **Muller YL, Bogardus C, Beamer BA, Shuldiner AR, and Baier LJ.** A functional variant in the peroxisome proliferator-activated receptor gamma2 promoter is associated with predictors of obesity and type 2 diabetes in Pima Indians. *Diabetes* 52: 1864-1871, 2003.

127. **Nakae J, Barr V, and Accili D.** Differential regulation of gene expression by insulin and IGF-1 receptors correlates with phosphorylation of a single amino acid residue in the forkhead transcription factor FKHR. *Embo J* 19: 989-996, 2000.

128. **Nakae J, Biggs WH, 3rd, Kitamura T, Cavenee WK, Wright CV, Arden KC, and Accili D.** Regulation of insulin action and pancreatic beta-cell function by mutated alleles of the gene encoding forkhead transcription factor Foxo1. *Nat Genet* 32: 245-253, 2002.

129. **Newsholme EA, Crabtree B, and Ardawi MS.** The role of high rates of glycolysis and glutamine utilization in rapidly dividing cells. *Biosci Rep* 5: 393-400, 1985.

130. **Noguchi T, Matozaki T, Inagaki K, Tsuda M, Fukunaga K, Kitamura Y, Kitamura T, Shii K, Yamanashi Y, and Kasuga M.** Tyrosine phosphorylation of p62(Dok) induced by cell adhesion and insulin: possible role in cell migration. *Embo J* 18: 1748-1760, 1999.

131. **Ntzani EE and Ioannidis JP.** Predictive ability of DNA microarrays for cancer outcomes and correlates: an empirical assessment. *Lancet* 362: 1439-1444, 2003.

132. **Obici S and Rossetti L.** Minireview: nutrient sensing and the regulation of insulin action and energy balance. *Endocrinology* 144: 5172-5178, 2003.

133. **Ong KK, Phillips DI, Fall C, Poulton J, Bennett ST, Golding J, Todd JA, and Dunger DB.** The insulin gene VNTR, type 2 diabetes and birth weight. *Nat Genet* 21: 262-263, 1999.

134. **Parikh H and Groop L.** Candidate genes for type 2 diabetes. *Rev Endocr Metab Disord* 5: 151-176, 2004.

135. **Park SY, Ryu J, and Lee W.** O-GlcNAc modification on IRS-1 and Akt2 by PUGNAc inhibits their phosphorylation and induces insulin resistance in rat primary adipocytes. *Exp Mol Med* 37: 220-229, 2005.

136. **Parker G, Taylor R, Jones D, and McClain D.** Hyperglycemia and inhibition of glycogen synthase in streptozotocin-treated mice: role of O-linked N-acetylglucosamine. *J Biol Chem* 279: 20636-20642, 2004.

137. **Parker GJ, Lund KC, Taylor RP, and McClain DA.** Insulin resistance of glycogen synthase mediated by o-linked N-acetylglucosamine. *J Biol Chem* 278: 10022-10027, 2003.

138. **Patti ME, Virkamaki A, Landaker EJ, Kahn CR, and Yki-Jarvinen H.** Activation of the hexosamine pathway by glucosamine in vivo induces insulin resistance

of early postreceptor insulin signaling events in skeletal muscle. *Diabetes* 48: 1562-1571, 1999.

139. **Pawson T and Scott JD.** Signaling through scaffold, anchoring, and adaptor proteins. *Science* 278: 2075-2080, 1997.

140. **Portais JC, Voisin P, Merle M, and Canioni P.** Glucose and glutamine metabolism in C6 glioma cells studied by carbon 13 NMR. *Biochimie* 78: 155-164, 1996.

141. **Porzio O, Federici M, Hribal ML, Lauro D, Accili D, Lauro R, Borboni P, and Sesti G.** The Gly972-->Arg amino acid polymorphism in IRS-1 impairs insulin secretion in pancreatic beta cells. *J Clin Invest* 104: 357-364, 1999.

142. **Pouwels MJ, Jacobs JR, Span PN, Lutterman JA, Smits P, and Tack CJ.** Short-term glucosamine infusion does not affect insulin sensitivity in humans. *J Clin Endocrinol Metab* 86: 2099-2103, 2001.

143. **Pouwels MJ, Span PN, Tack CJ, Olthaar AJ, Sweep CG, van Engelen BG, de Jong JG, Lutterman JA, and Hermus AR.** Muscle uridine diphosphate-hexosamines do not decrease despite correction of hyperglycemia-induced insulin resistance in type 2 diabetes. *J Clin Endocrinol Metab* 87: 5179-5184, 2002.

144. **Pouwels MJ, Tack CJ, Span PN, Olthaar AJ, Sweep CG, Huvers FC, Lutterman JA, and Hermus AR.** Role of hexosamines in insulin resistance and nutrient sensing in human adipose and muscle tissue. *J Clin Endocrinol Metab* 89: 5132-5137, 2004.

145. **Press WH, Teukolsky SA, Vetterling WT, and Flannery BP.** Modeling of Data. In: *Numerical Recipes in C++: The Art of Scientific Computing* (2nd ed.). New York, NY: Cambridge University Press, 1992, p. 661-666.

146. **Previs SF, Withers DJ, Ren JM, White MF, and Shulman GI.** Contrasting effects of IRS-1 versus IRS-2 gene disruption on carbohydrate and lipid metabolism in vivo. *J Biol Chem* 275: 38990-38994, 2000.

147. **Puigserver P, Rhee J, Donovan J, Walkey CJ, Yoon JC, Oriente F, Kitamura Y, Altomonte J, Dong H, Accili D, and Spiegelman BM.** Insulin-regulated hepatic gluconeogenesis through FOXO1-PGC-1alpha interaction. *Nature* 423: 550-555, 2003.

148. **Pyke DA.** The History of Diabetes. http://www.diabetesliving.com/basics/wiley.htm. June 21, 2005.

149. **Quillard M, Renouf S, Husson A, Meisse D, and Lavoinne A.** Glutamine and regulation of gene expression in mammalian cells. Special reference to phosphoenolpyruvate carboxykinase (PEPCK). *Biochimie* 79: 125-128, 1997.

150. **Reitzer LJ, Wice BM, and Kennell D.** Evidence that glutamine, not sugar, is the major energy source for cultured HeLa cells. *J Biol Chem* 254: 2669-2676, 1979.

151. **Rigoutsos I and Floratos A.** Combinatorial pattern discovery in biological sequences: The TEIRESIAS algorithm. *Bioinformatics* 14: 55-67, 1998.

152. **Rissanen J, Pihlajamaki J, Heikkinen S, Kekalainen P, Mykkanen L, Kuusisto J, Kolle A, and Laakso M.** New variants in the glycogen synthase gene (Gln71His, Met416Val) in patients with NIDDM from eastern Finland. *Diabetologia* 40: 1313-1319, 1997.

153. **Roach PJ.** Control of glycogen synthase by hierarchal protein phosphorylation. *Faseb J* 4: 2961-2968, 1990.

154. **Robinson KA, Sens DA, and Buse MG.** Pre-exposure to glucosamine induces insulin resistance of glucose transport and glycogen synthesis in isolated rat skeletal muscles. Study of mechanisms in muscle and in rat-1 fibroblasts overexpressing the human insulin receptor. *Diabetes* 42: 1333-1346, 1993.

155. **Rose IA and O'Connell EL.** Stereospecificity of the sugarphosphate isomerase reactions; a uniformity. *Biochim Biophys Acta* 42: 159-160, 1960.

156. **Rosella G, Zajac JD, Baker L, Kaczmarczyk SJ, Andrikopoulos S, Adams TE, and Proietto J.** Impaired glucose tolerance and increased weight gain in transgenic rats overexpressing a non-insulin-responsive phosphoenolpyruvate carboxykinase gene. *Mol Endocrinol* 9: 1396-1404, 1995.

157. **Rossetti L.** Perspective: Hexosamines and nutrient sensing. *Endocrinology* 141: 1922-1925, 2000.

158. **Rossetti L, Giaccari A, Barzilai N, Howard K, Sebel G, and Hu M.** Mechanism by which hyperglycemia inhibits hepatic glucose production in conscious rats. Implications for the pathophysiology of fasting hyperglycemia in diabetes. *J Clin Invest* 92: 1126-1134, 1993.

159. **Roth U, Curth K, Unterman TG, and Kietzmann T.** The transcription factors HIF-1 and HNF-4 and the coactivator p300 are involved in insulin-regulated glucokinase gene expression via the phosphatidylinositol 3-kinase/protein kinase B pathway. *J Biol Chem* 279: 2623-2631, 2004.

160. **Rui L, Fisher TL, Thomas J, and White MF.** Regulation of insulin/insulin-like growth factor-1 signaling by proteasome-mediated degradation of insulin receptor substrate-2. *J Biol Chem* 276: 40362-40367, 2001.

161. **Rumberger JM, Wu T, Hering MA, and Marshall S.** Role of hexosamine biosynthesis in glucose-mediated up-regulation of lipogenic enzyme mRNA levels: effects of glucose, glutamine, and glucosamine on glycerophosphate dehydrogenase, fatty acid synthase, and acetyl-CoA carboxylase mRNA levels. *J Biol Chem* 278: 28547-28552, 2003.

162. **Sacca L, Hendler R, and Sherwin RS.** Hyperglycemia inhibits glucose production in man independent of changes in glucoregulatory hormones. *J Clin Endocrinol Metab* 47: 1160-1163, 1978.

163. **Schmoll D, Walker KS, Alessi DR, Grempler R, Burchell A, Guo S, Walther R, and Unterman TG.** Regulation of glucose-6-phosphatase gene expression by protein kinase Balpha and the forkhead transcription factor FKHR. Evidence for insulin response unit-dependent and -independent effects of insulin on promoter activity. *J Biol Chem* 275: 36324-36333, 2000.

164. **Seeholzer SH.** Phosphoglucose isomerase: a ketol isomerase with aldol C2-epimerase activity. *Proc Natl Acad Sci U S A* 90: 1237-1241, 1993.

165. **Seglen PO.** Preparation of isolated rat liver cells. *Methods Cell Biol* 13: 29-83, 1976.

166. **Shaw RJ, Lamia KA, Vasquez D, Koo SH, Bardeesy N, Depinho RA, Montminy M, and Cantley LC.** The kinase LKB1 mediates glucose homeostasis in liver and therapeutic effects of metformin. *Science* 310: 1642-1646, 2005.

167. **Shulman GI.** Cellular mechanisms of insulin resistance. *J Clin Invest* 106: 171-176, 2000.

168. **Shulman GI, Lacy WW, Liljenquist JE, Keller U, Williams PE, and Cherrington AD.** Effect of glucose, independent of changes in insulin and glucagon secretion, on alanine metabolism in the conscious dog. *J Clin Invest* 65: 496-505, 1980.

169. **Shulman GI, Liljenquist JE, Williams PE, and Lacy WW.** Glucose disposal during insulinopenia in somatostatin-treated dogs. The roles of glucose and glucagon. *J Clin Invest* 62: 487-491, 1978.

170. **Simonson DC, Rossetti L., Giaccari, A., and DeFronzo, R.A.** In: *International Textbook of Diabetes Mellitus*, edited by Alberti KGMM, Zimmet, P., DeFronzo, R.A., and Kenn, H.: John Wiley & Sons, Ltd, 1997, p. 713-744.

171. **Song Y, Niu T, Manson JE, Kwiatkowski DJ, and Liu S.** Are variants in the CAPN10 gene related to risk of type 2 diabetes? A quantitative assessment of population and family-based association studies. *Am J Hum Genet* 74: 208-222, 2004.

172. **Soskin S and Levine R.** In: *Carbohydrate Metabolism*. Chicago: University of Chicago Press, 1946, p. 247-263.

173. **Spampinato D, Giaccari A, Trischitta V, Costanzo BV, Morviducci L, Buongiorno A, Di Mario U, Vigneri R, and Frittitta L.** Rats that are made insulin resistant by glucosamine treatment have impaired skeletal muscle insulin receptor phosphorylation. *Metabolism* 52: 1092-1095, 2003.

174. **Spellman PT, Sherlock G, Zhang MQ, Iyer VR, Anders K, Eisen MB, Brown PO, Botstein D, and Futcher B.** Comprehensive identification of cell cycle-regulated genes of the yeast Saccharomyces cerevisiae by microarray hybridization. *Mol Biol Cell* 9: 3273-3297, 1998.

175. **Sreenan SK, Zhou YP, Otani K, Hansen PA, Currie KP, Pan CY, Lee JP, Ostrega DM, Pugh W, Horikawa Y, Cox NJ, Hanis CL, Burant CF, Fox AP, Bell GI, and Polonsky KS.** Calpains play a role in insulin secretion and action. *Diabetes* 50: 2013-2020, 2001.

176. **St-Onge J, Joanisse DR, and Simoneau JA.** The stimulation-induced increase in skeletal muscle glycogen synthase content is impaired in carriers of the glycogen synthase XbaI gene polymorphism. *Diabetes* 50: 195-198, 2001.

177. **Streeper RS, Eaton EM, Ebert DH, Chapman SC, Svitek CA, and O'Brien RM.** Hepatocyte nuclear factor-1 acts as an accessory factor to enhance the inhibitory action of insulin on mouse glucose-6-phosphatase gene transcription. *Proc Natl Acad Sci U S A* 95: 9208-9213, 1998.

178. **Stumvoll M, Fritsche A, Volk A, Stefan N, Madaus A, Maerker E, Teigeler A, Koch M, Machicao F, and Haring H.** The Gly972Arg polymorphism in the insulin receptor substrate-1 gene contributes to the variation in insulin secretion in normal glucose-tolerant humans. *Diabetes* 50: 882-885, 2001.

179. **Summers SA, Kao AW, Kohn AD, Backus GS, Roth RA, Pessin JE, and Birnbaum MJ.** The role of glycogen synthase kinase 3beta in insulin-stimulated glucose metabolism. *J Biol Chem* 274: 17934-17940, 1999.

180. **Suzuki K, Hata S, Kawabata Y, and Sorimachi H.** Structure, activation, and biology of calpain. *Diabetes* 53 Suppl 1: S12-18, 2004.

181. **Tavazoie S, Hughes JD, Campbell MJ, Cho RJ, and Church GM.** Systematic determination of genetic network architecture. *Nat Genet* 22: 281-285, 1999.

182. **Taylor R and Agius L.** The biochemistry of diabetes. *Biochem J* 250: 625-640, 1988.

183. **Thomas PE and Hutton JJ.** Biochemical and tissue culture studies of transplantable mouse hepatomas H-4, H-6, and BW7756. *J Natl Cancer Inst* 47: 1025-1031, 1971.

184. **Trinh KY, O'Doherty RM, Anderson P, Lange AJ, and Newgard CB.** Perturbation of fuel homeostasis caused by overexpression of the glucose-6-phosphatase catalytic subunit in liver of normal rats. *J Biol Chem* 273: 31615-31620, 1998.

185. **Tripathy D, Eriksson KF, Orho-Melander M, Fredriksson J, Ahlqvist G, and Groop L.** Parallel manifestation of insulin resistance and beta cell decompensation is compatible with a common defect in Type 2 diabetes. *Diabetologia* 47: 782-793, 2004.

186. **Unger G, Fredman L, and Shapiro S.** Pharmacologic studies of a new oral hypoglycemic drug. *Proc Soc Exp Biol Med* 95: 190-192, 1957.

187. **Valera A, Pujol A, Pelegrin M, and Bosch F.** Transgenic mice overexpressing phosphoenolpyruvate carboxykinase develop non-insulin-dependent diabetes mellitus. *Proc Natl Acad Sci U S A* 91: 9151-9154, 1994.

188. **van 't Veer LJ, Dai H, van de Vijver MJ, He YD, Hart AA, Mao M, Peterse HL, van der Kooy K, Marton MJ, Witteveen AT, Schreiber GJ, Kerkhoven RM, Roberts C, Linsley PS, Bernards R, and Friend SH.** Gene expression profiling predicts clinical outcome of breast cancer. *Nature* 415: 530-536, 2002.

189. **van de Vijver MJ, He YD, van't Veer LJ, Dai H, Hart AA, Voskuil DW, Schreiber GJ, Peterse JL, Roberts C, Marton MJ, Parrish M, Atsma D, Witteveen A, Glas A, Delahaye L, van der Velde T, Bartelink H, Rodenhuis S, Rutgers ET, Friend SH, and Bernards R.** A gene-expression signature as a predictor of survival in breast cancer. *N Engl J Med* 347: 1999-2009, 2002.

190. **Vanhaesebroeck B and Alessi DR.** The PI3K-PDK1 connection: more than just a road to PKB. *Biochem J* 346 Pt 3: 561-576, 2000.

191. **Vaulont S, Munnich A, Decaux JF, and Kahn A.** Transcriptional and post-transcriptional regulation of L-type pyruvate kinase gene expression in rat liver. *J Biol Chem* 261: 7621-7625, 1986.

192. **Vidal-Puig A and O'Rahilly S.** Metabolism. Controlling the glucose factory. *Nature* 413: 125-126, 2001.

193. **Virkamaki A, Daniels MC, Hamalainen S, Utriainen T, McClain D, and Yki-Jarvinen H.** Activation of the hexosamine pathway by glucosamine in vivo induces insulin resistance in multiple insulin sensitive tissues. *Endocrinology* 138: 2501-2507, 1997.

194. **Waring JF, Jolly RA, Ciurlionis R, Lum PY, Praestgaard JT, Morfitt DC, Buratto B, Roberts C, Schadt E, and Ulrich RG.** Clustering of hepatotoxins based on mechanism of toxicity using gene expression profiles. *Toxicol Appl Pharmacol* 175: 28-42, 2001.

195. **Weedon MN, Schwarz PE, Horikawa Y, Iwasaki N, Illig T, Holle R, Rathmann W, Selisko T, Schulze J, Owen KR, Evans J, Del Bosque-Plata L, Hitman G, Walker M, Levy JC, Sampson M, Bell GI, McCarthy MI, Hattersley AT, and Frayling TM.** Meta-analysis and a large association study confirm a role for calpain-10 variation in type 2 diabetes susceptibility. *Am J Hum Genet* 73: 1208-1212, 2003.

196. **Weigert C, Thamer C, Brodbeck K, Guirguis A, Machicao F, Machann J, Schick F, Stumvoll M, Fritsche A, Haring HU, and Schleicher ED.** The -913 G/A glutamine:fructose-6-phosphate aminotransferase gene polymorphism is associated with measures of obesity and intramyocellular lipid content in nondiabetic subjects. *J Clin Endocrinol Metab* 90: 1639-1643, 2005.

197. **Wells L, Vosseller K, and Hart GW.** A role for N-acetylglucosamine as a nutrient sensor and mediator of insulin resistance. *Cell Mol Life Sci* 60: 222-228, 2003.

198. **Wen X, Fuhrman S, Michaels GS, Carr DB, Smith S, Barker JL, and Somogyi R.** Large-scale temporal gene expression mapping of central nervous system development. *Proc Natl Acad Sci U S A* 95: 334-339, 1998.

199. **White KP, Rifkin SA, Hurban P, and Hogness DS.** Microarray analysis of Drosophila development during metamorphosis. *Science* 286: 2179-2184, 1999.

200. **White MF.** IRS proteins and the common path to diabetes. *Am J Physiol Endocrinol Metab* 283: E413-422, 2002.

201. **Whitehead JP, Humphreys P, Krook A, Jackson R, Hayward A, Lewis H, Siddle K, and O'Rahilly S.** Molecular scanning of the insulin receptor substrate 1 gene in subjects with severe insulin resistance: detection and functional analysis of a naturally occurring mutation in a YMXM motif. *Diabetes* 47: 837-839, 1998.

202. **Wild S, Roglic G, Green A, Sicree R, and King H.** Global prevalence of diabetes: estimates for the year 2000 and projections for 2030. *Diabetes Care* 27: 1047-1053, 2004.

203. **Wolfe R.** *Radioactive and Stable Isotope Tracers in Biomedicine*. New York: Wiley-Liss, 1992.

204. **Wolfrum C, Besser D, Luca E, and Stoffel M.** Insulin regulates the activity of forkhead transcription factor Hnf-3beta/Foxa-2 by Akt-mediated phosphorylation and nuclear/cytosolic localization. *Proc Natl Acad Sci U S A* 100: 11624-11629, 2003.

205. **Yamauchi T, Tobe K, Tamemoto H, Ueki K, Kaburagi Y, Yamamoto-Honda R, Takahashi Y, Yoshizawa F, Aizawa S, Akanuma Y, Sonenberg N, Yazaki Y, and Kadowaki T.** Insulin signalling and insulin actions in the muscles and livers of insulin-resistant, insulin receptor substrate 1-deficient mice. *Mol Cell Biol* 16: 3074-3084, 1996.

206. **Yang Chou J and Mansfield BC.** Molecular Genetics of Type 1 Glycogen Storage Diseases. *Trends Endocrinol Metab* 10: 104-113, 1999.

207. **Yang Z, Whelan J, Babb R, and Bowen BR.** An mRNA splice variant of the AFX gene with altered transcriptional activity. *J Biol Chem* 277: 8068-8075, 2002.

208. **Ye JM, Dzamko N, Cleasby ME, Hegarty BD, Furler SM, Cooney GJ, and Kraegen EW.** Direct demonstration of lipid sequestration as a mechanism by which rosiglitazone prevents fatty-acid-induced insulin resistance in the rat: comparison with metformin. *Diabetologia* 47: 1306-1313, 2004.

209. **Yki-Jarvinen H.** Glucose toxicity. *Endocr Rev* 13: 415-431, 1992.

210. **Yki-Jarvinen H.** Thiazolidinediones. *N Engl J Med* 351: 1106-1118, 2004.

211. **Yoon JC, Puigserver P, Chen G, Donovan J, Wu Z, Rhee J, Adelmant G, Stafford J, Kahn CR, Granner DK, Newgard CB, and Spiegelman BM.** Control of hepatic gluconeogenesis through the transcriptional coactivator PGC-1. *Nature* 413: 131-138, 2001.

212. **Zachara NE and Hart GW.** The emerging significance of O-GlcNAc in cellular regulation. *Chem Rev* 102: 431-438, 2002.

213. **Zhang P, Klenk ES, Lazzaro MA, Williams LB, and Considine RV.** Hexosamines regulate leptin production in 3T3-L1 adipocytes through transcriptional mechanisms. *Endocrinology* 143: 99-106, 2002.

214. **Zhao X, Gan L, Pan H, Kan D, Majeski M, Adam SA, and Unterman TG.** Multiple elements regulate nuclear/cytoplasmic shuttling of FOXO1: characterization of phosphorylation- and 14-3-3-dependent and -independent mechanisms. *Biochem J* 378: 839-849, 2004.

215. **Zielke HR, Ozand PT, Tildon JT, Sevdalian DA, and Cornblath M.** Reciprocal regulation of glucose and glutamine utilization by cultured human diploid fibroblasts. *J Cell Physiol* 95: 41-48, 1978.

216. **Zinker BA, Rondinone CM, Trevillyan JM, Gum RJ, Clampit JE, Waring JF, Xie N, Wilcox D, Jacobson P, Frost L, Kroeger PE, Reilly RM, Koterski S, Opgenorth TJ, Ulrich RG, Crosby S, Butler M, Murray SF, McKay RA, Bhanot S,**

Monia BP, and Jirousek MR. PTP1B antisense oligonucleotide lowers PTP1B protein, normalizes blood glucose, and improves insulin sensitivity in diabetic mice. *Proc Natl Acad Sci U S A* 99: 11357-11362, 2002.